Journal of Machine Learning Research 26 (2025) 1-68 Submitted 10/23; Revised 10/24; Published 1/25

Deep Out-of-Distribution Uncertainty Quantification via Weight Entropy Maximization

Antoine de Mathelin[1,2] ANTOINE.DE_MATHELIN@ENS-PARIS-SACLAY.FR
François Deheeger[1] FRANCOIS.DEHEEGER@MICHELIN.COM
Mathilde Mougeot[2] MATHILDE.MOUGEOT@ENS-PARIS-SACLAY.FR
Nicolas Vayatis[2] NICOLAS.VAYATIS@ENS-PARIS-SACLAY.FR
[1]*Manufacture Française des pneumatiques Michelin, Clermont-Ferrand, 63000, France*
[2]*Centre Borelli, Université Paris-Saclay, CNRS, ENS Paris-Saclay, Gif-sur-Yvette, 91190, France*

Editor: Maya Gupta

Abstract

This paper deals with uncertainty quantification and out-of-distribution detection in deep learning using Bayesian and ensemble methods. It proposes a practical solution to the lack of prediction diversity observed recently for standard approaches when used out-of-distribution (Ovadia et al., 2019; Liu et al., 2021). Considering that this issue is mainly related to a lack of weight diversity, we claim that standard methods sample in "over-restricted" regions of the weight space due to the use of "over-regularization" processes, such as weight decay and zero-mean centered Gaussian priors. We propose to solve the problem by adopting the maximum entropy principle for the weight distribution, with the underlying idea to maximize the weight diversity. Under this paradigm, the epistemic uncertainty is described by the weight distribution of maximal entropy that produces neural networks "consistent" with the training observations. Considering stochastic neural networks, a practical optimization is derived to build such a distribution, defined as a trade-off between the average empirical risk and the weight distribution entropy. We provide both theoretical and numerical results to assess the efficiency of the approach. In particular, the proposed algorithm appears in the top three best methods in all configurations of an extensive out-of-distribution detection benchmark including more than thirty competitors.

Keywords: Epistemic uncertainty, out-of-distribution detection, deep ensemble, Bayesian neural networks, maximum entropy

1. Introduction

In many practical deep learning scenarios, neural network models are deployed on unknown data distributions that can significantly differ from the training distribution. For instance, when building deep learning models of object detection for autonomous cars, the training dataset cannot cover any potential situation that the model can encounter, in terms of weather conditions, geography, or camera obstructions for examples. In this context, the learner aims at providing confidence guarantees on the model prediction for any data belonging to the whole input space, including data outside the support of the training distribution. This task is related to *epistemic uncertainty* quantification and *out-of-distribution* (OOD) detection for deep learning (Kendall and Gal, 2017; Shen et al., 2021). In the epistemic uncertainty quantification framework, the learner aims at estimating the potential discrepancy between the estimated hypothesis and the optimal predictor. When dealing with neural networks, the set of hypotheses is typically very large and many of them provide a low empirical risk on the training observations. Informally, this collection of hypotheses that are *consistent* with the training data form a subset of relevant candidates for the optimal predictor. The prediction uncertainty for a novel input observation is then described by the prediction diversity of the consistent hypotheses (Hüllermeier and Waegeman, 2021).

In the case of universal approximators such as neural networks, a proxy of the epistemic uncertainty can be estimated by computing the distance to the support of the training set. For example, if the considered set of hypotheses is the set of k-Lipschitz functions, the pointwise prediction discrepancy between two consistent hypotheses is bounded by a value proportional to the distance to the training inputs (Sullivan et al., 2013; Malherbe and Vayatis, 2017; de Mathelin et al., 2022). Methods developed under this paradigm are referred to as *distance-based* uncertainty quantifiers, which include, for instance, derivative of Gaussian processes (Rasmussen, 2003), Deterministic Uncertainty Quantification (DUQ) (Van Amersfoort et al., 2020), Mahalanobis distance (Lee et al., 2018b) or Deep Nearest Neighbors (Sun et al., 2022). The main challenge faced by distance-based uncertainty approaches is to find a relevant notion of distance to use (Liu et al., 2022). For high-dimensional machine learning problems, using the Euclidean distance in the input space is generally irrelevant and one looks for geometric distances computed in encoded spaces. For instance, Liu et al. (2022) and Cao and Zhang (2022) develop distance preserving networks using spectral normalization. Finally, computing the distance to the training distribution support can also be performed by density estimation techniques, such as auto-encoders or GANs, which have been used for OOD detection (Zhou, 2022; Ryu et al., 2018). The distance to the training set is then computed through the reconstruction error of the decoder or by the predicted likelihood of the discriminator.

The main alternative to the distance-based approach consists in directly looking for a set of hypotheses that are consistent with the training observations and to use the diversity of their predictions as uncertainties. It essentially includes ensemble and Bayesian methods (Lakshminarayanan et al., 2017; Mackay, 1992). The ongoing challenge of this approach is to produce diversity in the ensemble of networks, i.e., to avoid sampling similar hypotheses. It has been observed, indeed, that most of the main baselines lead to a lack of prediction diversity, in particular outside the training support, i.e., for out-of-distribution data (Ovadia et al., 2019; Liu et al., 2021; Henning et al., 2021). Facing this issue, several attempts propose to increase the prediction diversity by adding a penalizing term to the loss. For instance, negative correlation methods penalize the correlation between the outputs of the ensemble members on the training data (Liu and Yao, 1999; Shui et al., 2018; Zhang et al., 2020). Related methods, referred to as *contrastive* approaches, penalize small output variances on synthetic OOD data produced by sampling uniformly in the input space (Jain et al., 2020; Mehrtens et al., 2022) or in the neighborhood of the training instances (Lakshminarayanan et al., 2017; Segonne et al., 2022). The drawback of these methods is the lack of generalization to any OOD data that the model can encounter (Cao and Zhang, 2022). Alternative approaches consist in penalizing the similarity between the ensemble members in the parameter space (Pearce et al., 2018; D'Angelo and Fortuin, 2021), with the underlying assumption that an ensemble of neural networks with weights distant from each other produces diversified outputs. In this work, we advocate that the key feature for producing accurate uncertainty quantification for any input data point is to sample in the *whole* space of consistent hypotheses. Indeed, we argue that standard Bayesian and ensemble methods often provide over-confident predictions for OOD data because the hypotheses they produce are sampled in restricted regions of the consistent hypothesis space due to weight decay regularization and hyper-parameters selection based on hold-out validation.

Considering stochastic neural networks with parameterized weight distribution (Jospin et al., 2022), we cast the problem as a trade-off between sampling in low empirical risk regions and increasing the weight diversity. We consider the entropy as a measure of weight diversity, and show that the optimization boils down to solving a maximum entropy problem (Jaynes, 1968), where we aim at selecting the weight distribution of maximal entropy under the constraint that the training loss is acceptable. We derive a practical optimization formulation to solve this problem, called Maximum Weight Entropy (**MaxWEnt**), and show that it can be tackled with stochastic variational inference (Hoffman et al., 2013) using the reparameterization trick (Kingma and Welling, 2014). The proposed optimization consists in penalizing the training loss with a term imposing the *increase* of the weight distribution entropy. We provide a theoretical framework to understand the dynamic of this approach and show that the spread of the weight distribution is inversely proportional to the neuron activation amplitude for the training data. Numerical experiments conducted on several regression and classification datasets demonstrate the strong benefit of this approach in OOD detection compared to state-of-the-art methods dedicated to this task (e.g., Figure 1).

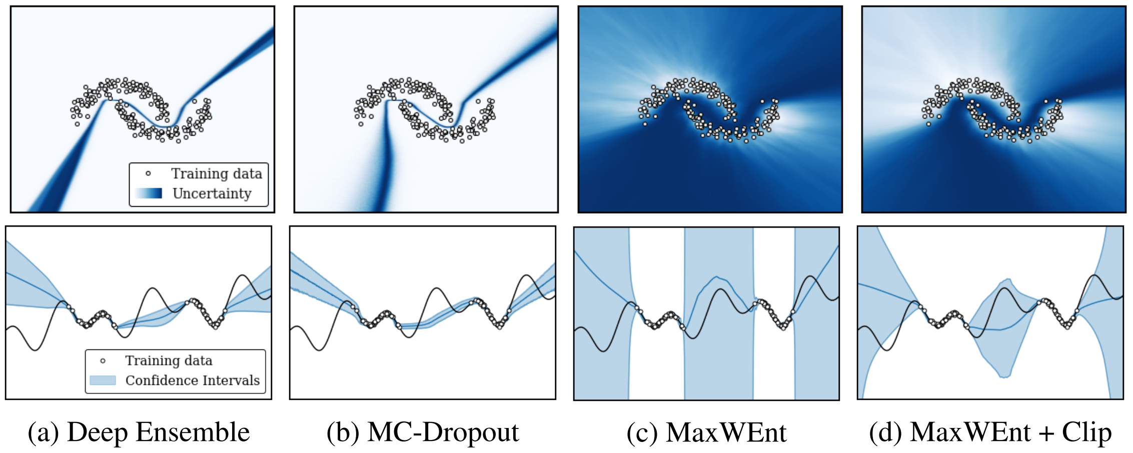

Figure 1: Uncertainty Estimation Comparison. Above: “two-moons” 2D classification dataset. Below: 1D-regression (Jain et al., 2020). Deep Ensemble (a) and MC-Dropout (b) produce overconfident estimations outside the training support due to a lack of hypothesis diversity. In the classification experiment, the hypotheses produced by both methods are restricted to half-space separators. There is no prediction uncertainty in the upper left and lower right areas of the input space, despite the lack of training data in these regions. In contrast, MaxWEnt (c, d) provides a clear discrimination between the in-distribution and out-of-distribution domains in terms of prediction uncertainty. Figure (c) presents the result obtained with MaxWEnt when no regularity assumption is made on the labeling function. In this case, the uncertainty quickly increases when leaving the training support, which truly represents the epistemic uncertainty in the absence of prior knowledge about the labeling function. Figure (d) reports the MaxWEnt uncertainty estimation when considering Lipschitz constraints. This result can be obtained with a small modification of the previous MaxWEnt model in the form of weight clipping. The full description of these synthetic experiments is reported in Section 7.1.

2. Assessing Epistemic Uncertainty for OOD Prediction: Setup and Challenges

2.1 Notations

We consider the supervised learning framework provided with the input space $\mathcal{X}$ of finite dimension $b \in \mathbb{N}$, and the output space $\mathcal{Y}$. We denote by $p^*(x, y)$ the "ground truth" law defined over $\mathcal{X} \times \mathcal{Y}$. Furthermore, we distinguish the *in-distribution* and *out-of-distribution* domains by considering that only a subset $\mathcal{D}_\mathcal{X} \subset \mathcal{X}$ can be sampled. The subset $\mathcal{D}_\mathcal{X}$ is called "training domain" and any data from the complementary $\mathcal{X} \setminus \mathcal{D}_\mathcal{X}$ is considered to be "out-of-distribution". We assume that the learner has access to the training set $\mathcal{S} = \{(x_1, y_1), ..., (x_n, y_n)\} \in \mathcal{D}_\mathcal{X} \times \mathcal{Y}$ of size $n \in \mathbb{N}$ where the training instances (x_i, y_i) are supposed independently identically distributed (iid) according to the joint distribution $p(x, y)$ defined over $\mathcal{D}_\mathcal{X} \times \mathcal{Y}$ and verifying $p(y|x) = p^*(y|x) \; \forall \, x \in \mathcal{D}_\mathcal{X}$. We consider a continuous loss function $\ell : \mathcal{Y} \times \mathcal{Y} \to \mathbb{R}_+$ and define the *optimal predictor* $f^* : \mathcal{X} \to \mathcal{Y}$ as follows:

$$f^*(x) = \underset{y' \in \mathcal{Y}}{\operatorname{argmin}} \int_{y \in \mathcal{Y}} \ell(y', y) \, dp^*(y|x).$$

We denote $\mathcal{H}$ a set of neural networks of a specified architecture, mapping $\mathcal{X}$ to $\mathcal{Y}$. The set $\mathcal{H}$ is assumed to be "large". We denote $\mathcal{W} \subset \mathbb{R}^d$ ($d \in \mathbb{N}$) the set of weights corresponding to the hypotheses in $\mathcal{H}$. The best hypothesis in the class, h^*, referred to as the *optimal hypothesis*, is defined according to the following expression:

$$h^* = \underset{h \in \mathcal{H}}{\operatorname{argmin}} \int_{x \in \mathcal{X}} \int_{y \in \mathcal{Y}} \ell(h(x), y) \, dp^*(x, y).$$

Finally, for any $h \in \mathcal{H}$, we define the empirical risk as follows:

$$\mathcal{L}_\mathcal{S}(h) = \frac{1}{n} \sum_{(x,y) \in \mathcal{S}} \ell(h(x), y),$$

denoted indifferently $\mathcal{L}_\mathcal{S}(w)$, when considering the weights $w \in \mathcal{W}$ associated to the hypothesis $h \in \mathcal{H}$, also referred as h_w.

2.2 The epistemic uncertainty is described by the set of consistent hypotheses

The general purpose of uncertainty quantification is to provide, for any $x \in \mathcal{X}$, a distribution in the label space $\mathcal{Y}$, describing the potential outputs that can be associated with x, knowing the training observations $\mathcal{S}$ and prior information about $p^*(x, y)$. In this work, we distinguish the following four sources of uncertainty:

1. **Aleatoric uncertainty**: the intrinsic random noise of the data, i.e., $p^*(y|x)$. This uncertainty cannot be reduced, even with an infinite number of observations (e.g., the outcome of a coin flip).

2. **Model uncertainty**: the discrepancy between f^* and h^*. The model uncertainty is related to the choice of the hypothesis set $\mathcal{H}$. It can be reduced by increasing the size of $\mathcal{H}$ or by acquiring prior knowledge about f^* (e.g., Lipschitz constraints).

3. **Statistical uncertainty**: the partial knowledge about $p(x, y)$ given by the finite number of data $\mathcal{S}$. This uncertainty, also referred to as *approximation uncertainty* (Hüllermeier and

Waegeman, 2021) or *data variability* (Huang et al., 2021b), is linked to the discrepancy between h^* and its estimation. It can be reduced by the acquisition of novel observations drawn according to $p(x, y)$ or by prior knowledge about the intrinsic random noise (e.g., a Gaussian homoscedastic noise of known variance).

4. **Out-of-distribution uncertainty**: the absence of observation over the out-of-distribution domain $\mathcal{X} \setminus \mathcal{D}_{\mathcal{X}}$. This uncertainty can remain large even with an infinite number of training observations. Indeed, for complex hypotheses as neural networks, different hypotheses can match $h^*(x)$ on $\mathcal{D}_{\mathcal{X}}$ but produce different outputs on $\mathcal{X} \setminus \mathcal{D}_{\mathcal{X}}$.

The first three sources of uncertainty are described in detail in Hüllermeier and Waegeman (2021), while source (4) is an additional distinction of the epistemic uncertainty similar to the framework introduced in Liu et al. (2022). The distinction between these four sources of uncertainty is useful for positioning our contribution. In this work, we focus essentially on the estimation of the statistical and OOD uncertainty. We assume, indeed, that f^* is close to $\mathcal{H}$, i.e., $h^* \simeq f^*$, and then neglect the model uncertainty, which is a common assumption when considering a large set of hypotheses such as a set of deep neural networks (Hüllermeier and Waegeman, 2021). In the following, the term *epistemic uncertainty* will refer to the combination of the statistical and OOD uncertainty.

It should be noted that, on the one hand, as we consider model uncertainty to be negligible, our approach may not effectively capture the epistemic uncertainty if this assumption does not hold. On the other hand, since our method is designed to address OOD uncertainty, it remains useful even when the statistical uncertainty is low (e.g., when a very large amount of training data is available). Indeed, multiple hypotheses can perform optimally on the training distribution while providing different predictions on OOD data. Our method specifically aims to capture this variability.

Because of lack of complete knowledge, the learner cannot perfectly determine the optimal hypothesis h^* and then the optimal predictions $h^*(x)$. If no data is available, the prediction uncertainty for $x \in \mathcal{X}$ is given by the distribution of the predicted values $h(x)$ for all hypotheses $h \in \mathcal{H}$. When acquiring more observations, the learner can discriminate between relevant and irrelevant candidates for h^*, i.e., between "consistent" and "inconsistent" hypotheses with respect to the observations $\mathcal{S}$ (assuming that a notion of "consistency" can be formally defined). By denoting $\mathcal{H}_{\mathcal{S}}$ the set of *consistent hypotheses*, the epistemic uncertainty for the prediction of the model for x is then given by the distribution of predictions $h(x)$ with $h \sim \mathcal{H}_{\mathcal{S}}$.

The notion of consistency depends on the underlying assumptions that the user considers about the data sample $\mathcal{S}$. A strong assumption is the "no noise" framework, where the user assumes that the optimal hypothesis necessarily verifies $h^*(x) = y$ for any $(x, y) \in \mathcal{S}$. In this case, the set of consistent hypotheses is the set: $\mathcal{H}_{\mathcal{S}} = \{h \in \mathcal{H};\ h(x) = y\}$ (Mitchell, 1977). In general, the user assumes a moderated noise level. Then, the notion of consistency is related to the empirical risk $\mathcal{L}_{\mathcal{S}}(h)$, such that consistent hypotheses provide "low" empirical risk on $\mathcal{S}$. For instance, if the user is only interested in deploying models with greater accuracy than $\tau = 0.99$, then the set of consistent hypotheses is defined as $\mathcal{H}_{\mathcal{S}} = \{h \in \mathcal{H};\ \mathcal{L}_{\mathcal{S}}(h) \leq 1 - \tau\}$ (assuming that ℓ is the 0-1 loss). In the Bayesian setting, a noise model, $p(y|x, h)$ is generally assumed (e.g., a Gaussian noise of unknown mean and variance), then a gradual notion of consistency is obtained through the likelihood of the hypothesis $h \in \mathcal{H}$ given the sample $\mathcal{S}$, i.e., $p(h|\mathcal{S})$ (D'Angelo and Fortuin, 2021).

2.3 The main limitation of epistemic uncertainty estimation for deep learning

Based on the previous considerations, the epistemic uncertainty estimation is then considered accurate when the learner is able to determine the whole set of consistent hypothesis $\mathcal{H}_\mathcal{S}$ (or to determine the likelihood of any hypotheses in the Bayesian framework). However, as $\mathcal{H}$ is an infinite set, computing the empirical risk for any hypothesis from $\mathcal{H}$ to determine which hypothesis belong to $\mathcal{H}_\mathcal{S}$ is impossible. Moreover, with deep neural network hypotheses, determining the subspace $\mathcal{H}_\mathcal{S}$ is generally intractable, because of the non-linear relationship between the neural network parameters and the empirical error.

To overcome this issue, common practice consists in using empirical risk minimization algorithms to produce a sample or a distribution of consistent hypotheses. To avoid sampling always the same empirical risk minimizer, deep ensemble methods use random initialization and random batch order with early stopping (Lakshminarayanan et al., 2017), while Bayesian neural networks algorithms learn a weight distribution (Kendall and Gal, 2017). Although such approaches foster hypothesis diversity, they cannot guarantee to produce a representative sample of the *whole* set of consistent hypotheses. Moreover, common practices in deep learning training induce important biases which narrow the sampling in a restricted region of the consistent hypotheses' subspace. For instance, the use of weight decay (ℓ_2 penalization) and random weights initialization of relatively small variance (e.g., equal to the inverse of the number of neurons in the layer, Glorot and Bengio 2010) drive the sample in low weight regions. Consistent hypotheses with high weights are then excluded, even though they can explain the observations as well, but in a different way, which would contribute to increase the potential prediction diversity. Similarly, in the Bayesian framework, it has been recently observed that the most commonly used prior, i.e., the Gaussian centered prior, is "unintentionally informative" (Wenzel et al., 2020a). Finally, the evaluation of uncertainty quantification methods and their hyper-parameters selection is traditionally driven by the negative-log-likelihood metric (NLL) computed over a validation dataset belonging to the training domain (Liu and Yao, 1999; Pearce et al., 2018; Jain et al., 2020). However, such practice does not account for the epistemic uncertainty out-of-distribution and then does not foster methods which accurately estimate it. This issue is illustrated by the four bottom graphics of Figure 1, the four methods provide almost the same prediction uncertainty on the training domain, their validation NLL is then similar, but their OOD epistemic uncertainty estimation is very different.

Therefore, we identify the inability of standard approaches to produce a representative sample of consistent hypotheses as their main limitation. We argue that this limitation is the principal cause of their lack of prediction diversity for OOD data, observed recently (Ovadia et al., 2019; Liu et al., 2021; Henning et al., 2021) (cf. Section 5.1).

3. Weight Entropy Maximization

The main contribution of this work is the development of a practical algorithm to produce a sample of hypotheses that tends to be representative of the whole space of consistent hypotheses. Considering stochastic neural networks, we propose to learn the scale parameters of a distribution over the network weights, centered on a hypothesis of low empirical risk, with the double objective of minimizing the average empirical risk and maximizing the distribution diversity, measured through the weight entropy.

3.1 A principle to sample the whole space of consistent hypotheses

We consider the stochastic neural network approach, where samples of hypotheses are produced through a parameterized weight distribution q_ϕ in the set $\Phi = \{q_\phi\}_{\phi \in \mathbb{R}^D}$ composed of several distributions over $\mathcal{W}$ parameterized by $\phi \in \mathbb{R}^D$, with $D \in \mathbb{N}$ the parameter dimension. We propose to penalize the average training risk over q_ϕ with the entropy of the weight distribution, leading to the following optimization formulation:

$$\min_{\phi \in \mathbb{R}^D} \; \mathbb{E}_{q_\phi}\left[\mathcal{L}_{\mathcal{S}}(w)\right] - \lambda \mathbb{E}_{q_\phi}\left[-\log(q_\phi(w))\right], \tag{1}$$

with $\lambda \in \mathbb{R}_+$ the trade-off parameter.

- The first term: $\mathbb{E}_{q_\phi}[\mathcal{L}_{\mathcal{S}}(w)]$ of the optimization objective in Equation (1) is the average empirical risk over the weight distribution. This term induces the increase of the probability mass $q_\phi(w)$ in regions where the weights $w \in \mathcal{W}$ produce accurate hypotheses on the training dataset, i.e., where $\mathcal{L}_{\mathcal{S}}(w)$ is small.

- The second term: $-\lambda \mathbb{E}_{q_\phi}\left[-\log(q_\phi(w))\right]$ in Equation (1) is a penalty that induces the increase of the weight entropy, which is generally related to expand the support of the weight distribution q_ϕ as broad as possible.

It should be underlined that both terms in Equation (1) evolve in opposite direction with respect to the weight distribution: the first term induces a weight distribution concentrated around any set of weights with minimal error on $\mathcal{S}$, while the second term induces a uniform distribution over the whole weight space. To solve this trade-off, the weight distribution tends to flatten in regions of little impact on the empirical risk, while remaining concentrated in directions where a small weight perturbation causes an important risk increase. The theoretical analysis in Section 4 shows, indeed, that the distribution spread of the weights is inversely proportional to the neuron activation amplitude. The weight variance is then larger for weights in front of neurons weakly activated by the training data. This theoretical result is supported by numerical results observed on synthetic datasets in Section 7.1 which provide a direct illustration of this link between the neuron activation and the weight variance (cf. Figure 6).

Objective (1) can be understood as a maximum entropy problem (Jaynes, 1957), where, in the presence of partial information about the optimal weight, the uncertainty is best described by the distribution of low-risk hypotheses with maximal entropy. In the Bayesian neural network setting, a similar objective can be derived through the ELBO formulation by using the prior of maximum entropy (Jaynes, 1968), which, in this case, is the uniform distribution over $\mathcal{W}$ (see Section 5.2). To highlight the link between our proposed approach and the maximum entropy principle, we call the method: Maximum Weight Entropy (**MaxWEnt**) in reference to the general maximum entropy modeling framework, commonly named MaxEnt (Berger et al., 1996). Formulating the epistemic uncertainty quantification as a maximum entropy problem offers a natural classification among the weight distributions $q_\phi \in \Phi$. Between two weight distributions that provide the same level of empirical risk on the training data, the user should select the one with the largest entropy. The maximum entropy paradigm also offers an interesting guideline to drive the selection of the weight distribution family Φ: the user should foster weight parameterization that enables larger increases of the entropy, as the SVD-parameterization described in Section 3.3.2.

3.2 The maximum weight entropy algorithm under general weight parameterization

Equation (1) is solved through stochastic gradient descent with mini-batches. To compute the expectation over q_ϕ, we use the reparameterization trick (Kingma and Welling, 2014; Rezende et al., 2014). We introduce a sampling variable $z \sim \mathcal{Z}$ with $\mathcal{Z}$ a distribution over $\mathbb{R}^d$ and a parameterization function $\omega : \mathbb{R}^d \times \mathbb{R}^d \to \mathbb{R}^d$ such that: $w = \omega(z, \phi)$. Typically, z follows a distribution that can be numerically sampled as the normal or uniform distribution. In case of simple parameterization, the weight entropy can be directly derived from the weight parameters ϕ, such that there exists a function $H : \mathbb{R}^d \to \mathbb{R}$ verifying $H(\phi) = \mathbb{E}_{\mathcal{Z}}\left[-\log(q_\phi(\omega(z,\phi)))\right]$. This leads to the following objective function, computed on a mini-batch of data $\mathcal{S}_b \subset \mathcal{S}$ of size $B > 0$:

$$G(\phi, \mathcal{S}_b) = \mathbb{E}_{\mathcal{Z}}\left[\mathcal{L}_{\mathcal{S}_b}(\omega(z,\phi))\right] - \lambda\, H(\phi). \tag{2}$$

By sampling $z^{(1)}, ..., z^{(N)}$ iid according to $\mathcal{Z}$, we can compute an estimation of the objective function gradient for each mini-batch as follows:

$$\nabla_\phi G(\phi, \mathcal{S}_b) \simeq \nabla_\phi \left[\frac{1}{N} \sum_{j=1}^{N} \mathcal{L}_{\mathcal{S}_b}(\omega(z^{(j)}, \phi)) - \lambda\, H(\phi) \right]. \tag{3}$$

Note that choosing $N = 1$ appears to be sufficient, in practice, to obtain efficient results (Kingma and Welling, 2014). Several gradient updates are performed until convergence to obtain the estimated parameters $\hat{\phi}$. The training part of the algorithm is summarized in Algorithm 1. For inference on $x \in \mathcal{X}$, a set of P predictions ($P \in \mathbb{N}^*$) is obtained by sampling multiple $z^{(j)} \sim \mathcal{Z}$ with $j \in [|1, P|]$, and computing the corresponding outputs $\{h_{w_j}(x);\ w_j = \omega(z^{(j)}, \hat{\phi})\}_{j \in [|1,P|]}$ (cf. Algorithm 2)

Algorithm 1 MaxWEnt Training

```
1: Inputs: Training set $\mathcal{S}$, learning rate $\nu$, trade-off $\lambda$, batch size $B$, parameterization $\omega$
2: Outputs: Scaling vector $\phi$
3: Init: $\phi \in \mathbb{R}^d$
4: while stopping criterion is not reached do
5:     $z \sim \mathcal{Z}, \mathcal{S}_b \sim \mathcal{U}(\mathcal{S}^B)$
6:     $\phi \leftarrow \phi - \nu \nabla_\phi \left[\mathcal{L}_{\mathcal{S}_b}(\omega(z,\phi)) - \lambda H(\phi)\right]$
7: end while
```

Algorithm 2 MaxWEnt Inference

```
1: Inputs: Input data $x$, parameterization $\omega$, scaling vector $\phi$, sample size $P$
2: Outputs: Prediction sample $(\hat{y}_1, ..., \hat{y}_P)$
3: for $1 \leq i \leq P$ do
4:     $z \sim \mathcal{Z}$;
5:     $w \leftarrow \omega(z, \phi)$
6:     $\hat{y}_i \leftarrow h_w(x)$
7: end for
```

3.3 Examples of weight parameterization

Obviously, the choice of the weight parameterization ω has an important impact on the resulting weight distribution. In line with the purpose of the MaxWEnt approach, the guidelines for choosing ω should follow these three principles: enable the sampling in regions of accurate hypotheses, foster the increase of the weight entropy and be practical to use. Moreover, one should consider weight parameterizations that provide a tractable formulation of the weight entropy $H(\phi)$.

3.3.1 SCALING PARAMETERIZATION

Following the aformentionned guidelines, we consider the sampling variable $z \sim \mathcal{Z}$ such that $\mathbb{E}[z] = 0, \mathbb{V}[z] = \text{Id}_d$ and propose the "scaling" parameterization defined as follows:

$$\omega(z, \phi) = \overline{w} + \phi \odot z. \tag{4}$$

Where $\odot$ is the element-wise product between two vectors, such that $\phi \odot z = (\phi_1 z_1, ..., \phi_d z_d)$ with $\phi = (\phi_1, ..., \phi_d) \in \mathbb{R}^d$ and $z = (z_1, ..., z_d) \in \mathbb{R}^d$. The weight vector $\overline{w} \in \mathbb{R}^d$ is the weight mean $\mathbb{E}_{q_\phi}[w] = \overline{w}$. It is typically defined as the weights of a pretrained network $h_{\overline{w}}$ fitted on the training data. For $\mathcal{Z}$ defined as a normal $\mathcal{N}(0, \text{Id}_d)$ or uniform distribution $\mathcal{U}([-\sqrt{3}, \sqrt{3}]^d)$, the parameters $\phi = (\phi_1, ..., \phi_d)$ act as scaling factors: the higher ϕ_k, the wider the distribution $w_k \sim \overline{w}_k + \phi_k z_k$.

The scaling parameterization (4) meets the three previous requirements for a relevant choice of stochastic model. The mean of the weight distribution verifies $\mathbb{E}_{q_\phi}[w] = \overline{w}$ with $\overline{w}$ the weights of a pretrained network fitted on $\mathcal{S}$, the weight distribution is then centered in a region of the weight space of low empirical risk. If $\phi \simeq 0$, the resulting weight distribution is equivalent to a peaked distribution around $\overline{w}$, which meets the first objective to provide samples of accurate hypotheses. Moreover, the weight entropy is directly controlled by the parameters ϕ : when ϕ increases, the weight distribution becomes wider and the entropy increases. We show, indeed, in the next section, that the weight entropy $H(\phi)$ can be expressed directly as a function of ϕ. Finally, it can be noticed that the scaling parameterization only involves element-wise multiplications, which makes it practical to compute.

3.3.2 SVD PARAMETERIZATION

We show, through the theoretical analysis developed in Section 4, that the increase of the ϕ parameters is inversely proportional to the neuron activation amplitude. Indeed, if a neuron is weakly activated by the training data, all the weights w_k in front of this neuron have little impact on the network predictions in the training domain. Therefore, the parameters ϕ_k can be enlarged without degrading the average empirical risk $\mathbb{E}_{q_\phi}\left[\mathcal{L}_\mathcal{S}(w)\right]$. In the extreme case, if the neuron is never activated by the training data (it always returns 0), then the parameters ϕ_k can go to infinity without impacting the network outputs on the training domain. Based on this theoretical observation, we argue that the weight entropy can be further increased without impacting the training risk by taking into account the correlation between neurons. Indeed, let's consider, for instance, two neurons of the same hidden layer, totally correlated, both with activation amplitude $a > 0$ on average on the training data. The scales of the weights w_k in front of these neurons will verify $\phi_k \propto 1/a$. However, by expressing the outputs of these neurons in their singular value decomposition basis, the novel representation is now composed of one component of average amplitude a and the other of null amplitude. In that case, some parameters ϕ_k can be further increased without impacting the training risk. Motivated by these arguments, we propose the "SVD" parameterization described in the following subsection.

Let's consider a pretrained neural network $h_{\overline{w}}$ of L hidden layers. We denote $\psi_{(l)}(X) \in \mathbb{R}^{n \times b_l}$ the hidden representation of the input data $X \in \mathbb{R}^{n \times b}$ in the l^{th} layer of $h_{\overline{w}}$, with b_l the hidden layer dimension (i.e., the number of neurons). The singular values decomposition of $\psi_{(l)}(X)$ is written: $\psi_{(l)}(X) = U_{(l)} S_{(l)} V_{(l)}$ with $U_{(l)} \in \mathbb{R}^{n \times n}, S_{(l)} \in \mathbb{R}^{n \times b_l}$ and $V_{(l)} \in \mathbb{R}^{b_l \times b_l}$. We propose the SVD parameterization, which consists in "aligning" the weight distribution with the principal components of $\psi_{(l)}(X)$ such that:

$$w_{(l)} = \overline{w}_{(l)} + V_{(l)}^T(\phi_{(l)} \odot z_{(l)}), \tag{5}$$

for any $l \in [|0, L|]$, where $w_{(l)}, \overline{w}_{(l)}, \phi_{(l)}, z_{(l)} \in \mathbb{R}^{b_l \times b_{l+1}}$ are respectively the matrix of weights, average weights, scaling parameters and sampling variables between the l^{th} layer and the next layer. A compact formulation of the parameterization can be written as follows:

$$\omega(z, \phi) = \overline{w} + V(\phi \odot z). \tag{6}$$

Where V denotes the block matrix: $V = \left[V_{(1)}^T, ..., V_{(1)}^T, V_{(2)}^T, ..., V_{(L)}^T\right]$ of dimension $\sum b_l \times b_{l+1}$.

Similar to the previous one, the SVD parameterization fulfills the guidelines. Indeed, the weight distribution is still centered on $\overline{w}$, which ensures to sample in a weight space region of low empirical risk. Moreover, the weight entropy can be increased by enlarging the ϕ parameters. This can be done more efficiently compared to the previous approach due to the integration of the neurons' correlations (cf. Section 4.1.3). The SVD parameterization requires additional computational time compared to the scaling one, due to the SVD decomposition and the matrix multiplication. It should be noticed that the SVD decomposition for each layer is computed only once. Before the stochastic gradient descent, a forward pass of the training data in $h_{\overline{w}}$ is required to compute each hidden representation $\psi_{(l)}(X)$, then the SVD decomposition of $\psi_{(l)}(X)$ is performed to compute the matrix $V_{(l)}$. However, the matrix multiplications between $V_{(l)}$ and $\phi_{(l)} \odot z_{(l)}$ are performed at each gradient update, which requires an additional computational burden during the gradient descent compared to the scaling parameterization (cf. Section 5.3 for the complexity calculation). Finally, we show in the next section, that a similar expression of the weight entropy $H(\phi)$ can be written in function of ϕ for both parameterizations.

3.3.3 Weight Entropy Formulation Under Scaling and SVD Parameterizations

The following proposition states that the previous weight parameterizations provide a closed-form expression of the weight entropy $H(\phi)$:

Proposition 1 (Closed-form expression of the weight entropy) *Let q_ϕ be a weight distribution described by Equation (4) or (6) with $z \sim \mathcal{Z}$ and $\phi > 0$. If $\mathcal{Z}$ is defined as the normal $\mathcal{N}(0, \text{Id}_d)$ or the uniform distribution $\mathcal{U}([-\sqrt{3}, \sqrt{3}]^d)$, there exists two constants C_1, C_2 such that the weight entropy $H(\phi)$ is expressed as follows:*

$$H(\phi) = C_1 \sum_{k=1}^{d} \log(\phi_k^2) + C_2, \tag{7}$$

with $\phi = (\phi_1, ..., \phi_d) \in \mathbb{R}^d$, the scaling parameters of the weight distribution q_ϕ.

Proof The full proof is reported in Appendix A.1. The proof consists in considering that, for a normal distribution $\mathcal{N}(0, \Sigma)$ or for a uniform distribution defined over a parallelotope described by Σ, the entropy verifies $H(\phi) \propto \log(|\det(\Sigma)|)$. Then, by showing that for both parameterizations $\det(\Sigma) \propto \det(\text{diag}(\phi))$, the above result can be derived. ■

Note that, the C_2 constant can be removed in the objective function of Equation (2) as it does not impact the optimization and the C_1 constant can be integrated in the trade-off parameter λ. This expression of the entropy function is easy to implement. It highlights the direct link between the scale parameter ϕ_k and the weight entropy. When ϕ_k grows, the weight distribution becomes wider and the entropy increases.

4. Theoretical Analysis

In this section, we develop a theoretical framework to understand the MaxWEnt approach in the specific case where the loss function is defined by the mean squared error. We first develop theoretical results in the linear regression case, and further extend these results to deep fully-connected neural networks.

4.1 Linear regression

Linear regression can be seen as a particular case of deep fully-connected neural networks where the networks are composed of exactly two layers: the input layer of b neurons and the output layer of 1 neuron with linear activation function. The linear regression case is not representative of the framework considered in this work, as the hypotheses $h \in \mathcal{H}$ can no longer be considered as universal approximators. However, the following study provides valuable insights on what happen between the neurons of one hidden layer and one neuron of the next layer. In particular, we highlight the link between the scale parameters ϕ and the amplitude of the input features.

4.1.1 NOTATIONS

We consider the linear regression framework, where the learner has access to an input dataset $X \in \mathbb{R}^{n \times b}$ composed of n row data $x_i \in \mathbb{R}^b$ drawn iid according to the distribution $p(x)$ and an output vector $y \in \mathbb{R}^n$ such that $y = (y_1, ..., y_n)$. Each input x_i is associated to the scalar output $y_i \in \mathbb{R}$ drawn according to $p(y|x_i)$. We denote $\mathcal{S} = \{(x_1, y_1), ..., (x_n, y_n)\}$ the set of training observations. We consider the set $\mathcal{H} = \{x \to \sum_{k=1}^{b} x_k w_k;\ w \in \mathbb{R}^b\}$ of linear hypotheses. The loss function is the mean squared error, and we define the empirical risk for any weight $w \in \mathbb{R}^b$ as $\mathcal{L}_{\mathcal{S}}(w) = \frac{1}{n}||Xw - y||_2^2$. We denote by $a = (a_1, ..., a_b) \in \mathbb{R}_+^b$ the *amplitude* of the input features of the training set, such that $a_j^2 = \frac{1}{n}||X_j||_2^2$ for any $j \in [|1, b|]$, with X_j the j^{th} column of X. We assume that $a_j > 0$ for any $j \in [|1, b|]$.

4.1.2 SCALING WEIGHT PARAMETERIZATION

We first consider the weight parameterization defined in Equation (4) such that $q_\phi \sim \overline{w} + \phi \odot z$ with $z \sim \mathcal{Z}$ such that $\mathcal{Z} \sim \mathcal{N}(0, \text{Id}_b)$ or $\mathcal{Z} \sim \mathcal{U}([-\sqrt{3}, \sqrt{3}]^b)$. The weight vector $\overline{w} \in \mathbb{R}^b$ is the weight mean: $\mathbb{E}_{q_\phi}[w] = \overline{w}$. Finally, we consider the entropy penalty $H(\phi)$ defined by $H(\phi) = \sum_{k=1}^{b} \log(\phi_k^2)$. The optimization problem (1) can then be written:

$$\min_{\phi \in \mathbb{R}^b} \mathbb{E}_{\mathcal{Z}} \left[\frac{1}{n} ||X(\overline{w} + \phi \odot z) - y||_2^2 \right] - \lambda \sum_{k=1}^{b} \log(\phi_k^2). \tag{8}$$

We show that the MaxWEnt optimization problem of Equation (8) has a unique solution, which can be expressed with the following closed-form expression:

Proposition 2 (Closed-form solution for the scaling parameterization) *Equation (8) has a unique solution $\phi^* \in \mathbb{R}^b$ verifying for any $k \in [|1, b|]$:*

$$\phi_k^{*2} = \frac{\lambda}{a_k^2}.$$

Proof The proof consists in first developing the average risk as follows:

$$\mathbb{E}_{\mathcal{Z}} \left[\frac{1}{n} ||X(\overline{w} + \phi \odot z) - y||_2^2 \right] = \sum_{k=1}^{b} a_k^2 \phi_k^2 + \frac{1}{n} ||X\overline{w} - y||_2^2.$$

Optimization (8) can then be written:

$$\min_{\phi \in \mathbb{R}^b} \sum_{k=1}^{b} a_k^2 \phi_k^2 - \lambda \sum_{k=1}^{b} \log(\phi_k^2). \tag{9}$$

This is a convex problem, for which the derivative of the objective function with respect to ϕ^2 is null for:

$$a_k^2 - \lambda / \phi_k^2 = 0.$$

A detailed proof is provided in Appendix A.2. ■

This closed-form solution of ϕ^* is particularly insightful: ϕ_k^* is inversely proportional to a_k^2, which means that the optimal scale parameters ϕ_k^* are larger for weights in front of low amplitude features a_k^2. Applied to the hidden layers of a neural network, Proposition (2) states that the weight distribution is wider in front of neurons weakly activated by the training data. As a consequence, if an OOD data activates these neurons, large values are propagated through the network, which produces an important output variance. These statements are formalized in Section 4.2 when considering deep fully connected neural networks.

It can be further noticed that Equation (9) is equivalent to a log determinant optimization problem (Boyd et al., 2006). The maximum entropy optimization can then be interpreted as a maximum ellipsoid volume problem, where the volume $\prod \phi_k^2$ is maximized under the linear constraint $\sum_k a_k^2 \phi_k^2 \leq \lambda b$. If $\mathcal{Z}$ is a uniform distribution, this boils down to maximizing the support of the weight distribution while maintaining the average empirical risk on the training data under an acceptable threshold. This is in line with the purpose of the approach to find the weight distribution that covers as many consistent weights as possible.

4.1.3 SVD WEIGHT PARAMETERIZATION

According to Proposition (2), the optimal scale parameters verify $\phi^{*2} = \lambda / a^2$. When injecting this solution in the entropy formulation, we obtain: $H(\phi) = -\sum \log(a_k^2) + \text{cste}$. Considering this formula, it appears clearly that the weight entropy is particularly important if some a_k^2 are small, i.e., if some input features have a low amplitude. However, in the presence of correlated features, all amplitudes a_k^2 may be high while the input training data may present small variation in some directions of the input space. The SVD parameterization (6) proposes to exploit these directions of small variation by aligning the weight distribution with the singular value components of the input data. For this purpose, we now consider $V \in \mathbb{R}^{b \times b}$, the matrix of eigenvectors of $\frac{1}{n}X^T X$ and $s^2 = (s_1^2, ..., s_b^2) \in \mathbb{R}_+^b$ the vector of eigenvalues, and assume that $s_j > 0$ for any $j \in [|1, b|]$. The SVD weight parameterization is written $w = \overline{w} + V(\phi \odot z)$ with $z \sim \mathcal{Z}$ and the MaxWEnt optimization problem (1) becomes:

$$\min_{\phi \in \mathbb{R}^b} \mathbb{E}_{\mathcal{Z}} \left[\frac{1}{n} ||X(\overline{w} + V(\phi \odot z) - y||_2^2 \right] - \lambda \sum_{k=1}^{b} \log(\phi_k^2). \tag{10}$$

In comparison to the previous optimization problem in Equation (8), there is now the presence of the matrix V between X and $\phi \odot z$. By definition of V, the matrix XV is the expression of X in its singular values basis. Thus, the vector $\phi \odot z$ is now aligned with the singular value components. As for the previous parameterization, the optimal parameter vector ϕ^* admits a closed-form expression as follows:

Proposition 3 (Closed-form solution for the SVD parameterization) *Equation (10) has a unique solution $\phi^* \in \mathbb{R}^b$ verifying for any $k \in [|1, b|]$:*

$$\phi_k^{*2} = \frac{\lambda}{s_k^2}.$$

Proof The proof consists in developing the average risk, such that:

$$\mathbb{E}_{\mathcal{Z}} \left[\frac{1}{n} ||X(\overline{w} + V(\phi \odot z)) - y||_2^2 \right] = \sum_{k=1}^{b} s_k^2 \phi_k^2 + \frac{1}{n} ||X\overline{w} - y||_2^2.$$

Optimization (10) is then written:

$$\min_{\phi \in \mathbb{R}^b} \sum_{k=1}^{b} s_k^2 \phi_k^2 - \lambda \sum_{k=1}^{b} \log(\phi_k^2),$$

which is similar to Equation (9) with s_k^2 instead of a_k^2 (see Appendix A.3 for a detailed proof). ■

Proposition (3) states that the optimal parameters ϕ^* are now inversely proportional to the singular values of the training data instead of the feature amplitudes. We show, with the next Proposition, that this difference implies a larger weight entropy for the same level of average empirical risk.

Proposition 4 (Comparison between scaling and SVD parameterization) *Let $q_{\phi^*}^{(1)}$, $q_{\phi^*}^{(2)}$ be the respective optimal weight distributions for the scaling and the SVD parameterization. The following propositions hold:*

$$\mathbb{E}_{q_{\phi^*}^{(1)}} [\mathcal{L}_{\mathcal{S}}(w)] = \mathbb{E}_{q_{\phi^*}^{(2)}} [\mathcal{L}_{\mathcal{S}}(w)]$$
$$\mathbb{E}_{q_{\phi^*}^{(1)}} \left[-\log(q_{\phi^*}^{(1)}(w)) \right] \leq \mathbb{E}_{q_{\phi^*}^{(2)}} \left[-\log(q_{\phi^*}^{(2)}(w)) \right].$$

Proof The average empirical risk equality can be derived as follows:

$$\mathbb{E}_{q_{\phi^*}^{(1)}} [\mathcal{L}_{\mathcal{S}}(w)] = \lambda \sum_{k=1}^{b} \frac{a_k^2}{a_k^2} + \epsilon = \lambda\, b + \epsilon = \lambda \sum_{k=1}^{b} \frac{s_k^2}{s_k^2} + \epsilon = \mathbb{E}_{q_{\phi^*}^{(2)}} [\mathcal{L}_{\mathcal{S}}(w)],$$

with $\epsilon = \frac{1}{n}||X\overline{w} - y||_2^2$. The weight entropy inequality is derived from Hadamard's inequality. The detailed proof is reported in Appendix A.4. ■

In light of Proposition (4), it appears that the SVD parameterization leads to a more efficient weight distribution according to the maximum entropy principle. Indeed, for the same level of explanation of the observations (same average empirical risk), the SVD parameterization provides more entropy. Experiments conducted on both synthetic and real datasets show that this last weight parameterization provides, indeed, a better evaluation of the epistemic uncertainty (cf. Section 7) which advocates in favor of the use of the entropy as a measure of weight distribution quality.

4.2 Deep fully connected neural network

In this subsection, we extend the previous result to deep fully connected networks under the mean squared error loss. In particular, we formally derive the connection between the neuron activation amplitude and the optimal scaling parameters suggested by Proposition (2).

4.2.1 NOTATIONS

We consider fully-connected neural networks $h_w \in \mathcal{H}$ of L hidden layers with $w \in \mathcal{W}$. For the sake of simplicity, we assume that every hidden layer is composed of b neurons with b the dimension of the input data, the last layer is composed of 1 neuron such that the neural networks produce scalar outputs. For any $x \in \mathcal{X}$ and for any $l \in [|1, L|]$, $\psi_{(l)}(x) \in \mathbb{R}^b$ denotes the hidden representation of the input data x in the l^{th} layer; $\psi_{(0)}(x) \in \mathbb{R}^b$ and $\psi_{(L+1)} \in \mathbb{R}$ are respectively the input and output layer representation, such that $\psi_{(0)}(x) = x$ and $\psi_{(L+1)}(x) = h_w(x)$. Notice that the hidden representations depend on w; the notation $\psi_{(l)}(x)$ is a contraction of $\psi_{(l)}(x, w)$ or ${\psi_{(l)}}_w(x)$. The set of network weights verifies $\mathcal{W} \subset \mathbb{R}^d$, with $d = Lb^2 + b$ the number of weights in the network (bias parameters are not considered here). For any weights $w \in \mathcal{W}$, $w_{(l,j)} \in \mathbb{R}^b$ denotes the weights between the layer l and the j^{th} components of the layer $l + 1$ for $l \in [|0, L|]$ and $j \in [|1, b_l|]$, with $b_l = 1$ if $l = L$ and $b_l = b$ otherwise. We consider the activation function $\zeta : \mathbb{R} \to \mathbb{R}$ such that, for any $x \in \mathcal{X}$, any $l \in [|0, L - 1|]$ and any $j \in [|1, b|]$, $\psi_{(l+1,j)}(x) = \zeta\left(\psi_{(l)}(x)^T w_{(l,j)}\right)$ with $\psi_{(l+1,j)}(x)$ the j^{th} component of the hidden representation $\psi_{(l+1)}(x)$. The weight distributions are denoted q_ϕ with $\phi \in \mathbb{R}^d$. The loss function ℓ is the mean squared error and the problem to be solved is written:

$$\min_{\phi \in \mathbb{R}^d} \mathbb{E}_{q_\phi}\left[\mathcal{L}_\mathcal{S}(w)\right] - \lambda \sum_{k=1}^{d} \log(\phi_k^2). \tag{11}$$

We assume that Problem (11) has a unique solution, denoted $\phi^* \in \mathbb{R}^d$.

4.2.2 SCALING WEIGHT PARAMETERIZATION

We focus our deep neural networks analysis on the scaling parameterization (4) such that $q_\phi \sim \overline{w} + \phi \odot z$ with $z \sim \mathcal{Z}$ where $\mathcal{Z} \sim \mathcal{N}(0, \text{Id}_d)$ or $\mathcal{Z} \sim \mathcal{U}([-\sqrt{3}, \sqrt{3}]^d)$ and $\overline{w}$ the weight of a pretrained network $h_{\overline{w}}$. In the following, we aim at extending the results of Proposition (2) to the hidden layers of deep neural networks and show that the MaxWEnt optimization leads to scaling parameters inversely proportional to the neuron activation amplitude. For this purpose, we consider the following assumption on the activation function ζ. Assumption (5) states that the order of the first and second moment of the neuron activation are preserved by ζ. This assumption is verified, for instance, for most of the common activation functions, as ReLU or Leaky-ReLU, if the neuron activation follows a centered independent Gaussian distribution.

Assumption 5 (Moments preserving property of the activation function) *For any $\phi_1, \phi_2 \in \Phi$, $l \in [|0, L-1|]$ and any $j \in [|1, b|]$, the activation function ζ verifies:*

$$\sum_{i=1}^{n} \mathbb{E}_{q_{\phi_1}}\left[U_{ij}\right] \leq \sum_{i=1}^{n} \mathbb{E}_{q_{\phi_2}}\left[U_{ij}\right] \implies \sum_{i=1}^{n} \mathbb{E}_{q_{\phi_1}}\left[\zeta\left(U_{ij}\right)\right] \leq \sum_{i=1}^{n} \mathbb{E}_{q_{\phi_2}}\left[\zeta\left(U_{ij}\right)\right]$$

$$\sum_{i=1}^{n} \mathbb{E}_{q_{\phi_1}}\left[U_i U_i^T\right] \preccurlyeq \sum_{i=1}^{n} \mathbb{E}_{q_{\phi_2}}\left[U_i U_i^T\right] \implies \sum_{i=1}^{n} \mathbb{E}_{q_{\phi_1}}\left[\zeta\left(U_i\right)\zeta\left(U_i\right)^T\right] \preccurlyeq \sum_{i=1}^{n} \mathbb{E}_{q_{\phi_2}}\left[\zeta\left(U_i\right)\zeta\left(U_i\right)^T\right]$$

Where $U_i = (U_{i1}, ..., U_{ib})$ and $U_{ij} = \psi_{(l)}(x_i)^T w_{(l,j)}$ $\forall i \in [|1, n|]$, $\forall j \in [|1, b|]$. For two matrices A, B, the notation $A \preccurlyeq B$ states that $B - A$ is a positive semi-definite matrix.

Proposition 6 (Optimal scaling parameters) *Let $\phi^* \in \mathbb{R}^d$ be the unique solution of Problem (11), then ϕ^* verifies:*

$$\begin{aligned} \phi^* &= \bigotimes_{l=0}^{L} \bigotimes_{j=1}^{b_l} \left(\phi^*_{(l,j,1)}, ..., \phi^*_{(l,j,b)}\right) \\ {\phi^*_{(l,j,k)}}^2 &= \frac{\sigma^2_{(l,j)}}{b\, a^2_{(l,k)}} \quad \forall\, l \in [|1, L|];\ j \in [|1, b_l|];\ k \in [|1, b|]. \end{aligned} \tag{12}$$

Where $\bigotimes$ is the concatenation operator and for any $l \in [|0, L|]$, $j \in [|1, b_l|]$ and $k \in [|1, b|]$:

$$a^2_{(l,k)} = \frac{1}{n} \sum_{i=1}^{n} \mathbb{E}_{q_{\phi^*}}\left[\psi_{(l,k)}(x_i)^2\right]$$

$$\sigma^2_{(l,j)} = \frac{1}{n} \sum_{i=1}^{n} \mathbb{V}_{q_{\phi^*}}\left[\psi_{(l)}(x_i)^T \left(w_{(l,j)} - \overline{w}_{(l,j)}\right)\right].$$

Proof The full proof is reported in Appendix A.5. The main idea of the proof consists in first dividing Problem (11) by layer and output neurons. The parameters $\phi_{(l,j,k)}$ defined in Equation (12) provide the solution for each sub-problem. Then, considering Assumption (5) on the activation function and the uniqueness of the solution, it can be shown that $\phi = \phi^*$. ■

Proposition (6) states that the solution ϕ^* of the MaxWEnt optimization (11) is the inverse of the average neuron activation amplitude over the training data. We emphasize that the aim of Proposition (6) is not to provide an exact solution (as the quantities $a^2_{(l,k)}$ and $\sigma^2_{(l,j)}$ are intractable) but to offer a theoretical understanding of MaxWEnt in the case of deep fully connected neural networks. Numerical observations described in Section 7.1.4 confirm this "inverse proportionality" relationship between the scaling parameters and the neuron activation amplitude. This means that maximizing the weight entropy leads to put more emphasis on the activation of neurons that are weakly activated by the training data. Thus, it can be considered that these neurons act as "detectors" for the out-of-distribution data that activate them.

5. Discussion

5.1 Overfitting, weight diversity and evaluation

In Section 2.3, we identify the main limitation of standard ensemble and Bayesian approaches as their inability to produce a representative sample of the whole consistent hypothesis set. We argue that this limitation is related to the use of weight decay regularization and hyper-parameters selection driven by hold-out validation. Indeed, the use of weight decay for deep neural networks is first designed as a tool to avoid overfitting (Krogh and Hertz, 1991), with the underlying idea that large weights induce the over-specification of the network on the observations. This technique has proven to improve the model accuracy in most cases. However, when applied in ensemble and Bayesian learning, it induces the counter effect of penalizing the diversity of the resulting sample of neural networks. On the contrary, our approach aims at jointly regularizing the sample of neural networks by increasing the entropy of their underlying weight distribution. Additionally, the use of a broad weight distribution avoids overfitting thanks to the marginalization process (Wilson, 2020).

Regarding the use of hold-out validation for hyper-parameters selection, we claim that such a technique fosters narrowed weight distributions. As q_ϕ cannot model complex distribution, the covering of a large portion of consistent hypotheses generally comes with the inclusion of inconsistent weights in the support of the weight distribution. As a consequence, the in-distribution performance for distributions of high entropy is usually degraded (confirmed numerically in our experiments). Moreover, for a large number of training data, the in-distribution epistemic uncertainty becomes negligible in front of the aleatoric uncertainty. Its accurate estimation is then not required to obtain good validation NLL. However, for out-of-distribution data, the main source of uncertainty is epistemic, and its estimation is critical. Then, narrowed weights distributions, although improving the validation NLL, fail to produce relevant uncertainty quantification out-of-distribution (Ovadia et al., 2019; Liu et al., 2021; Henning et al., 2021).

It should be underlined that, although MaxWEnt tends to enlarge the weight distribution, it cannot fully guarantee to capture the whole set of consistent hypotheses due to the technical limitation of the stochastic model q_ϕ. However, the MaxWEnt approach is an important step in this direction. It already provides significant improvements compared to the baselines, as demonstrated by our numerical experiments.

5.2 Bayesian neural networks

In the Bayesian variational inference framework, the learner aims at approximating the posterior distribution $p(w|\mathcal{S})$ with a parameterized distribution q_ϕ defined over $\mathcal{W}$. The minimization of the Kullback-Leibler (KL) divergence between $p(w|\mathcal{S})$ and q_ϕ leads to the maximization of the *evidence lower bound* (ELBO) expressed as follows (Wenzel et al., 2020a):

$$\max_{\phi \in \mathbb{R}^D} \mathbb{E}_{q_\phi} \left[\sum_{(x,y) \in \mathcal{S}} \log(p(y|h_w(x)) \right] - D_{\text{KL}} \left(q_\phi(w), p(w) \right). \tag{13}$$

Where $p(y|h_w(x))$ is the log likelihood of y with respect to $h_w(x)$, D_{KL} is the Kullback-Leibler divergence and $p(w)$ is the prior distribution defined over $\mathcal{W}$.

If we consider a uniform prior over the whole weight space: $p(w) \sim \mathcal{U}(\mathcal{W})$ (assuming $\mathcal{W}$ bounded), the second term of the ELBO maximization: $D_{\text{KL}} \left(q_\phi(w), p(w) \right)$, is equal to the negative entropy of q_ϕ (up to a constant). Therefore, if the empirical risk $\mathcal{L}_\mathcal{S}(w)$ can be written as a quantity proportional to the negative log-likelihood, the ELBO maximization (13) is equivalent to the MaxWEnt optimization problem (1). This is in line with the application of the maximum entropy principle to the Bayesian framework (Jaynes, 1968), which states that the prior should be selected as the distribution of maximal entropy that integrates prior information. In our case, without any regularity assumption about the optimal hypothesis, the maximum entropy principle then leads to consider a uniform prior over the whole weight space $\mathcal{W}$ (bounded), i.e., $p(w) \sim \mathcal{U}(\mathcal{W})$.

The use of "uninformative" parameter priors is considered as the guideline to model epistemic uncertainty in the Bayesian framework (Wilson, 2020). In practice, however, the most commonly used priors for Bayesian neural networks are Dropout (Gal and Ghahramani, 2016; Kendall and Gal, 2017; Boluki et al., 2020) which has been shown to produce over-confident predictions for out-of-distribution data (Liu et al., 2021) and the isotropic Gaussian prior $p(w) \sim \mathcal{N}(0, \sigma_0^2 \operatorname{Id}_d)$ (Zhang et al., 2018; Osawa et al., 2019; Jospin et al., 2022), which is recently considered to be often "non-optimal" or "unintentionally informative" (Wenzel et al., 2020a; Fortuin et al., 2021).

When considering a Gaussian isotropic prior $p(w) \sim \mathcal{N}(0, \sigma_0^2 \operatorname{Id}_d)$ with $\sigma_0 \in \mathbb{R}$ and an independent multivariate Gaussian stochastic model $q_\phi \sim \mathcal{N}(\mu, \operatorname{diag}(\sigma^2))$ with $\mu, \sigma \in \mathbb{R}^d$ the mean and scale parameters such that $\phi = (\mu, \sigma)$, the following expression can be derived for the KL divergence between the approximate posterior and the prior (Duchi, 2007):

$$D_{\text{KL}}\left(q_\phi(w), p(w)\right) = \frac{||\mu||_2^2}{2\sigma_0^2} + \frac{1}{2}\sum_{k=1}^{d}\left(\frac{\sigma_k^2}{\sigma_0^2} - \log\left(\frac{\sigma_k^2}{\sigma_0^2}\right)\right) - \frac{d}{2}.$$

From this expression, it appears that the KL divergence operates a "double" regularization regime on the scale parameters σ. When σ_k^2 is below σ_0^2, the term $-\log(\sigma_k^2/\sigma_0^2)$ dominates σ_k^2/σ_0^2, which induces the increase of the σ_k^2 parameter similar to the MaxWEnt penalization. Whereas, for σ_k^2 above σ_0^2, the dominant term becomes σ_k^2/σ_0^2 which stops the increase of the scaling parameter. Then, for $\sigma_0 \to +\infty$, the regularization over σ^2 induced by the KL divergence converges to the maximum entropy penalization. However, as a side effect, the term $||\mu||_2^2/2\sigma_0^2$ is reduced to zero and no regularization on the mean is operated, which is generally avoided. In many previous works which consider isotropic Gaussian priors, the commonly considered prior bandwidth σ_0^2 are relatively small (Zhang et al., 2018; Osawa et al., 2019; Ashukha et al., 2019), or at least, not designed in a maximum entropy perspective. Moreover, a trade-off parameter $\lambda < 1$ is often added between the log likelihood and the KL divergence in optimization (13) (Wenzel et al., 2020a) which further tempers the KL divergence regularization. Our interpretation is that the hyper-parameter selection is often driven by the in-distribution performances (computed on a validation set for instance) which fosters narrowed posterior distributions. Indeed, extending the weight distribution to any consistent weight, generally penalizes the test performances as observed in our experiments (cf. Sections 7.1.3 and 7.2.2). However, we argue that such penalization could be accepted when considering OOD detection. Further insights on the key components that enable a Bayesian Neural Network (BNN) with a Gaussian prior to exhibit behaviors similar to those of MaxWEnt and MaxWEnt-SVD are provided in Appendix C.

5.3 SVD-parameterization

The SVD-parameterization has been introduced in Section 3.3.2 (cf. Equation 6) with the aim of allowing a larger increase of the weight entropy while limiting the average empirical risk penalty. We argue, indeed, that using independent weight components in the stochastic model sets the directions of weight distribution expansion to the canonical basis of $\mathbb{R}^d$, which seems intuitively sub-optimal. We could include correlations between weight components as additional parameters to optimize in ϕ. However, this solution would require the optimization of $\mathcal{O}(d^2)$ parameters which may become intractable, especially for large neural networks such as ResNet (He et al., 2016), for instance, for which $d > 10^6$. Through the SVD-parameterization, we propose to set the correlation between weight components, at each hidden layer, according to the singular value decomposition of the neuron activation on the training data. Our theoretical analysis in Section 4.1.3 shows, in the case of linear regression, that this weight parameterization provides the same level of average empirical risk as independent weight components but with larger weight entropy.

Previous works consider the use of weight correlations in stochastic model in the form of matrix Gaussian distribution (Louizos and Welling, 2016; Sun et al., 2017) or through more sophisticated models such as weight distributions defined over "well-chosen" subspace of $\mathbb{R}^d$ (Izmailov et al., 2020), as well as normalizing flows (Louizos and Welling, 2017) and implicit weight models (Pawlowski et al., 2017). A notable use of correlation between weights is the Laplace approximations (MacKay, 1992; Foong et al., 2019; Ritter et al., 2018), where the correlation matrix for a Gaussian model is given by a "closed-form" solution which can be computed using one forward and backward step through the network. Similarities can be observed between the Kronecker Laplace approximation (Ritter et al., 2018) and the SVD-parameterization, as both method involve the correlation matrix of the neuron activation, but identifying the link between both methods would require further investigation. In our case, the parameters ϕ are still optimized through stochastic variational gradient descent, whereas the Laplace approximation does not require multiple gradient updates. As we manage to find a closed-form expression for ϕ^* in the linear case (cf. Propositions 2 and 3), interesting future work directions include "Laplace-like" approximation in the MaxWEnt framework, which can potentially speed up the computation of the parameters ϕ^*.

Regarding the complexity of the SVD parameterization, we can consider the case of a fully connected neural network with L layers of b neurons each. Computing the SVD decomposition matrix V (cf. Section 3.3.2) requires one forward pass of the training inputs and the computation of the SVD decomposition at each layer with complexity $\mathcal{O}(Lb^3)$ (Pan and Chen, 1999). Storing the matrices adds $\mathcal{O}(Lb^2)$ of memory burden, which is equivalent to $\mathcal{O}(d)$ with $d \in \mathbb{N}$ the dimension of the network weight vector. During the variational gradient descent, the matrix multiplication between the matrix V and the vector $\phi \odot z$ has a complexity of order $\mathcal{O}(Lb^3)$. For comparison, a forward pass with a batch of size B, for the scaling parameterization, is of complexity $\mathcal{O}(LBb^2)$. If we consider that $b \simeq B$ with B the batch size, we can say that the SVD parameterization requires twice as much computational time as the scaling one, which corresponds approximately to what we observed in our experiments.

5.4 Entropy function

In the case of scaling (Equation 4) or SVD parameterization (Equation 6), we manage to provide an expression of the entropy $H(\phi)$ function of ϕ (cf. Equation 7), which is a convenient property to speed up the MaxWEnt optimization. For other weight parameterizations, one may not be able to derive such a closed-form expression. If the probability density function $q_\phi(w)$ can be computed, one can estimate the entropy through sampling, as done for the empirical risk. An alternative solution is to use a proxy of the entropy which is directly linked to the parameters ϕ. If the entropy is a growing function of ϕ_k for any $k \in [|1, d|]$, we propose to consider the following general expression for the penalization term related to the entropy:

$$H(\phi) = \sum_{k=1}^{d} g_k(\phi_k^2), \tag{14}$$

with $g_k : \mathbb{R}_+ \to \mathbb{R}$ predefined growing functions such that ϕ_k^2 grows with $H(\phi)$. Typical choices are $g_k(u) = \log(u)$ or $g_k(u) = \sqrt{u}$. In the case, $g_k(u) = \log(u)$, Equation (14) matches the entropy expression derived in Proposition (1) within a constant factor. Equation (14) can be seen as a "proxy" of the weight "entropy" as it increases with ϕ_k as the entropy.

We observe in our numerical experiments that alternative functions g_k lead to improved results compared to the logarithm. Our interpretation is that the logarithm function over-penalizes small components ϕ_k. Then, at initialization, the gradient norm of the objective function is large (as ϕ_k are initialized close to 0) and the first gradient steps push the ϕ_k too far. We then advocate for the use of proxy functions, as $g_k(u) = \sqrt{u}$, to improve the optimization stability in practice.

5.5 Assessing epistemic uncertainty quantification methods

Our work focuses on better quantifying epistemic uncertainty using Bayesian and ensemble approaches, as we identify the underestimation of epistemic uncertainty as the key reason why standard methods tend to provide overconfident predictions on OOD data.

As discussed in Section 2.2, epistemic uncertainty is characterized by the set of consistent hypotheses. We argue that an optimal estimation of epistemic uncertainty should account for the entire set of these consistent hypotheses. This makes evaluating uncertainty quantification methods inherently challenging, as it requires knowledge of the full set of consistent hypotheses, which is the very goal these methods aim to uncover. Additionally, commonly used metrics for evaluating uncertainty—such as negative log-likelihood (NLL), coverage, expected calibration error (ECE)—do not adequately assess epistemic uncertainty. These metrics rely on the ground truth label and evaluate the probability assigned to it or whether it is covered by a predictive interval. However, epistemic uncertainty is more accurately evaluated by determining if all potential labels, given the observation set $\mathcal{S}$, are identified, rather than checking if the correct label is included in the confidence intervals.

Therefore, a commonly used "proxy" to evaluate the epistemic uncertainty quantification methods is OOD detection scores, with the underlying assumption that epistemic uncertainty should be larger for OOD data than ID data. This boils down to compute uncertainty scores for test data coming from the same distribution as the training data and an OOD dataset from a different distribution. If epistemic uncertainty is well estimated, the uncertainty scores should be larger for OOD data than test data. AUROC and FPR95 metrics can be used on the uncertainty scores to evaluate the OOD detection ability of the methods (Yang et al., 2022).

A good illustration of the difficulty to evaluate epistemic uncertainty quantification methods with metrics such as NLL or coverage is provided in Figure 7 presenting the results of uncertainty quantifiaction for a counting vehicle task. We can see that, after 17:30, because of water drops landing on the camera, many cars are hidden and are difficult to count. The human annotator has only counted visible cars, resulting in an under-estimation of the true number of vehicles present at this time. We can see that Deep Ensemble is rather confident in the number of vehicles and almost matches the number given by the human annotator. On the contrary, MaxWEnt detects the domain shift and triggers large prediction variances. If we evaluate the NLL or the coverage, Deep Ensemble will likely provide better scores than MaxWEnt. However, in this case, MaxWEnt is closer to the "true" epistemic uncertainty, as it is not possible to accurately count the actual number of vehicles.

6. Related Work

The main related works in distance-based and ensemble-based uncertainty quantification are presented in Section 1. The vast uncertainty estimation literature also includes notable methods as conformal prediction (Vovk et al., 2005; Lei et al., 2018; Angelopoulos et al., 2020), calibration (Guo et al., 2017b; Kuleshov et al., 2018) and evidential learning (Sensoy et al., 2018; Amini et al., 2020). Our focus in this present work is on the Bayesian and ensemble approaches, for which we propose a specific improvement through the MaxWEnt algorithm. Readers interested in the alternative approaches will find further details in the following surveys (Abdar et al., 2021; Shen et al., 2021).

6.1 Deep ensembles and prediction diversity out-of-distribution

The main challenge, faced by Bayesian and ensemble methods, is the lack of explicit correlation between the prediction diversity and the distance to the training domain, leading to the observation that standard methods in this category often produce over-confident predictions for OOD data (Henning et al., 2021; Ovadia et al., 2019; Liu et al., 2021).

As described in Section 1, two main approaches are considered to increase the prediction diversity of deep ensemble, especially out-of-distribution: the first approach works on the diversity of the network outputs, gradients or hidden representations (Liu and Yao, 1999; Shui et al., 2018; Zhang et al., 2020; Ross et al., 2020; Ramé and Cord, 2021; Sinha et al., 2021). In this category, contrastive approaches make use of auxiliary real or synthetic OOD data (Pagliardini et al., 2022; Tifrea et al., 2022; Kristiadi et al., 2022; Jain et al., 2020; Mehrtens et al., 2022; Yu and Aizawa, 2019; Wang et al., 2022b). The second approach works on the hypothesis diversity through random initialization and different architectures (Lakshminarayanan et al., 2017; Wen et al., 2020; Wenzel et al., 2020b; Zaidi et al., 2021) or by imposing the weight diversity (Pearce et al., 2018; Tagasovska and Lopez-Paz, 2019; D'Angelo and Fortuin, 2021; de Mathelin et al., 2023).

These last methods particularly relate to MaxWEnt. In particular, the DARE algorithm (de Mathelin et al., 2023) produces a deep ensemble at the edge of the consistent hypothesis set by enlarging the network weights while maintaining the loss under an acceptable threshold. However, the DARE approach is limited to the use of the mean squared error loss function with linear end activation. Moreover, the DARE training requires the control of the penalization term to avoid numerical issues when the weights become too large. With the MaxWEnt approach, the training is more stable, as the weight distribution is centered on the weights $\overline{w}$ of a pretrained network. It also works with softmax activation because of the symmetric expansion of the weight distribution.

6.2 Bayesian neural network priors and stochastic models

Since the seminal work of Jaynes on Bayesian priors (Jaynes, 1968), an ongoing discussion has been opened about the use of the maximum entropy method for assigning priors in Bayesian modeling. This method, considered "thought-provoking" (MacKay, 2003), is generally not recommended (Gelman, 2020). With the proposed MaxWEnt approach, we do not plan to further extend this discussion. We do not argue that the maximum entropy method is the "optimal" way to select a prior, as such a statement depends on the considered notion of optimality. Actually, we advocate for the use of MaxWEnt for OOD detection but do not recommend this method to improve the test accuracy. Enlarging the weight entropy may, indeed, induce a loss of test accuracy due to the large weight variance. However, we show in our experiments that one can always use a "shrunk" version of the weight distribution learned by MaxWEnt when looking for accurate inference while sampling over the whole distribution for OOD detection (cf. Section 7.2.2).

The question of the prior choice has been extensively discussed in the Bayesian literature, a recent review provides the main considered approaches (Fortuin et al., 2021). For Bayesian neural networks, two main groups of priors can be distinguished: weight-space priors and function-space priors. The latter includes priors defined in function space, i.e., over $\mathcal{H}$. Many recent works consider this approach (Sun et al., 2018; Louizos et al., 2019; Tran et al., 2022; Fortuin, 2022; Rudner et al., 2023), which mainly use Gaussian process priors. These methods can be related to the distance-based uncertainty approach, as they make explicit the link between uncertainty and distance to training data through Gaussian processes. The former group corresponds to priors defined over the weights of the neural network, i.e., over $\mathcal{W}$. Our work relates particularly to this approach, as discussed in Section 5.2. The main considered priors in this category are Dropout (Gal and Ghahramani, 2016; Gal et al., 2017; Boluki et al., 2020; Nguyen et al., 2022), isotropic Gaussians (Zhang et al., 2018; Osawa et al., 2019; Jospin et al., 2022), mixture of Gaussians (Blundell et al., 2015), hierarchical (Wu et al., 2018) and horseshoe priors (Ghosh et al., 2019). Some methods also propose to define the prior based on empirical observation of the weight distribution of non-Bayesian networks (Atanov et al., 2018; Fortuin et al., 2021).

Regarding the stochastic model of the weight distribution, previous works have considered the use of diagonal Gaussian (Graves, 2011) and matrix Gaussian to include the weight correlations (Louizos and Welling, 2016; Sun et al., 2017). In the case of multivariate Gaussian model with fixed mean, approximation methods can be used to derive the posterior distribution without using gradient descent as Laplace approximations (MacKay, 1992; Foong et al., 2019; Ritter et al., 2018; Kristiadi et al., 2020) and tractable approximate Gaussian inference (TAGI) (Goulet et al., 2021). More sophisticated stochastic models have been developed with techniques as normalizing flows (Rezende and Mohamed, 2015; Louizos and Welling, 2017), implicit distribution (Pawlowski et al., 2017) or distribution defined over subspaces of $\mathcal{W}$ (Izmailov et al., 2020).

7. Experiments

We conduct several experiments on both synthetic and real datasets. We primarily focus on OOD detection performances to compare the methods. The implementation details for the MaxWEnt algorithm are presented in Section 7.5. The source code of the experiments is available on GitHub.[1]

7.1 Synthetic experiments

In this section, we provide a qualitative analysis of the MaxWEnt algorithm on low dimensional synthetic datasets. Specifically, we compare the uncertainty estimation produced by MaxWEnt and standard ensemble and Bayesian methods.

1. `https://github.com/antoinedemathelin/maxwent-expe`

7.1.1 SETUP

We consider both classification and regression experiments, performed respectively on the two following datasets:

- **Two Moons Classification**: We consider the *two-moons* classification dataset from scikit-learn[2] which simulates a two-dimensional binary classification task with moons like distributed classes. The training set is composed of 200 data points generated from the *two-moons* generator; 50 additional instances are generated to form a validation dataset. The noise level of the generator is set to 0.1.

- **1D Regression** : We reproduce the synthetic univariate regression experiment from Jain et al. (2020) with 100 training and 20 validation instances. The input instances are drawn in $\mathcal{X} \subset \mathbb{R}$ according to the mixture of two Gaussians centered respectively in -0.5 and 0.75 with standard deviation 0.1. The outputs $y \in \mathcal{Y} \subset \mathbb{R}$ are drawn according to the conditional distribution: $p(y|x) \sim f^*(x) + \epsilon$ with $\epsilon \sim \mathcal{N}(0, 0.02)$ the noise variable and $f^*(x)$ the "ground truth" defined as:

$$f^*(x) = 0.3\,(x + \sin(2\pi x) + \sin(4\pi x))\,.$$

In both experiments, the base estimator is a fully-connected neural network with three layers of 100 neurons, each with ReLU activations. For classification, the end layer is composed of one layer with sigmoid activation to produce probabilistic outputs. The end layer for regression is made of two neurons which respectively encode for the conditional mean $\mu_w(x)$ and conditional standard deviation $\sigma_w(x)$ of the univariate Gaussian $\mathcal{N}(\mu_w(x), \sigma_w(x))$ as suggested in Nix and Weigend (1994) to produce probabilistic outputs in the regression setting. We consider the five following uncertainty quantification methods:

- **Vanilla Network**, the baseline, which produces uncertainty estimation based on the network probabilistic outputs $h_w(x) \in [0, 1]$ for classification and $\sigma_w(x) \in \mathbb{R}_+$ for regression. Notice that an ensemble of Vanilla Networks corresponds to the **Deep Ensemble** method.

- **MC-Dropout** (Gal and Ghahramani, 2016), with dropout rate selected through hold-out validation NLL, computed using the validation data, among $[0.05, 0.1, 0.2, 0.3, 0.5]$;

- standard **BNN** (Bayesian Neural Network) (MacKay, 1992; Graves, 2011), trained with stochastic variational inference and reparameterization trick (Hoffman et al., 2013; Kingma and Ba, 2015), we use an independent multivariate Gaussian stochastic model $q_{(\mu,\sigma)} \sim \mathcal{N}(\mu, \text{diag}(\sigma^2))$ and a Normal prior $p(w) \sim \mathcal{N}(0, \text{Id})$. Following common practices for variational Bayes approach to BNNs, we consider a trade-off parameter λ between the NLL and the KL divergence (Wenzel et al., 2020a). The trade-off parameter is selected in $\{10^k\}_{k \in [|-3,3|]}$ through hold-out validation NLL.

- **MaxWEnt**, with an independent multivariate uniform stochastic model centered on the resulting weights of the Vanilla Network.

2. `https://scikit-learn.org/stable/modules/generated/sklearn.datasets.make_moons.html`

- **MaxWEnt-SVD**, which uses the "SVD" parameterization of Equation (6) in addition to the previous MaxWEnt settings.

We use the Adam optimizer (Kingma and Ba, 2015) with learning rate 0.001 and batch size 32. 10k iterations are used to train the Vanilla Network and 20k iterations for other methods, as the stochastic variational inference requires more iterations to converge. For both tasks, the loss function is the Negative Log Likelihood (NLL). It can be written for the respective classification and regression settings as follows:

$$\mathcal{L}_{\mathcal{S}}(w) = -\frac{1}{n} \sum_{(x,y)\in\mathcal{S}} y \log(h_w(x)) + (1-y)\log(1-h_w(x)) \quad \text{(Classification)} \tag{15}$$

$$\mathcal{L}_{\mathcal{S}}(w) = \frac{1}{n} \sum_{(x,y)\in\mathcal{S}} \frac{1}{2} \left(\log(\sigma_w(x)^2) + \frac{(y-\mu_w(x))^2}{\sigma_w(x)^2} \right) \quad \text{(Regression),} \tag{16}$$

with $h_w \in \mathcal{H}$ the neural network of weights $w \in \mathcal{W}$ such that, for any $x \in \mathcal{X}$, $h_w(x) = (\mu_w(x), \sigma_w(x))$ for the regression setting (cf. Lakshminarayanan et al. 2017).

To compute uncertainty estimates, we use the entropy metric for classification and the standard deviation of the "Gaussian mixture approximation" introduced in (Lakshminarayanan et al., 2017) for regression. All uncertainty quantification methods except the Vanilla Network produce stochastic outputs, i.e., for any $x \in \mathcal{X}$, $h_w(x)$ is a random variable as w follows a stochastic model. To produce uncertainty estimates at inference, we then compute $P = 50$ predictions $\{h_{w_i}(x)\}_{i\in[|1,P|]}$ with w_i drawn iid according to the learned weight distribution. Then, the uncertainty estimation for each setting becomes, for any $x \in \mathcal{X}$:

$$u(x) = -\overline{h}_w(x)\log\big(\overline{h}_w(x)\big) - \big(1-\overline{h}_w(x)\big)\log\big(1-\overline{h}_w(x)\big) \quad \text{(Classification)} \tag{17}$$

$$u(x) = \frac{1}{P}\sum_{i=1}^{P} \left(\sigma_{w_i}(x)^2 + \mu_{w_i}(x)^2\right) - \overline{\mu}_w(x)^2 \quad \text{(Regression),} \tag{18}$$

with $\overline{h}_w(x), \overline{\mu}_w(x)$, the average of the respective sets $\{h_{w_i}(x)\}_i$ and $\{\mu_{w_i}(x)\}_i$. It should be underlined that the uncertainty metric for classification in Equation (17) is the entropy metric applied to the average predicted output over the P stochastic inferences, while the uncertainty metric for regression in Equation (18) is the variance formula for the Gaussian mixture composed of P Gaussians of mean $\mu_{w_i}(x)$ and variance $\sigma_{w_i}(x)^2$ (Lakshminarayanan et al., 2017). Notice also that, for the Vanilla Network, the estimated uncertainty is independent of P as the method produces the deterministic outputs $h_w(x)$. In the regression case, the Vanilla Network uncertainty is $u(x) = \sigma_w(x)^2$.

To complete the experiments, we also consider ensembles of the previously mentioned uncertainty quantification methods. We build ensembles of $N = 5$ networks trained independently with different random weight initializations. In this case, the uncertainty metrics are computed in the same way as in the single-network setting through Equation (17) and (18) with P predictions for each network in the ensemble, i.e., with a total of $NP = 250$ predictions.

7.1.2 RESULTS

The regression experiment results are reported in Figure 2. Predicted uncertainties for each method are presented in the form of confidence intervals in light blue. We observe that the Deep Ensemble, MC-Dropout and BNN methods provide larger uncertainty estimates out-of-distribution than in-distribution, which offers an efficient way to detect OODs in this case. However, the three methods fail to capture the full epistemic uncertainty, as a significant part of the ground-truth lies outside the confidence intervals. In contrast, MaxWEnt provides relevant confidence intervals outside the training support when extrapolating on the right and left sides of the domain. Although the predicted uncertainties between the two separated parts of the training domain are still under-estimated. This behavior is corrected by MaxWEnt-SVD which fully manages to produce tight confidence intervals in-distribution and uncertainties as large as possible out-of-distribution.

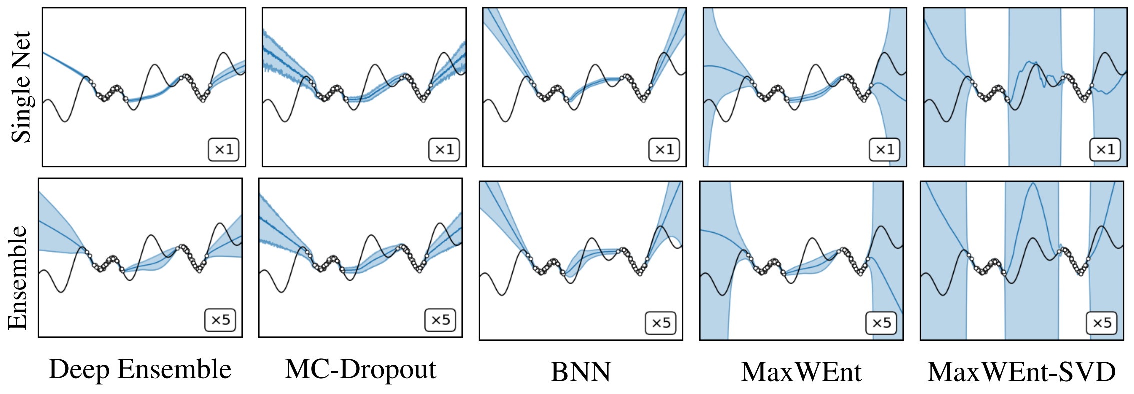

Figure 2: 1D-Regression Uncertainty Estimation. The horizontal and vertical axes correspond respectively to the 1D input space $\mathcal{X}$ and the 1D output space $\mathcal{Y}$. The black line represents the ground truth $f^*(x)$ and the blue line the average predictions $\overline{\mu}_w(x)$. Training instances are reported as white dots. Uncertainty estimations are reported in the form of confidence intervals centered around the average prediction (in light blue). The length of the intervals is equal to $4\sqrt{u(x)}$ with $u(x)$ defined according to Equation (18).

The results of the classification experiment are reported in Figure 3. As for the regression experiment, we observe that Deep Ensemble, MC-Dropout and BNN fail to provide relevant uncertainty estimations whereas MaxWEnt and MaxWEnt-SVD are close to the expected behavior of an ideal uncertainty quantifier. Moreover, in this experiment, the first three methods do not offer proper discrimination between out-of-distribution and in-distribution data. The produced uncertainties are concentrated in the margin between classes and do not increase in the OOD areas behind the training instances. We observe that MaxWEnt and MaxWEnt-SVD manage to increase the uncertainty outside the margin between classes.

7.1.3 DISCUSSION

Both experiments on synthetic data strongly highlight the benefit of using MaxWEnt for uncertainty quantification over standard Bayesian and ensemble methods. As discussed in Section 5.2, the MaxWEnt implementation is related to BNN algorithms, however, the predicted uncertainties of MaxWEnt and BNN are very different (cf. Figures 2 and 3). These observed discrepancies between the two methods can be explained by their different paradigms. In standard BNN optimization, the main objective is to produce relevant uncertainty estimation inside the training domain. In this perspective, the prior distribution and the trade-off parameters are selected in order to minimize

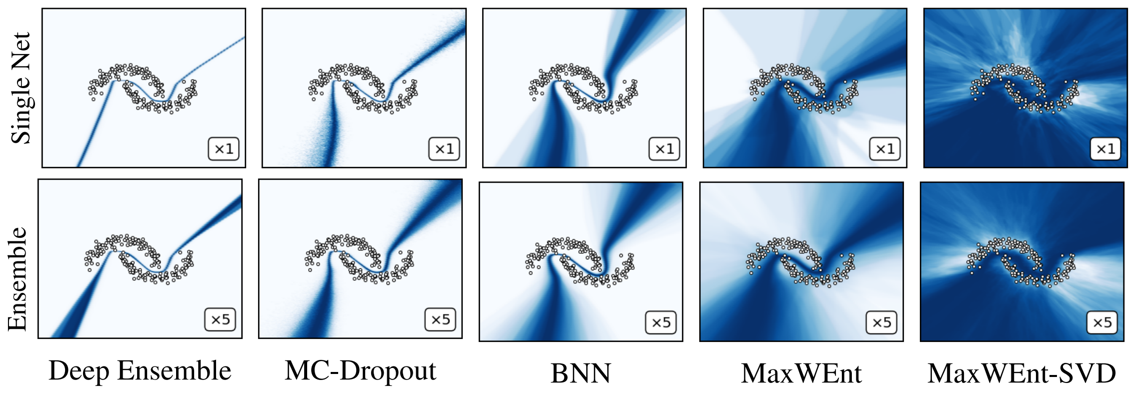

Figure 3: Two-Moons Classification Uncertainty Estimation. The horizontal and vertical axes correspond to both dimensions of the input space $\mathcal{X}$. Training instances are represented by white dots. The two "moons" formed by the training instances correspond to two different classes. Predicted uncertainties $u(x)$, computed through Equation (17), are reported in shades of blue (darker areas correspond to larger uncertainties).

the validation NLL. Consequently, the expansion of the weight distribution is generally limited. In MaxWEnt optimization, the primary goal is to maximize the entropy of the weight distribution as long as the sampled weights are consistent. Although this approach induces a slight penalization of the validation NLL as suggested in Figure 3 (predicted uncertainties in the training domain are larger for MaxWEnt and MaxWEnt-SVD than for BNN), it significantly improves the predicted epistemic uncertainties outside the training domain. Notice that one can sample from the whole MaxWEnt weight distribution to detect OOD and then from "shrunk" weight distribution to provide more accurate prediction for data identified as in-distribution (cf. Figure 4).

When considering the MaxWEnt-SVD results for both experiments (cf. right side of Figures 2 and 3), we might judge that the produced out-of-distribution uncertainties are over-estimated; especially in the regression experiment, where the predicted uncertainties become very large almost instantly at the borders of the training domain. However, this behavior is optimal according to the notion of epistemic uncertainty considered in this work. Indeed, epistemic uncertainty is defined through the set of potential candidates for the optimal hypothesis h_{w^*}. Then, as soon as there exists a neural network h in $\mathcal{H}$ which fits the training instances and produces very high outputs out-of-distribution, the user has no reason, in the absence of further regularity consideration, to exclude that the optimal hypothesis can be modeled by h. If, for some reason, the user wants to add some prior information on h_{w^*}, such as Lipschitz constraints on the network output, this can be achieved, for example, by clipping the scaling variable $\phi \odot z$ during the MaxWEnt inference as done for the weights of the Wasserstein-GAN to impose the 1-Lipschitz constraint (Arjovsky et al., 2017). This boils down to considering a reduced hypothesis space $\mathcal{H}$, which de facto reduces the epistemic uncertainty estimation, but potentially increases the discrepancy between $\mathcal{H}$ and f^*. We present in Figure 4 the impact of weight clipping on the predicted uncertainties of MaxWEnt-SVD on the regression dataset. We observe that the clipping parameter enables the interpolation between the behavior of the vanilla probabilistic network and the MaxWEnt-SVD behavior. Notice that clipping is performed at "test time", i.e., after the MaxWEnt optimization, which is convenient as the clipping parameter can be selected "a posteriori", without further training.

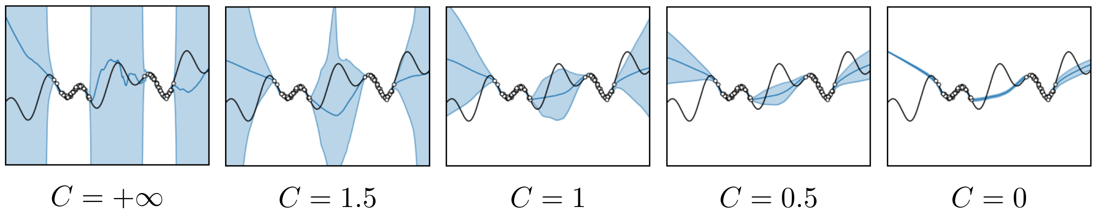

Figure 4: MaxWEnt-SVD Uncertainties for different clipping parameters. Clipping is performed "a posteriori" on the scaling variable $\hat{\phi} \odot z$ (cf. Equation 6) with $\hat{\phi}$ the parameters of the fitted MaxWEnt-SVD network, such that $q_{\hat{\phi}} \sim \overline{w} + V \min(\hat{\phi} \odot z, C)$, with C the clipping parameter.

The comparison between the regression and classification results suggests that out-of-distribution detection is a more difficult task in the classification setting. Indeed, in this setting, the uncertainty quantification methods do not fully manage to increase uncertainty for OOD data behind the training instances of each class. This behavior can be explained by the use of the sigmoid activation at the end-layer, which hardens the epistemic uncertainty estimation as different large outputs are reduced in the same probabilistic output (close to 1 if positive or 0 if negative). In fact, recent out-of-distribution detection methods often abandon the use of softmax and sigmoid activation functions at the end layer in favor of distance-based approaches where class assignment is computed through distance to class prototypes (Van Amersfoort et al., 2020). Notice that, we do not consider distance-based uncertainty methods in these synthetic experiments. For these low dimensional problems, using the Euclidean distance to the training instances would provide an almost perfect OOD detector. However, for high dimensional datasets, ensemble-based approaches generally provide better performances (Yang et al., 2022).

In both experiments, we observe that MaxWEnt-SVD produces uncertainty estimates of better quality than MaxWEnt. The theoretical analysis in Section 4.1.3 suggests that this improvement is related to the weight entropy increase. To evaluate this theoretical claim, we report the evolution of the predicted uncertainties and the weight entropy $H(\phi)$ through the epochs for both methods in the regression setting (cf. Figure 5). We observe, for both methods, a strong correlation between the increase of the weight diversity (measured by $H(\phi)$) and the increase of the uncertainty estimates out-of-distribution. Moreover, the predicted uncertainties of MaxWEnt-SVD quickly increase around epoch 100 as well as its distribution entropy $H(\phi)$, which becomes higher than the MaxWEnt entropy ($H(\phi) = -0.03$ at epoch 125 for MaxWEnt-SVD while $H(\phi) = -2.51$ for MaxWEnt). After this stage, the predicted OOD uncertainties are better for MaxWEnt-SVD than for MaxWEnt, especially in the interpolation regime between the two parts of the training domain. These observations support the idea that higher weight diversity for the same level of in-distribution risk produces better uncertainty quantification out-of-distribution.

7.1.4 NEURON ACTIVATION AMPLITUDE AND SCALING PARAMETERS

In the theoretical analysis in Section 4, we show, in the case of fully-connected neural networks, that the scaling parameters ϕ_k are inversely proportional to the neuron activation amplitude on the

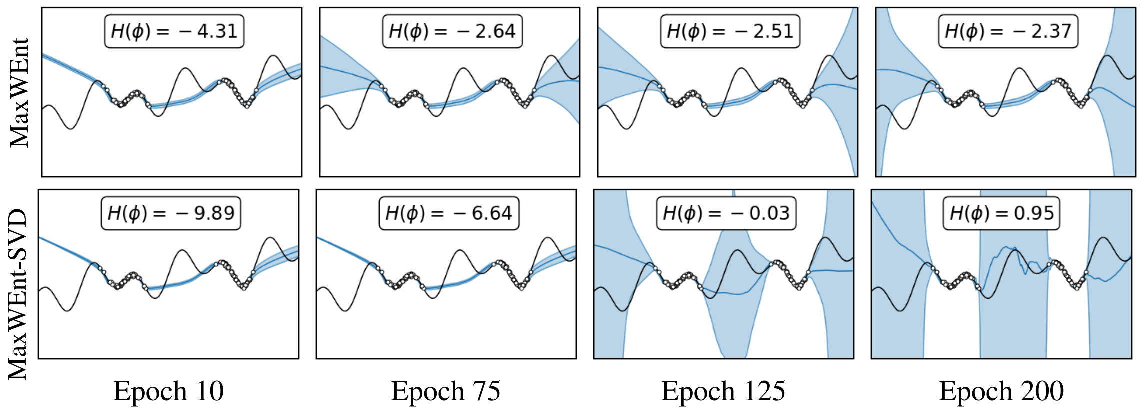

Figure 5: MaxWEnt Uncertainties Evolution through Epochs. One epoch corresponds to 100 iterations. The entropy term $H(\phi)$ is defined here as $H(\phi) = \frac{1}{d}\sum_{k=1}^{d} \log(\phi_k^2)$ with ϕ the scale parameters of the weight distribution. Notice that MaxWEnt and MaxWEnt-SVD have different parameter initialization, respectively: $\phi_{\text{init}} = \text{softplus}(-5)$ and $\phi_{\text{init}} = \text{softplus}(-10)$.

training data denoted $a^2_{(l,k)}$ for the l^{th} layer (cf. Proposition 6). We aim at supporting this theoretical result with empirical observations. For this purpose, we estimate the activation amplitudes in each layer of the MaxWEnt neural network and compare their values with the average of their corresponding scaling parameters $(1/b_l)\sum_{j=1}^{b_l}\phi_{(l,j,k)}$. We report the result in Figure 6. The top three graphics present the scaling parameters as a function of the activation amplitudes in the three layers of the MaxWEnt neural network trained on the two moons dataset. We observe a clear relation of inverse proportionality between the two quantities, in line with the theoretical outcomes. The three graphics below present the results for the standard BNN method. We observe the inverse proportionality relationship for the first layer but to a lesser extent than for MaxWEnt. This relationship is diminished in the two next layers. Moreover, we observe that the scaling parameters in the two last layers are globally larger for MaxWEnt than for BNN.

7.2 UCI regression datasets

7.2.1 SETUP

In this section, we consider the most common UCI regression datasets used to evaluate uncertainty quantification methods. Most previous works evaluate the methods based on the in-distribution NLL computed on a test set drawn from the same distribution as the training set (Lakshminarayanan et al., 2017). In this work, we focus on the method's ability to detect whether a data point is outside the training support or not. For this purpose, we build OOD detection problems by splitting each dataset into two distinct parts, with one part modeling the training domain and the other part the OOD data. Inspired by Foong et al. (2019) and Jain et al. (2020), which propose OOD splits for UCI datasets, we split the dataset along the first component of the input PCA: we define the *internal* domain with the data between the 25% and 75% percentiles of the first component of the input PCA, while the rest of the data forms the *external* domain. We then consider the two following experimental setups:

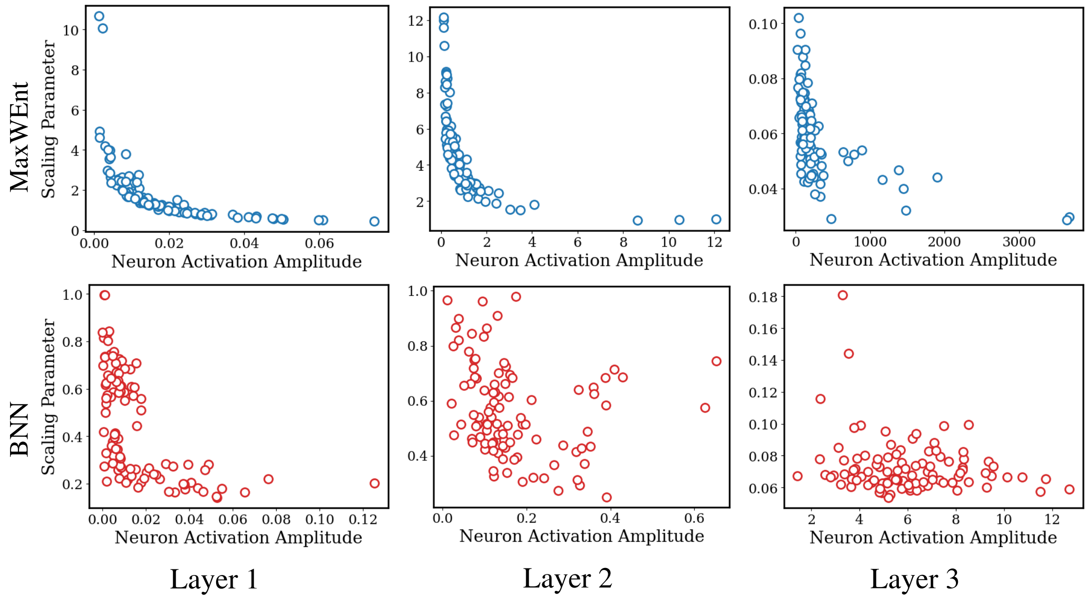

Figure 6: Neuron activation amplitude for the three hidden layers of MaxWEnt and BNN for the synthetic classification experiment: The top three graphics correspond to MaxWEnt while the three bottom to BNN. Each graphic reports the value of the average scaling parameter as a function of the training neuron activation amplitude in the three layers of the neural network.

- **Extrapolation**: The training data are defined by the *internal* domain, while the data from the *external* domain are considered as OOD.
- **Interpolation**: The training data are defined by the *external* domain, while the data from the *internal* domain are considered as OOD.

In all experiments, we consider a fully-connected network with three hidden layers of 100 neurons each and ReLU activation for the base estimator. The end-layer is composed of two neurons, which respectively predict the conditional mean and standard deviation $\mu_w(x), \sigma_w(x)$ (cf. Section 7.1.1). We consider 13 different uncertainty quantification approaches: five deep ensemble methods: **Deep Ensemble** (Lakshminarayanan et al., 2017), **Negative Correlation** (Liu and Yao, 1999; Shui et al., 2018), **Maximize-Overall-Diversity (MOD)** (Jain et al., 2020), **Anchored-Networks** (Pearce et al., 2018), **Repulsive-Deep-Ensemble (RDE)** (D'Angelo and Fortuin, 2021) and four "Bayesian" methods: **MC-Dropout**, **BNN**, **MaxWEnt**, **MaxWEnt-SVD** (described in Section 7.1.1), and ensemble version of these four previous Bayesian methods. The competitor characteristics are summarized in Table 1. We use the Gaussian NLL loss for regression, as defined in Equation (16) and the Adam optimizer (Kingma and Ba, 2015) with learning rate 0.001 and batch size 128. The number of iterations is chosen such that the minimum validation NLL is generally reached by every method on every dataset. We then consider 10k iterations for ensemble methods and 50k iterations for Bayesian and Bayesian ensemble methods, as stochastic variational inference converges slower than stochastic gradient descent. A callback process is used to monitor the validation NLL of the model every 100 iterations, the network weights corresponding to the iteration of best validation NLL are restored at the training end. For MaxWEnt, the scale parameters are saved if the validation NLL is below the threshold defined in Section 7.5. Notice that the OOD dataset is not used during the network training, as well as a test dataset, selected uniformly in the training domain. 10% of the in-distribution data are selected to form the test set and 5% of the remaining data to form the validation set.

Methods	Abrv.	Kind	Nets	Preds	Total	Parallel	Hyper-parameters
Deep Ensemble	DE	Ensemble	5	1	5	✓	None
Negative Correlation	NC	Ensemble	5	1	5	✓	$\lambda \in \{10^{-k};\ k \in [\|0, 5\|]\}$
Maximize-Overall-Diversity	MO	Ensemble	5	1	5	$\times$	$\lambda \in \{10^{-k};\ k \in [\|0, 5\|]\}$
Anchored-Networks	AN	Ensemble	5	1	5	✓	$\Sigma, \lambda \in [0.1, 1, 10]$
Repulsive-Deep-Ensemble	RE	Ensemble	5	1	5	$\times$	$\sigma =$ median heuristic
MC-Dropout $(\times 1)$	MD	Bayesian	1	50	50	N/A	rate $\in [0.05, 0.1, 0.2, 0.3, 0.5]$
Bayesian Neural Net $(\times 1)$	BN	Bayesian	1	50	50	N/A	$\lambda \in \{10^{k};\ k \in [\|-3, 3\|]\}$
MaxWEnt $(\times 1)$	ME	Bayesian	1	50	50	N/A	$\lambda = 10$, $\phi_{\text{init}} = \text{soft}(-5)$
MaxWEnt-SVD $(\times 1)$	ME+	Bayesian	1	50	50	N/A	$\lambda = 10$, $\phi_{\text{init}} = \text{soft}(-10)$
MC-Dropout $(\times 5)$	MD	Bay Ens	5	50	250	✓	rate $\in [0.05, 0.1, 0.2, 0.3, 0.5]$
Bayesian Neural Net $(\times 5)$	BN	Bay Ens	5	50	250	✓	$\lambda \in \{10^{k};\ k \in [\|-3, 3\|]\}$
MaxWEnt $(\times 5)$	ME	Bay Ens	5	50	250	✓	$\lambda = 10$, $\phi_{\text{init}} = \text{soft}(-5)$
MaxWEnt-SVD $(\times 5)$	ME+	Bay Ens	5	50	250	✓	$\lambda = 10$, $\phi_{\text{init}} = \text{soft}(-10)$

Table 1: Competitors Summary. The columns "Nets" and "Preds" respectively report the number of networks in the ensemble and the number of predictions at inference for one network. "Total" is the total number of predictions (Nets $\times$ Preds). The "Parallel" column reports whether the ensemble can be trained in parallel or not. When a list is given in the "Hyper-parameters" section, the value is selected based on hold-out validation NLL. "soft" is the abbreviation for the "softplus" function: $\text{soft}(x) = \log(1 + \exp(x))$.

7.2.2 RESULTS

To evaluate the model performances, we use the metric defined in Equation (18) which defines an uncertainty score for each data point, this score is used to compute the AUROC metric between in-distribution and OOD data which is a commonly used metric in the OOD detection setting (Yang et al., 2022). All results are reported in Table 2. Each experiment is performed only once to reduce the computational time of the experiments. As many different datasets are used, this is sufficient to obtain statistically significant results. We report the results by kind of methods: ensemble, Bayesian and Bayesian ensemble. The best result for each dataset in each category is emphasized in bold. We report the average AUROC among extrapolation and interpolation experiments and the rank of the methods. Our observations can be summarized as follows:

- **MaxWEnt-SVD (ME+) outperforms all other approaches**, with or without ensembling. The second-best non-MaxWEnt approach is 11.3 points behind in extrapolation and 18 points behind in interpolation in terms of average AUROC. Ensembling improves from 4.5 points in extrapolation and 1.2 points in interpolation.

	Meth	**Ensemble**					**Bayesian**				**Bayesian Ensemble**			
	Data	DE	NC	MO	AN	RE	BN	MD	ME	ME+	BN	MD	ME	ME+
Extrapolation	yacht	98.9	99.1	99.1	98.1	**99.5**	89.5	78.2	97.1	**99.4**	95.3	83.1	**99.6**	99.1
	energy	81.0	**93.6**	91.3	79.9	92.9	88.2	55.6	74.3	**99.6**	92.0	81.9	91.7	**99.9**
	concrete	78.4	**89.8**	88.9	83.8	87.7	75.7	68.7	74.3	**90.8**	79.5	72.1	81.8	**95.6**
	wine	38.8	**48.7**	36.8	45.8	39.3	70.9	62.3	79.1	**85.9**	66.7	64.2	83.8	**88.4**
	power	**84.9**	78.5	75.3	75.1	79.4	82.1	79.8	78.4	**93.0**	82.4	86.7	93.1	**93.3**
	naval	97.5	97.7	85.3	**99.7**	96.0	89.5	96.1	96.9	**97.2**	96.8	96.8	98.9	**99.6**
	protein	82.5	**83.0**	82.8	78.0	79.7	82.9	74.7	**81.6**	79.6	84.0	79.9	**89.3**	87.6
	kin8nm	45.4	45.0	45.0	45.9	**46.1**	52.5	51.4	39.1	**60.3**	54.5	52.8	49.1	**78.2**
	Avg AUC	75.9	**79.4**	75.6	75.8	77.6	78.9	70.8	77.6	**88.2**	81.4	77.2	85.9	**92.7**
	Rank	9	**5**	11	10	7	6	12	7	**2**	4	8	3	**1**
Interpolation	yacht	77.5	78.4	**80.6**	76.1	79.7	46.7	48.4	71.4	**98.9**	51.9	48.0	90.1	**98.6**
	energy	99.2	**99.7**	99.6	98.7	99.5	95.5	78.8	88.5	**99.5**	98.2	96.4	98.8	**100.0**
	concrete	60.8	72.7	72.4	46.2	**73.6**	48.6	57.4	46.7	**93.4**	60.3	60.6	62.5	**95.0**
	wine	43.3	42.7	42.7	41.1	**43.8**	34.8	41.6	32.2	**52.5**	33.9	41.0	37.0	**62.1**
	power	43.5	42.8	17.8	**67.3**	48.5	38.1	42.7	58.6	**94.7**	57.2	47.1	65.5	**96.0**
	naval	81.8	73.5	73.6	**83.6**	71.2	22.8	83.8	54.6	**98.6**	46.9	91.5	88.9	**98.4**
	protein	70.6	72.5	65.9	**73.7**	73.3	66.0	71.6	64.2	**83.8**	71.0	76.1	71.9	**80.6**
	kin8nm	63.7	63.2	63.3	64.7	**64.8**	53.1	56.2	55.8	**67.1**	54.2	58.1	56.9	**67.7**
	Avg AUC	67.6	68.2	64.5	68.9	**69.3**	50.7	60.1	59.0	**86.1**	59.2	64.8	71.4	**87.3**
	Rank	7	6	9	5	**4**	13	10	12	**2**	11	8	3	**1**

Table 2: UCI experiments OOD detection results. AUROC scores for OOD detection are reported. The best score for each category is emphasized in bold (higher scores are better). The two last rows for the extrapolation and interpolation settings report the average AUROC over the eight datasets (Avg AUC) and the rank of the method among all methods according to the average score (Rank).

- **The ensemble version of MaxWEnt (ME) is third best** behind the two versions of MaxWEnt-SVD. The single-network MaxWEnt, however, provides poor performances, which advocates for the use of ensembling or SVD parameterization.
- **AUROC scores are higher in extrapolation than in interpolation**, suggesting that the second task is more difficult. This seems reasonable, as the network is conditioned on both sides of the OOD domain in the interpolation case while being conditioned only on one side of the OOD domain in extrapolation.
- **Ensembling of Bayesian methods generally improves the results compared to the single-net from 7 points on average**. However, using Bayesian combined in ensemble increases the training and inference time by the number of members as well as the required memory size. Note that, for these methods, the ensemble training can be conducted in parallel, which can alleviate the training time burden.

Finally, to evaluate the in-distribution performance of the methods, we compute, on the test set, the Negative Log Likelihood (NLL) as well as the Expected Calibration Error (ECE) (Levi et al., 2022). To further assess the in-distribution performance of the methods, we also introduce two additional metrics: coverage and average interval width. Coverage measures the proportion of labels that fall within the predicted uncertainty intervals, while interval width evaluates the average length

		Baselines			MaxWEnt				MaxWEnt + Clip			
	Metric	DE	BN1	BN5	ME1	ME1+	ME5	ME5+	ME1	ME1+	ME5	ME5+
Extrapolation	Avg NLL	-0.69	-0.61	**-0.75**	-0.44	-0.33	-0.41	-0.04	-0.61	-0.71	-0.59	-0.71
	Avg ECE	0.37	0.37	0.35	0.36	0.33	0.36	0.39	0.31	0.36	**0.29**	0.35
	Cov.	0.61	0.58	0.65	0.73	0.75	0.79	**0.82**	0.65	0.68	0.63	0.64
	Int. Width	**1.00**	1.33	1.85	> 50	> 50	> 50	> 50	3.07	1.19	1.07	1.12
	Coverage Conform	0.91	0.93	0.86	0.93	0.92	0.91	**0.94**	0.93	0.93	0.90	0.90
	Int. Width Conform	1.00	1.41	1.68	> 50	> 50	> 50	> 50	3.34	1.42	**0.99**	**0.99**
Interpolation	Avg NLL	-0.45	-0.49	**-0.54**	-0.26	-0.12	-0.23	-0.06	-0.27	-0.45	-0.28	-0.45
	Avg ECE	0.33	0.32	**0.30**	0.32	**0.30**	**0.30**	0.34	0.33	0.33	0.33	0.33
	Coverage	0.65	0.57	0.64	0.74	0.78	0.81	**0.84**	0.59	0.59	0.65	0.65
	Int. Width	1.00	1.21	1.74	> 50	> 50	> 50	> 50	0.90	**0.88**	1.00	1.02
	Coverage Conform	0.91	0.90	0.90	0.93	**0.96**	**0.94**	0.92	0.93	**0.94**	0.91	0.91
	Int. Width Conform	1.00	1.25	1.68	> 50	> 50	3.54	> 50	1.14	1.20	1.00	**0.99**

Table 3: UCI experiments In-distribution performances. The average Negative Log Likelihood (NLL) and Expected Calibration Error (ECE) over the eight datasets are reported. The scores are computed on the test set, the lower the score the better. The number at the end of the acronyms corresponds to the number of networks (ME1 refers to a MaxWEnt single network and ME5 to an ensemble of 5 MaxWEnt networks). The coverage target level is 95%. "Int. Width" indicates the average confidence interval width and "Conf" denotes conformalized metrics, i.e., the metrics computed after conformalization of the intervals on the validation dataset.

of these intervals. The average metrics computed over the eight datasets are reported in Table 3. To evaluate the impact of clipping on the in-distribution performance, we also report the average metrics for the "clipped" MaxWEnt weight distribution: $q_\phi \sim \overline{w} + \min(\phi \odot z, C)$ (independent) and $q_\phi \sim \overline{w} + V \min(\phi \odot z, C)$ (SVD), with C the clipping parameter selected in $[+\infty, 10, 5, 2, 1, 0.5, 0.2, 0.1, 0]$ according to the validation NLL performance. We observe that the MaxWEnt algorithms generally penalize the test NLL and ECE compared to the baselines. In particular, the average NLL of MaxWEnt-SVD (x5) is larger than the ones produced by the other methods, suggesting that stronger OOD detection results come with weaker test performances. However, we observe that the use of weight clipping improves the MaxWEnt test performances, which become comparable to those of the baselines. Our results reveal that, in the absence of clipping, the predicted uncertainty intervals tend to be overestimated, which, while resulting in better coverage, leads to excessively large interval widths. After applying clipping, we observe that both the length of the intervals and the coverage improve, becoming comparable to those achieved by the baseline methods, especially for the MaxWEnt-SVD (x5) and MaxWEnt-SVD (x5) (Me5 and Me5+). These results suggest that the user should use the "unclipped" MaxWEnt predicted uncertainties to perform OOD detection and the "clipped" MaxWEnt inferences to provide predictions for data identified as in-distribution. This requires two different inferences: one for OOD detection and one for prediction.

We emphasize that clipping is not used during training; but only in inference after the model has been trained. Additionally, clipping is not essential for out-of-distribution (OOD) detection, but rather for in-distribution (ID) prediction. Therefore, the choice of clipping parameter does not affect the training nor the OOD detection score. Regarding the impact of clipping on the entropy, clipping intuitively reduces the weight entropy as suggested by the reduction of the prediction uncertainty shown in Figure 4 for the synthetic experiment. Deriving the formula of the weight entropy after clipping is not straightforward because the clipped distribution is a mixture of continuous and discrete distributions. Insights to compute the entropy in such cases can be found in (Nair et al., 2006).

7.3 CityCam regression datasets

7.3.1 SETUP

This section is dedicated to uncertainty quantification on the real-world dataset CityCam (Zhang et al., 2017). This dataset is composed of images gathered from several cameras monitoring the traffic in a city. Each camera records between 1k and 6k images dispatched over several days and hours. The task consists in counting the number of vehicles in the image using a neural network. This task is useful, for instance, to monitor the traffic in the city. To produce in-distribution vs OOD splits, we consider the three following experiments:

- **Camera-Shift**: Images coming from ten different cameras are selected for this experiment. At each round, five cameras are randomly selected to form the training dataset, while the five remaining cameras are used as OOD dataset. On average, both datasets contain around 20k images.

- **BigBus-Shift**: Images from five cameras are considered in this experiment. Some of them are marked as “big-bus” if a large vehicle masks a significant part of the image (cf. Zhang et al. 2017). These images are selected to form the OOD dataset, while the remaining ones compose the training set. The in-distribution and OOD datasets respectively contain around 17k and 1k images.

- **Weather-Shift**: For this experiment, we consider the images gathered from three cameras recorded during February the 23$^{\text{th}}$ from 9 am to 6 pm. On this particular day, weather conditions changed considerably between the beginning and end of the day. The dataset is split into two subsets: images recorded before 2 pm are considered in-distribution, while the others are out-of-distribution. After 4 pm, water drops landed on the cameras blur the images, causing a clear domain shift (cf. Table 4).

The three previous experiments model different out-of-distribution scenarios. OOD data for the BigBus-Shift and Weather-Shift experiments can be considered as “anomalies”. When a large vehicle masks an important part of the image or when the images become too blurry due to raindrops, it becomes very difficult to produce accurate predictions even for a human (cf. Table 4). In this case, the user may expect uncertainty quantification methods to provide large prediction uncertainty in order to detect such abnormal events. The paradigm slightly differs for the Camera-Shift experiment. In this setting, the domain shift essentially lies in the background differences between cameras. Since the model is trained on five different cameras, the user might expect the model to “generalize” and to provide accurate predictions for the images of the novel cameras.

As preprocessing, we use the features of the last layer of a ResNet50 (He et al., 2016) pretrained on ImageNet (Deng et al., 2009). We consider the same setting as for the UCI experiments in terms of base estimator, optimization parameters, callbacks and competitors.

	Camera-Shift	**BigBus-Shift**	**Weather-Shift**
In-Dist			
OOD			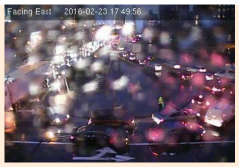

Table 4: CityCam Experiments setup. An example of a webcam image is given for each domain for the three settings: Camera-Shift, BigBus-Shift and Weather-Shift.

7.3.2 RESULTS

For each experiment, we compute the AUROC metric and the False Positive Rate at 95 percent (FPR@95) (Yang et al., 2022), using the uncertainty scores given in Equation (18). The computed metrics are reported in Table 5. We observe an important discrepancy between the scores produced by MaxWEnt-SVD and the ones of other methods. The gap is particularly large for the Camera-Shift experiments, where every method produces an average FPR@95 score around 97% while MaxWEnt-SVD provides a false positive rate of 29.4% in the single-net setting and 15.3% with ensembling. Similarly, MaxWEnt-SVD outperforms every other method for the BigBus-Shift and Weather-Shift experiments. The MaxWEnt algorithm without SVD parameterization provides the second-best results in the Bayesian and ensemble category, however, the performance gains compared to the baselines are much smaller than the ones obtained with the SVD parameterization. Notice, however, that MaxWEnt-SVD requires more computational time because of the additional matrix multiplication caused by the SVD alignment (cf. Section 5.3).

A visualization of the MaxWEnt uncertainty evolution on the Weather-Shift experiment is presented in Figure 7. We compare the evolution of the confidence intervals produced by Deep Ensemble and MaxWEnt (x1) along the day. The left part of Figure 7 corresponds to the images recorded between 2:00 pm and 2:30 pm which are the closest OOD data to the training domain. We observe that, in this time interval, both methods produce tight uncertainty intervals which well cover the ground-truth. The right part of Figure 7 corresponds to the time interval 4:00 pm to 6:00 pm. During this period of time, raindrops progressively land on the camera objective and blur the image. At some point around 5:30 pm, the deterioration of the image becomes critical for the vehicles' counting. We observe that, in this case, the size of the confidence intervals produced by Deep Ensemble does not increase. Paradoxically, the Deep Ensemble method seems to produce more confident predictions around 5:30 pm than before 2:30 pm. Conversely, the MaxWEnt predicted uncertainty progressively grows after 5:00 pm in correlation with the increasing task difficulty. Notice that, at some point, even the ground-truth is not reliable anymore, as the human annotator was not able to accurately count the actual number of vehicles.

Method	Camera-Shift		BigBus-Shift		Weather-Shift	
	FPR@95	AUROC	FPR@95	AUROC	FPR@95	AUROC
DE	98.3 (1.4)	52.1 (4.9)	82.0 (2.2)	77.9 (1.3)	79.7 (2.1)	77.5 (1.0)
NegCorr	**95.6 (0.6)**	56.5 (4.3)	78.4 (3.6)	**79.9 (1.0)**	80.0 (1.1)	78.5 (1.9)
MOD	97.0 (1.7)	**57.2 (2.2)**	78.0 (4.0)	79.0 (2.1)	76.7 (2.4)	78.5 (1.9)
AnchorNet	99.4 (0.4)	51.0 (5.9)	84.0 (1.7)	78.2 (0.9)	**73.4 (7.2)**	**80.9 (3.2)**
RDE	97.4 (0.4)	54.6 (3.9)	**78.0 (1.4)**	78.4 (1.1)	77.1 (1.0)	78.0 (0.6)
BNN (x1)	98.0 (2.8)	51.0 (2.3)	93.3 (2.1)	62.3 (7.6)	76.6 (1.4)	76.7 (1.8)
MCDropout (x1)	99.9 (0.1)	43.5 (4.4)	92.2 (1.4)	71.7 (1.8)	77.1 (4.3)	77.7 (1.9)
MaxWEnt (x1)	95.4 (0.0)	51.2 (0.0)	86.6 (0.0)	78.7 (0.0)	70.4 (0.0)	77.3 (0.0)
MaxWEnt-SVD (x1)	**29.4 (6.3)**	**92.3 (2.5)**	**57.5 (5.9)**	**87.0 (2.5)**	**61.1 (3.0)**	**85.7 (0.7)**
BNN (x5)	98.1 (2.5)	53.5 (2.9)	94.1 (1.4)	64.0 (7.9)	75.3 (1.9)	80.2 (1.1)
MCDropout (x5)	99.8 (0.1)	56.5 (1.8)	87.4 (1.4)	78.0 (0.1)	76.1 (2.5)	80.6 (2.7)
MaxWEnt (x5)	93.6 (2.1)	58.5 (5.9)	79.1 (4.9)	80.5 (1.2)	67.8 (2.7)	80.8 (0.3)
MaxWEnt-SVD (x5)	**15.3 (6.3)**	**96.9 (1.5)**	**53.5 (3.4)**	**88.6 (0.7)**	**59.8 (7.6)**	**86.7 (2.5)**

Table 5: CityCam Experiments: OOD Detection Results. Average AUROC and FPR@95 over three repetitions of the experiment are reported for each dataset and each method.

7.4 OSR-OOD detection benchmark on classification datasets

7.4.1 SETUP

We consider the Open-Set-Recognition (OSR) and Out-of-Distribution detection extensive benchmark (OpenOOD), developed in Yang et al. (2022) which compares more than 30 OSR and OOD detection methods on various classification datasets. The source code for the MaxWEnt experiments, conducted within the OpenOOD benchmark, is available on GitHub.[3] We focus on the OSR and OOD detection experiments:

- **Open-Set-Recognition**: For the OSR benchmark, each dataset is divided into two parts by removing the instances corresponding to some classes from the training set. The goal is to detect whether an instance comes from a training class or a removed one. Each experiment is repeated five times with random selections of the training classes. Four datasets are considered: MNIST (Deng, 2012), CIFAR10, CIFAR100 (Krizhevsky et al., 2009) and TinyImageNet (Torralba et al., 2008).
- **Out-Of-Distribution Detection**: For the OOD detection benchmark, data coming from all classes are used at training time. The goal is then to discriminate between the test set and data coming from other datasets (with no overlapping classes). Two types of OOD datasets are considered: **Far-OOD** which corresponds to images very different from the training instances (e.g., CIFAR10 vs MNIST) and **Near-OOD** which corresponds to images close to the training instances (e.g., CIFAR10 vs CIFAR100). This last type of OOD detection is considered more challenging and is closely related to the OSR setting (Yang et al., 2022). Three datasets are considered: MNIST, CIFAR10 and CIFAR100.

A summary of the datasets used in each experiment is presented in Table 6. The AUROC score is used to evaluate the discrimination accuracy between test and OOD datasets. To compute the "OOD scores", a variety of algorithms are considered. They can be classified into two main categories:

3. `https://github.com/antoinedemathelin/OpenOOD`

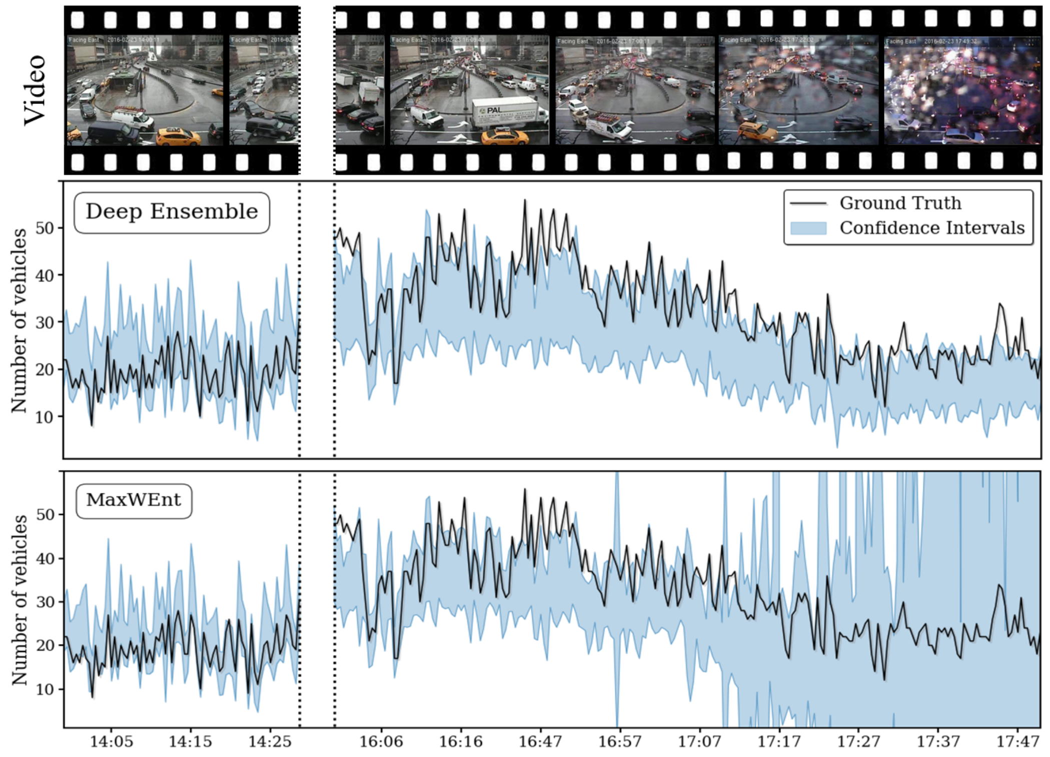

Figure 7: Comparison of the uncertainty evolution across time for Deep Ensemble and MaxWEnt on the Weather-Shift OOD dataset. The top images are examples of the camera's recording. The length of confidence intervals (in light blue) is equal to $2\sqrt{u(x)}$.

- **post-hoc Methods**, defined as methods that can be applied "directly" on a pretrained single network, independently of the training process. These methods are considered practical and model-agnostic (Yang et al., 2022). Among them, we can further distinguish the methods that do not require the training data: MSP (Hendrycks and Gimpel, 2017), MLS (Hendrycks et al., 2022a), ODIN (Liang et al., 2017), EBO (Liu et al., 2020), GradNorm (Huang et al., 2021a), ReAct (Sun et al., 2021), KLM (Hendrycks et al., 2022a) and TempScale (Guo et al., 2017a) and the methods that uses the training set: OpenMax (Bendale and Boult, 2016), MDS (Lee et al., 2018a), Gram (Sastry and Oore, 2020), VIM (Wang et al., 2022a), KNN (Sun et al., 2022), DICE (Sun and Li, 2022). Notice that, except for MSP and MLS, all post-hoc methods at least require the use of a validation dataset to fine-tune their hyper-parameters.

- **Non post-hoc Methods**, including all methods which do not belong to the previous category, essentially because they require a specific training process (in terms of training loss or data augmentation for instance). This category of methods includes anomaly detection approaches: DeepSVDD (Ruff et al., 2018), CutPaste (Li et al., 2021), DRAEM (Zavrtanik et al., 2021); OOD detection methods with specific training process: ConfBranch (DeVries and Taylor, 2018), G-ODIN (Hsu et al., 2020), CSI (Tack et al., 2020), ARPL (Chen et al., 2021), MOS (Huang and Li, 2021), OpenGAN (Kong and Ramanan, 2021), VOS (Du et al., 2022), LogitNorm (Wei et al., 2022); uncertainty-based approaches: MCdropout (Gal and Ghahramani, 2016), Deep Ensemble (Lakshminarayanan et al., 2017); and data augmentation methods: MixUp (Thulasidasan et al., 2019), CutMix (Yun et al., 2019), PixMix (Hendrycks et al., 2022b).

Experiment	In-Distribution Dataset	Out-Of-Distribution Datasets
OSR	MNIST6	MNIST4
	CIFAR6	CIFAR4
	CIFAR50	CIFAR50
	TIN20	TIN180
Near-OOD	MNIST	NOTMNIST, FashionMNIST
	CIFAR10	CIFAR100, TIN200
	CIFAR100	CIFAR10, TIN200
Far-OOD	MNIST	CIFAR10, TIN200, Texture, Places-365
	CIFAR10	MNIST, SVHN, Texture, Places-365
	CIFAR100	MNIST, SVHN, Texture, Places-365

Table 6: OpenOOD Experiments Summary.

According to Yang et al. (2022), a fair comparison between methods should be done among each category, as non-post-hoc methods may benefit from their specific training process. Notice that this classification is not perfect. Post-hoc methods are considered model-agnostic, as they can generally be "plugged" into any pretrained network. However, most post-hoc methods generally require the end-layer of the network to produce logits. Post-hoc methods are considered practical because they generally require less computational time than the non post-hoc methods. This computational efficiency is mainly due to the training process economy. It should be mentioned, however, that inference time for some post-hoc methods may become important for large training datasets. For instance, KNN computes the distance between test data and all training data in the penultimate network layer. This may lead to important memory and computational burden if the training dataset is very large.

The MaxWEnt algorithm can be plugged directly into a pretrained neural network $h_{\overline{w}}$. It may not be totally considered as post-hoc, as it requires the additional training of the scale parameters ϕ. However, this training may be done with a few epochs and also on a small extract of the training dataset. For our experiments, we trained MaxWEnt with the Adam optimizer (Kingma and Ba, 2015) with learning rate $5 \cdot 10^{-4}$ and 20 epochs. We also consider an ensemble of five MaxWEnt networks. For inference, we use $P = 10$ predictions.

7.4.2 RESULTS

The results are reported in Figure 8, we compare AUROC scores between MaxWEnt (x1) and MaxWEnt (x5) (in red) to the previously mentioned methods (in blue). Note that we do not include OOD detection methods that require auxiliary OOD datasets during training for the comparison, as MaxWEnt does not use this kind of additional information. post-hoc methods are marked with a dagger †. We group all experiments in the three main categories: OSR, NearOOD and FarOOD as described in Table 6. The reported AUROC scores are averaged over all experiments inside each category and over five different random seeds. We observe that MaxWEnt (x1) is ranked 3rd, 8th and

2nd for respectively the OSR, FarOOD and NearOOD experiments compared to all methods. When restricting the comparison to post-hoc methods, the MaxWEnt (x1) rankings become 1st, 3rd and 1st which demonstrates the effectiveness of the approach. It should be underlined that MaxWEnt (x1) is outperforming all other methods in the particular setting OSR and Near-OOD which are known to be the more challenging. For these two experiments, the MaxWEnt (x1) performances closely match those of Deep Ensemble, which requires the training of five neural networks and thus more computational resources. The ensemble of MaxWEnt networks provides an additional gain of around 2 points of AUROC scores and is then ranked 1st, 3rd and 1st compared to all methods. However, this improvement requires the training of five networks, which increases the computational time.

7.5 Implementation choices

We present hereafter the implementation choices that we consider as "good practices" for MaxWEnt:

7.5.1 INITIALIZATION

In our proposed setup, the weight mean $\mathbb{E}_{q_\phi}[w] = \overline{w}$ is frozen during the MaxWEnt optimization and independent of the parameters ϕ. The weight vector $\overline{w}$ is derived from a pretrained network $h_{\overline{w}}$ fitted on the training data. The ϕ parameters are initialized with a small constant value $C \ll 1$. Therefore, the weight distribution q_ϕ is initialized as a peaked distribution around $\overline{w}$, which already provides low empirical risk. Notice that the use of pretrained weights to initialize the mean of q_ϕ is similar to the common practice in Laplace approximation (Ritter et al., 2018), where the mean of the posterior distribution is set to the maximum a posteriori estimation (MAP). Moreover, in the case where a pretrained network is already available, the use of pretrained weights reduces the computational time. Note, finally, that we also consider a "softplus" activation of the ϕ parameters to smooth the increase of the weight entropy in earlier stages: $\phi = \log(1 + \exp(u))$.

7.5.2 ENTROPY FUNCTION

In our implementation, we use a proxy for the entropy given by $H(\phi) \propto \sum_{k=1}^{d} |\phi_k|$. This choice smooths the increase of ϕ during the initial stages of training, offering improved optimization stability compared to the logarithmic function $\log(\phi_k^2)$, which can over-penalize small components and cause excessive initial gradients (cf. Section 5.4).

7.5.3 TRADE-OFF PARAMETER

The MaxWEnt optimization (1) involves a trade-off between empirical risk minimization and entropy maximization, which is controlled by the trade-off parameter λ. A small λ penalizes larger average risks, while a large λ favors the weight distribution expansion. Obviously, the learner has to accept to penalize the empirical risk to offer room for the weight distribution to expand. In this perspective, we do not recommend selecting the trade-off parameter based on validation risk minimization. The λ value should be selected large enough to speed up the increase of the weight entropy, while not too large to avoid optimization instabilities. In all our experiments, we choose to consider a fixed trade-off $\lambda = 10$ for simplicity.[4]

4. In practice the entropy is scaled by the number of parameters such that $\lambda = 10/d$.

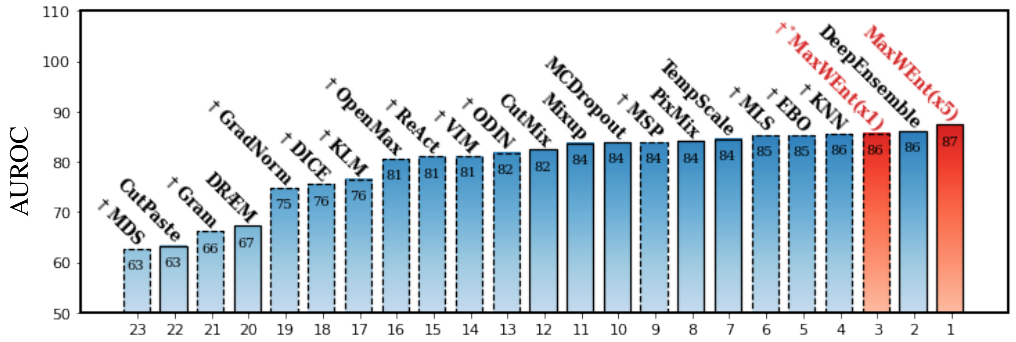

(a) OSR: MNIST6 + CIFAR6 + CIFAR50 + TIN20

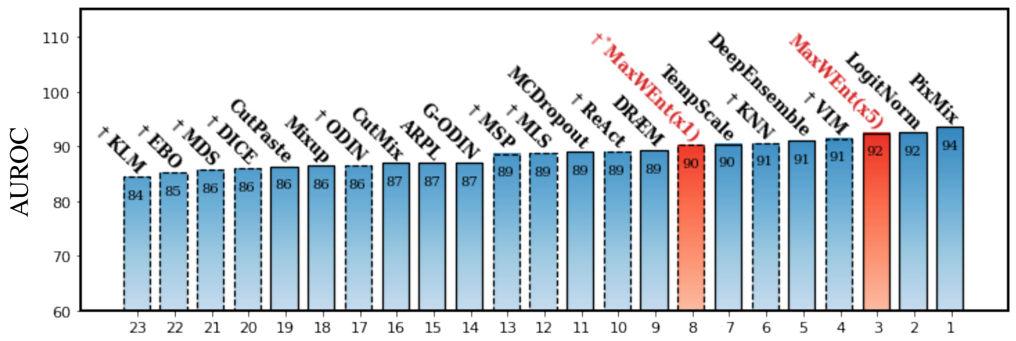

(b) FarOOD: MNIST + CIFAR10 + CIFAR100

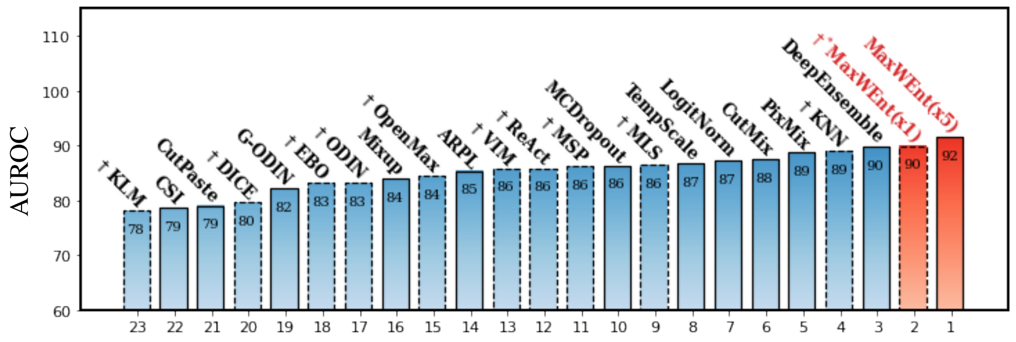

(c) NearOOD: MNIST + CIFAR10 + CIFAR100

Figure 8: OpenOOD benchmark ranking. Each method is ranked according to the average AUROC score computed for the three "global" experiments: OSR, Far-OOD, Near-OOD. Each experiment is performed on 3 or 4 different datasets (cf. Table 6). The top 23 scores among the 32 competitors are reported. post-hoc methods are marked with daggers, MaxWEnt(x1) can be considered as post-hoc as it applies on a pretrained network, although it requires additional training steps to learn the scaling parameters ϕ.

An extended analysis of the impact of λ on the training and the OOD detection performances is reported in Appendix B. This analysis reveals that OOD performances and entropy generally increase with higher λ values, but when λ is too large, the training becomes unstable and the validation loss quickly increases. As a result, a recommended approach is to use a stopping criterion to maintain a reasonable validation loss and select λ based on the resulting weight entropy. A well-performing model is characterized by high entropy and reasonable validation loss. Both metrics can be measured without using OOD data, which enables a practical approach to select the λ parameter.

7.5.4 STOPPING CRITERION

In standard training of neural networks, a sufficiently large number of epochs is generally performed until the full convergence of the training loss. Then the learner restores the weights of the network for the epoch which provides the best validation risk. Of course, we cannot consider such a technique for the MaxWEnt optimization, as increasing the weight entropy generally induces a small degradation of the validation risk. We then propose to save the network weights if the validation risk is below a threshold τ computed at the beginning of the optimization. We propose to estimate the performance threshold τ by the validation risk of the pretrained network $h_{\overline{w}}$ plus a statistical error:

$$\tau = \mathcal{L}_{\mathcal{S}_{\text{val}}}(\overline{w}) + \frac{2}{n_{\text{val}}} \sqrt{\sum_{(x,y)\in\mathcal{S}_{\text{val}}} \left(\ell(h_{\overline{w}}(x), y) - \mathcal{L}_{\mathcal{S}_{\text{val}}}(\overline{w})\right)^2}.$$

The second term is proportional to the standard deviation of the errors on the validation dataset.

The hyperparameter impact study presented in Appendix B reveals that, in some cases, a significant variance in OOD detection metrics is observed for late epochs, coinciding with an important increase in the validation loss. In these cases, the stopping criterion effectively selects an epoch with lower variance in OOD metrics and a reasonable validation loss. This indicates that the stopping criterion heuristic provides a relevant guideline to end the training, which does not add further hyperparameter tuning.

7.5.5 ENSEMBLE

It should be underlined that the proposed parameterizations (4) and (6) limit the range of the weight distribution around a neighborhood of $\overline{w}$. A straightforward improvement would be to apply Algorithm (1) on a set of weights $\overline{w}^{(j)}$ coming from a pretrained deep ensemble (Lakshminarayanan et al., 2017). Conceptually, this comes down to describing q_ϕ as a mixture with, for any $j \in [|1, m|]$, $\phi^{(j)} \in \mathbb{R}^d$, $z^{(j)} \sim \mathcal{Z}$ and $\pi \sim \mathcal{U}(\{1, ..., m\})$:

$$q_\phi \sim \sum_{j=1}^{m} \mathbb{1}(\pi = j)\, \omega(\phi^{(j)}, z^{(j)}),$$

with $\omega(\phi^{(j)}, z^{(j)}) = \overline{w}^{(j)} + \phi^{(j)} \odot z^{(j)}$ or $\omega(\phi^{(j)}, z^{(j)}) = \overline{w}^{(j)} + V\left(\phi^{(j)} \odot z^{(j)}\right)$. In practice, we apply Algorithm (1) to each of the pretrained networks with the scaling parameterization $\omega(\phi^{(j)}, z^{(j)})$. Notice that, if there is no overlap between the mixture components, the ensemble parameterization necessarily results in a weight distribution of higher entropy for the same empirical risk level, and then leads to a more efficient parameterization than the single network setting. A guideline to choose the centers $\overline{w}^{(j)}$ is then to avoid overlapping, which can be achieved with centers distant from each other. Thus, combining MaxWEnt with techniques such as RDE (D'Angelo and Fortuin, 2021) and AnchorNet (Pearce et al., 2018) may offer increased performances.

8. Limitations and Perspectives

In this work, we develop the MaxWEnt algorithm to improve OOD detection with stochastic neural networks. The main goal of MaxWEnt is to produce samples with larger weight diversity compared to standard Bayesian and ensemble methods. Our experiments show that MaxWEnt fulfills its promise, it increases the weight entropy and provides better OOD detection results. Moreover, we show that the more the weight entropy, the better the OOD detection (for the same level of average empirical error).

- **Increasing the weight entropy**: The weight entropy increase is strongly conditioned by the weight parameterization. We show that the use of the SVD-parameterization is already an important improvement compared to the use of independent scaling parameters. However, more efficient parameterization may be obtained with other techniques such as normalizing flows (Louizos and Welling, 2017) or weight subspaces (Izmailov et al., 2020). Nevertheless, the maximum entropy framework provides a general guideline for selecting the weight parameterization: an efficient stochastic model should enable a large increase of the weight entropy in low empirical risk regions of the weight space.

- **Penalized performances in-distribution**: We have seen that increasing the entropy penalizes the in-distribution performances. However, this negative result can be mitigated by the use of "shrunk" weight distribution obtained through weight clipping (cf. Sections 7.1.3 and 7.2.2). The user can use the MaxWEnt uncertainties to discriminate between ID and OOD data, and then use the prediction obtained with "shrunk" weight distribution for the ID data.

- **SVD-parameterization for Convolutions**: For now, the SVD-parameterization is only developed for fully connected neural networks, but it may also be applied to convolutional layers. Convolutions apply the same kernel to multiple windows of one channel. To use the SVD-parameterization in this context, one idea is to concatenate all the windows on which the kernel is applied for all training data and then compute the SVD decomposition of the resulting dataset.

- **General Bayesian and ensemble limitations**: The developed MaxWEnt approach improves upon Bayesian and ensemble methods in terms of weight diversity. However, it still inherits the other limitations of these approaches, which principally include the computational burden in training and inference. Future work will then consider the use of "Laplace-like" approximation to reduce the computational time of MaxWEnt (cf. Section 5.3).

9. Conclusion

In this work, we tackle the over-confidence issue encountered with standard Bayesian and ensemble methods outside the training domain. Building on the maximum entropy principle, we show that penalizing the empirical average error with the weight entropy leads to larger hypothesis diversity and, then, to improved OOD detection. Theoretical analysis shows that the behavior of the developed MaxWEnt approach is related to the amplitude of the neuron activation on the training data.

In MaxWEnt neural networks, weakly activated neurons play a more important role in the OOD detection in comparison to vanilla probabilistic networks. Motivated by this quest of entropy maximization and by the outcomes of our theoretical analysis, we propose the SVD parameterization to take advantage of correlations between weights with limited additional complexity. Numerical experiments show the benefit of the method and highlight the link between weight entropy and OOD detection performances. We show that the maximum entropy framework offers a guideline to rank two weight distributions with the same empirical risk, the one with the largest entropy should be preferred to improve OOD detection. Moreover, we advocate for the use of stochastic models that foster the increase of the weight entropy, as the SVD parameterization. We are convinced that this approach is a step forward in the safety of deep learning. Although many challenges have to be resolved such as the training and inference computational time.

Appendix A. Proofs

A.1 Proof of Proposition 1

Let's consider a matrix $A \in \mathbb{R}^{d \times d}$ and a vector $\phi \in \mathbb{R}^d$, $\phi > 0$, such that the weights w are written:

$$w = \overline{w} + A(\phi \odot z),$$

with $z \sim \mathcal{Z}$ following either a multivariate normal or a uniform distribution. We demonstrate Proposition (1) for any orthogonal matrix A. Indeed, the weight parameterizations (4) and (6) correspond respectively to the specific cases $A = \text{Id}_d$ and $A = V$ which are both orthogonal matrices.

A.1.1 Gaussian Case

To demonstrate the result in the Gaussian case $z \sim \mathcal{N}(0, \text{Id}_d)$, we first derive the two following preliminary results:

- $z \sim \mathcal{N}(0, \text{Id}_d) \implies A(z \odot \phi) \sim \mathcal{N}(0, A^T \text{diag}(\phi^2) A)$, with $\text{diag}(\phi^2)$ the diagonal matrix of diagonal values ϕ^2 (cf. Lemma 7).
- The entropy of a multivariate Gaussian $\mathcal{N}(0, \Sigma)$ is written $C + \frac{1}{2}\log(|\text{det}(\Sigma)|)$ with $C > 0$ a constant (independent of Σ) and $\text{det}(\Sigma)$ the determinant of Σ (cf. Lemma 8).

Lemma 7 *For any $A \in \mathbb{R}^{d \times d}$ and any $\phi \in \mathbb{R}^d$, we have:*

$$z \sim \mathcal{N}(0, \text{Id}_d) \implies A(z \odot \phi) \sim \mathcal{N}(0, A\, \text{diag}(\phi^2) A^T).$$

Proof We first notice that linear combinations of Gaussian variables are Gaussians. Then, it appears that:

$$\mathbb{E}[A(z \odot \phi)] = A(\mathbb{E}[z] \odot \phi) = 0,$$

and:

$$\begin{aligned}
\mathbb{V}[A(z \odot \phi)] &= \mathbb{E}[(A(z \odot \phi))\,(A(z \odot \phi))^T] \\
&= \mathbb{E}[A(z \odot \phi)(z \odot \phi)^T A^T] \\
&= A\, \mathbb{E}[(z \odot \phi)(z \odot \phi)^T] A^T \\
&= A\, \mathbb{V}[z \odot \phi] A^T \\
&= A\, \text{diag}(\phi^2) A^T.
\end{aligned}$$

From which we conclude that $A(z \odot \phi) \sim \mathcal{N}(0, A\, \text{diag}(\phi^2) A^T)$

■

Lemma 8 *The entropy of a multivariate Gaussian $\mathcal{N}(0, \Sigma)$ is written $C + \frac{1}{2}\log(|\text{det}(\Sigma)|)$ with $C > 0$ a constant (independent of Σ) and $\text{det}(\Sigma)$ the determinant of Σ.*

Proof Let's consider the multivariate Gaussian variable $Z \sim \mathcal{N}(0, \Sigma)$ with $\Sigma \in \mathbb{R}^{d \times d}$. We denote $p_Z(z)$ its probability density function such that, for any $z \in \mathbb{R}^d$:

$$p_Z(z) = \frac{1}{\sqrt{(2\pi)^d |\text{det}(\Sigma)|}} \exp\left(-\frac{1}{2} z^T \Sigma^{-1} z\right).$$

Then,

$$-2\log(p_Z(z)) = d\log(2\pi) + \log(|\text{det}(\Sigma)|) + z^T \Sigma^{-1} z.$$

We now consider the eigen-decomposition of Σ^{-1}, such that $\Sigma^{-1} = Q^T \text{diag}(1/\lambda) Q$ with $Q \in \mathbb{R}^{d \times d}$ an orthogonal matrix and λ the vector of eigenvalues of Σ. The following equality holds:

$$z^T \Sigma^{-1} z = (Qz)^T \text{diag}(1/\lambda)(Qz) = u^T \text{diag}(1/\lambda) u = \sum_{k=1}^{d} \frac{u_k^2}{\lambda_k}.$$

Moreover, for any $z \sim \mathcal{N}(0, \Sigma)$, the variable $u = Qz$ follows the distribution $\mathcal{N}(0, Q\Sigma Q^T) = \mathcal{N}(0, \text{diag}(\lambda))$. We then deduce that:

$$\mathbb{E}[z^T \Sigma^{-1} z] = \sum_{k=1}^{d} \frac{\mathbb{E}[u_k^2]}{\lambda_k^2} = \sum_{k=1}^{d} \frac{\lambda_k^2}{\lambda_k^2} = d.$$

Finally, we can derive the following formula for the entropy of Z:

$$-\mathbb{E}[\log(p_Z(z))] = C + \frac{1}{2}\log(|\text{det}(\Sigma)|),$$

with $C \in \mathbb{R}$ verifying: $C = \frac{d}{2}\log(2\pi) + \frac{d}{2}$

■

Let's now consider the variable $z \sim \mathcal{N}(0, \text{Id}_d)$. According to Lemma (7), the variable $A(z \odot \phi)$ follows the distribution $\mathcal{N}(0, A\,\text{diag}(\phi^2) A^T)$. Then, according to Lemma (8) and by invariance of the entropy by translation, the entropy of the distribution $q_\phi(w) \sim \overline{w} + A(z \odot \phi)$ is written:

$$\begin{aligned} H(\phi) &= -\mathbb{E}[\log(q_\phi(w))] \\ &= C + \frac{1}{2}\log(|\text{det}(A\,\text{diag}(\phi^2) A^T)|) \\ &= C + \frac{1}{2}\log(|\text{det}(A)\,\text{det}(\text{diag}(\phi^2))\text{det}(A^T)|), \end{aligned}$$

with $C \in \mathbb{R}$ a constant. Then, as A is an orthogonal matrix, we have $|\text{det}(A)| = |\text{det}(A^T)| = 1$ and:

$$\begin{aligned} H(\phi) &= C + \frac{1}{2}\log(|\text{det}(\text{diag}(\phi^2))|) \\ &= C + \frac{1}{2}\log(|\prod_{k=1}^{d} \phi_k^2|) \\ &= C + \frac{1}{2}\sum_{k=1}^{d} \log(\phi_k^2). \end{aligned}$$

A.1.2 UNIFORM CASE

The probability density function $p_Z(z)$ of a uniform distribution defined over the parallelotope $\mathcal{P}$ described by the matrix $\Sigma \in \mathbb{R}^{d \times d}$ is written:

$$p_Z(z) = \begin{cases} 1/\mathcal{V}(\mathcal{P}) & z \in \mathcal{P} \\ 0 & z \notin \mathcal{P} \end{cases},$$

with $\mathcal{P}$ the subset of $\mathbb{R}^d$ defined as $\mathcal{P} = \{\Sigma x\,;\ x \in [0,1]^d\}$ and $\mathcal{V}(\mathcal{P})$ the volume of $\mathcal{P}$ which verifies $\mathcal{V}(\mathcal{P}) = |\text{det}(\Sigma)|$.

Let's now consider the variable Z of probability density function $p_Z(z)$, the entropy of Z is then written:

$$\mathbb{E}[-\log(p_Z(z))] = \log(|\text{det}(\Sigma)|).$$

We notice that, if $z \sim \mathcal{U}([-\sqrt{3}, \sqrt{3}]^d)$, then the variable $A(z \odot \phi) = A\,\text{diag}(\phi)z$ is defined as the uniform distribution over the parallelotope $\mathcal{P} = \{A\,\text{diag}(\phi)x\,;\ x \in [-\sqrt{3}, \sqrt{3}]^d\}$, which is well-defined as $\text{det}(A\,\text{diag}(\phi)) \neq 0$. As the volume of a subset is invariant by translation, we have $\mathcal{V}(\mathcal{P}) = \mathcal{V}(\tilde{\mathcal{P}})$ with $\tilde{\mathcal{P}}$ the parallelotope defined as $\tilde{\mathcal{P}} = \{A\,\text{diag}(\phi)x\,;\ x \in [0, 2\sqrt{3}]^d\} = \{2\sqrt{3}A\,\text{diag}(\phi)x\,;\ x \in [0,1]^d\}$. We then deduce that the entropy of $q_\phi(w) \sim \overline{w} + A(z \odot \phi)$

$$\begin{aligned} H(\phi) &= \mathbb{E}[-\log(q_\phi(w))] \\ &= \log(|\text{det}(2\sqrt{3}A\,\text{diag}(\phi))|) \\ &= \log(|\text{det}(A)|\,|\text{det}(2\sqrt{3}\,\text{diag}(\phi))|). \end{aligned}$$

Finally, as A is an orthogonal matrix, we have $|\text{det}(A)| = 1$ and:

$$\begin{aligned} H(\phi) &= \log(|\text{det}(2\sqrt{3}\,\text{diag}(\phi))|) \\ &= 2^{d-1}\sqrt{3}^d \sum_{k=1}^{b} \log(\phi_k^2). \end{aligned}$$

A.2 Proof of Proposition 2

Proof Let's consider $\phi \in \mathbb{R}^b$ and $z \sim \mathcal{Z}$. The training risk for the weight $w = \overline{w} + \phi \odot z$ can be written as follows:

$$\begin{aligned} ||X(\overline{w} + \phi \odot z) - y||_2^2 &= ||X(\phi \odot z) + X\overline{w} - y||_2^2 \\ &= ||X(\phi \odot z)||_2^2 + \langle X(\phi \odot z), X\overline{w} - y\rangle + ||X\overline{w} - y||_2^2. \end{aligned}$$

When averaging over $z \sim \mathcal{Z}$, considering that $\mathbb{E}[z] = 0$, we obtain:

$$\begin{aligned} \mathbb{E}_{\mathcal{Z}}\left[||X(\overline{w} + \phi \odot z) - y||_2^2\right] - ||X\overline{w} - y||_2^2 &= \mathbb{E}_{\mathcal{Z}}\left[||X(\phi \odot z)||_2^2\right] \\ &= \sum_{i=1}^{n} \mathbb{E}_{\mathcal{Z}}\left[\left(\sum_{k=1}^{b} X_{ik}\phi_k z_k\right)^2\right] \\ &= \sum_{i=1}^{n}\sum_{k=1}^{b} X_{ik}^2 \phi_k^2 \\ &= n\sum_{k=1}^{b} a_k^2 \phi_k^2 \end{aligned} \tag{19}$$

The objective function of Problem (8) can then be written, for any $\phi \in \mathbb{R}^b$:

$$G(\phi) = \sum_{k=1}^{b} \left(a_k^2 \phi_k^2 - \lambda \log(\phi_k^2) \right).$$

The objective function of Problem (8) is convex and admits a solution. Moreover, the partial derivative of the objective with respect to ϕ_k^2 is written:

$$\frac{\partial G(\phi)}{\partial \phi_k^2} = a_k^2 - \frac{\lambda}{\phi_k^2}.$$

As a consequence, the gradient of G is null if and only if

$$\phi_k^2 = \frac{\lambda}{a_k^2},$$

which is well-defined when assuming $a_k^2 > 0$.

■

A.3 Proof of Proposition 3

Proof Let's consider $\phi \in \mathbb{R}^b$, V the matrix of eigenvectors of $\frac{1}{n}X^T X$ with s^2 the corresponding vector of eigenvalues and $z \sim \mathcal{Z}$. The average training risk for the weight $w = \overline{w} + V(\phi \odot z)$ can be written as follows:

$$\mathbb{E}_{\mathcal{Z}} \left[\frac{1}{n} ||X(\overline{w} + V(\phi \odot z)) - y||_2^2 \right] = \mathbb{E}_{\mathcal{Z}} \left[\frac{1}{n} ||XV(\phi \odot z)||_2^2 \right] + \frac{1}{n} ||X\overline{w} - y||_2^2.$$

We notice that:

$$\begin{aligned}
\frac{1}{n}||XV(\phi \odot z)||_2^2 &= \frac{1}{n}||XV \,\text{diag}(\phi) z||_2^2 \\
&= z^T \text{diag}(\phi)^T V^T \left(\frac{1}{n} X^T X \right) V \text{diag}(\phi) z \\
&= z^T \text{diag}(\phi)^T \text{diag}(s^2) \text{diag}(\phi) z \\
&= z^T \text{diag}(s^2 \phi^2) z \\
&= \sum_{k=1}^{b} s_k^2 \phi_k^2 z_k^2.
\end{aligned}$$

Then,

$$\mathbb{E}_{\mathcal{Z}} \left[\frac{1}{n} ||X(\overline{w} + V(\phi \odot z)) - y||_2^2 \right] = \sum_{k=1}^{b} s_k^2 \phi_k^2 + \frac{1}{n} ||X\overline{w} - y||_2^2. \tag{20}$$

The continuation of the proof is similar to the proof in Appendix (A.2) with s_k^2 instead of a_k^2.

■

A.4 Proof of Proposition 4

Proof Let $q_{\phi^*}^{(1)}$, $q_{\phi^*}^{(2)}$ be the respective optimal weight distributions for the scaling and the SVD parameterization. Then,

$$q_{\phi^*}^{(1)} \sim \overline{w} + \frac{\lambda}{a} \odot z$$
$$q_{\phi^*}^{(2)} \sim \overline{w} + V(\frac{\lambda}{s} \odot z),$$

with $z \sim \mathcal{Z}$. Considering Equations (19) and (20), both average empirical losses are written:

$$\mathbb{E}_{q_{\phi^*}^{(1)}} [\mathcal{L}_{\mathcal{S}}(w)] = \sum_{k=1}^{b} \frac{\lambda a_k^2}{a_k^2} + \frac{1}{n} ||X\overline{w} - y||_2^2$$
$$\mathbb{E}_{q_{\phi^*}^{(2)}} [\mathcal{L}_{\mathcal{S}}(w)] = \sum_{k=1}^{b} \frac{\lambda s_k^2}{s_k^2} + \frac{1}{n} ||X\overline{w} - y||_2^2.$$

Then,

$$\mathbb{E}_{q_{\phi^*}^{(1)}} [\mathcal{L}_{\mathcal{S}}(w)] = \mathbb{E}_{q_{\phi^*}^{(2)}} [\mathcal{L}_{\mathcal{S}}(w)] = \lambda\, b + \frac{1}{n} ||X\overline{w} - y||_2^2.$$

Moreover, both entropy can be written as:

$$\mathbb{E}_{q_{\phi^*}^{(1)}} \left[-\log(q_{\phi^*}^{(1)}) \right] = - \sum_{k=1}^{b} \log(a_k^2) + b \log(\lambda)$$
$$\mathbb{E}_{q_{\phi^*}^{(2)}} \left[-\log(q_{\phi^*}^{(2)}) \right] = - \sum_{k=1}^{b} \log(s_k^2) + b \log(\lambda).$$

Let's denote $M = \frac{1}{n} X^T X$, by definition, we have the following equalities:

$$M = V^T \operatorname{diag}(s^2) V \tag{21}$$
$$M_{ii} = a_i^2 \ \forall i \in [|1, b|]. \tag{22}$$

Equation (21) implies that $M = UU^T$ with $U = V^T \operatorname{diag}(s) V$. For any $i \in [|1, b|]$, we denote $u_i \in \mathbb{R}^b$ the i^{th} row vector of the matrix U and $||u_i||_2 = \sqrt{\sum_{j=1}^{b} U_{ij}^2}$ its corresponding Euclidean norm.

Applying the Hadamard inequality to the matrix U, we obtain that:

$$\det(U) \leq \prod_{i=1}^{b} ||u_i||_2.$$

Then, the formula $U = V^T \operatorname{diag}(s) V$ implies that $\det(U) = \prod_{i=1}^{b} s_i$ and the equality $M = UU^T$ implies that $M_{ii} = \sum_{j=1}^{b} U_{ij}^2 = ||u_i||_2^2$. Considering Equation (22), we then deduce that:

$$\prod_{i=1}^{b} s_i^2 \leq \prod_{i=1}^{b} a_i^2.$$

From which we conclude that:

$$\begin{aligned} -\log\left(\prod_{i=1}^{b} s_i^2\right) \geq -\log\left(\prod_{i=1}^{b} a_i^2\right) &\implies -\sum_{i=1}^{b}\log(s_i^2) \geq -\sum_{i=1}^{b}\log(a_i^2) \\ &\implies \mathbb{E}_{q^{(2)}_{\phi^*}}\left[-\log(q^{(2)}_{\phi^*})\right] \geq \mathbb{E}_{q^{(2)}_{\phi^*}}\left[-\log(q^{(1)}_{\phi^*})\right]. \end{aligned}$$

■

A.5 Proof of Proposition 6

The proof consists in first rewriting the optimization problem (11) as a maximum entropy problem with a constraint over the average empirical risk. Then, we show that ϕ^* is solution of the optimization problem (OP) augmented with additional equality constraints in the hidden layers. We then remove the constraint over the average empirical risk and show that the solution $\phi^\dagger$ of the resulting OP provides a distribution with higher entropy than ϕ^*. By splitting the OP in sub-optimization problems by hidden layer, we show that $\phi^\dagger$ verifies Equation (12). Then, using recursively Assumption (5) on the activation function, we show that, for any layer, the first and second moments of the neuron activation are the same for both distribution $q_{\phi^\dagger}$ and q_{ϕ^*}. We then prove the equality of empirical risk for $q_{\phi^\dagger}$ and q_{ϕ^*}, leading to show that $\phi^\dagger$ is solution of Problem (11), from which we conclude that $\phi^\dagger = \phi^*$, as the solution is unique.

Proof Let's consider $\overline{w} \in \mathbb{R}^d$ and, for any $\phi \in \mathbb{R}^d$, the distribution $q_\phi \sim \overline{w} + \phi \odot z$ with $z \sim \mathcal{Z}$ such that $\mathcal{Z} \sim \mathcal{U}([-\sqrt{3}, \sqrt{3}]^d)$ or $\mathcal{Z} \sim \mathcal{N}(0, \mathrm{Id}_d)$. The optimization problem (11) is written:

$$\min_{\phi \in \mathbb{R}^d} \mathbb{E}_{q_\phi}\left[\mathcal{L}_\mathcal{S}(w)\right] - \lambda \sum_{k=1}^{d} \log(\phi_k^2). \tag{23}$$

It is assumed that the above optimization problem has a unique solution, denoted $\phi^* \in \mathbb{R}^d$. Then, there exists $\tau \in \mathbb{R}_+$ such that ϕ^* verifies the following optimization problem:

$$\begin{aligned} \max_{\phi \in \mathbb{R}^d} \quad & \sum_{k=1}^{d} \log(\phi_k^2) \\ \text{subject to} \quad & \mathbb{E}_{q_\phi}\left[\mathcal{L}_\mathcal{S}(w)\right] \leq \tau. \end{aligned} \tag{24}$$

Indeed, for $\tau = \mathbb{E}_{q_{\phi^*}}\left[\mathcal{L}_\mathcal{S}(w)\right]$, if we denote $\phi^{**} \in \mathbb{R}^d$ the solution of problem (24), then $\sum_{k=1}^{d} \log(\phi_k^{**2}) \geq \sum_{k=1}^{d} \log(\phi_k^{*2})$ and $\mathbb{E}_{q_{\phi^{**}}}\left[\mathcal{L}_\mathcal{S}(w)\right] \leq \tau$ which implies that:

$$\mathbb{E}_{q_{\phi^{**}}}\left[\mathcal{L}_\mathcal{S}(w)\right] - \lambda \sum_{k=1}^{d} \log(\phi_k^{**2}) \leq \mathbb{E}_{q_{\phi^*}}\left[\mathcal{L}_\mathcal{S}(w)\right] - \lambda \sum_{k=1}^{d} \log(\phi_k^{*2}).$$

From which we deduce that $\phi^{**} = \phi^*$, as the solution of Problem (23) is assumed unique. Moreover, ϕ^* is the unique solution of Problem (24).

For each layer, we define the amplitude of the input neuron activation on average over the training data:

$$a_{(l,k)}^2 = \frac{1}{n} \sum_{i=1}^{n} \mathbb{E}_{q_{\phi^*}} [\psi_{(l,k)}(x_i)^2] \quad \forall\, l \in [|0, L|]; k \in [|1, b|].$$

We also define the quantities $\sigma_{(l,j)}^2$, related to the variance of the output neurons, before activation, on average over the training data:

$$\sigma_{(l,j)}^2 = \frac{1}{n} \sum_{i=1}^{n} \mathbb{V}_{q_{\phi^*}} \left[\psi_{(l)}(x_i)^T \left(w_{(l,j)} - \overline{w}_{(l,j)} \right) \right] \quad \forall\, l \in [|0, L|]; j \in [|1, b_l|],$$

with $b_l = 1$ if $l = L$ and $b_l = b$ otherwise.
Let's now take $l \in [|0, L|]$ and $j \in [|1, b_l|]$, considering the independence between $\psi_{(l)}$ and $z_{(l,j)}$, we have:

$$\begin{aligned}
n\sigma_{(l,j)}^2 &= \sum_{i=1}^{n} \mathbb{V}_{q_{\phi^*}} [\psi_{(l)}(x_i)(\phi^*_{(l,j)} \odot z_{(l,j)})] \\
&= \sum_{i=1}^{n} \mathbb{V}_{q_{\phi^*}} \left[\sum_{k=1}^{b} \psi_{(l,k)}(x_i) \phi^*_{(l,j,k)} z_{(l,j,k)} \right] \\
&= \sum_{i=1}^{n} \sum_{u=1}^{b} \sum_{v=1}^{b} \phi^*_{(l,j,u)} \phi^*_{(l,j,v)} \text{Cov} \left(\psi_{(l,u)}(x_i) z_{(l,j,u)}, \psi_{(l,v)}(x_i) z_{(l,j,v)} \right) \\
&= \sum_{i=1}^{n} \sum_{u=1}^{b} \sum_{v=1}^{b} \phi^*_{(l,j,u)} \phi^*_{(l,j,v)} \mathbb{E}_{q_{\phi^*}} \left[\psi_{(l,u)}(x_i) \psi_{(l,v)}(x_i) \right] \mathbb{E}_{q_{\phi^*}} \left[z_{(l,j,u)} z_{(l,j,v)} \right].
\end{aligned}$$

For $u \neq v$, $z_{(l,j,u)} \perp\!\!\!\perp z_{(l,j,v)}$ and $\mathbb{E}_{q_{\phi^*}} \left[z_{(l,j,u)} z_{(l,j,v)} \right] = \mathbb{E}_{q_{\phi^*}} \left[z_{(l,j,u)} \right] \mathbb{E}_{q_{\phi^*}} \left[z_{(l,j,v)} \right] = 0$, then:

$$\begin{aligned}
\sigma_{(l,j)}^2 &= \frac{1}{n} \sum_{i=1}^{n} \sum_{k=1}^{b} \mathbb{E}_{q_{\phi^*}} [\psi_{(l,k)}(x_i)^2] {\phi^*_{(l,j,k)}}^2 \\
&= \sum_{k=1}^{b} a_{(l,k)}^2 {\phi^*_{(l,j,k)}}^2.
\end{aligned}$$

The optimization problem (24) is then equivalent to:

$$\begin{aligned}
&\max_{\phi \in \mathbb{R}^d} \quad \sum_{k=1}^{d} \log(\phi_k^2) \\
&\text{subject to:} \begin{cases} \mathbb{E}_{q_\phi} \left[\mathcal{L}_\mathcal{S}(w) \right] \leq \tau \\ \sum_{k=1}^{b} a_{(l,k)}^2 {\phi_{(l,j,k)}}^2 = \sigma_{(l,j)}^2 \quad \forall\, l \in [|0, L|]; j \in [|1, b_l|]. \end{cases}
\end{aligned} \tag{25}$$

Indeed, as problem (25) includes more constraints than problem (24), its solution necessarily provides a distribution of lower or equal entropy than q_{ϕ^*}. However, as the additional constraints are verified by ϕ^*, ϕ^* is the unique solution of problem (25).

We now remove the constraint over the average empirical risk and consider the following alternative optimization problem:

$$\begin{aligned} &\max_{\phi \in \mathbb{R}^d} \quad \sum_{k=1}^{d} \log(\phi_k^2) \\ &\text{subject to:} \quad \sum_{k=1}^{b} a_{(l,k)}^2 {\phi_{(l,j,k)}}^2 = \sigma_{(l,j)}^2 \quad \forall\, l \in [|0, L|]; j \in [|1, b_l|]. \end{aligned} \tag{26}$$

Considering a similar argument as before, the solution $\phi^\dagger$ of problem (26) necessarily provides a distribution of larger or equal entropy than ϕ^*, i.e.,

$$\sum_{k=1}^{d} \log({\phi_k^*}^2) \leq \sum_{k=1}^{d} \log({\phi_k^\dagger}^2). \tag{27}$$

Moreover, the optimization problem (26) can be decomposed in multiple sub-problems such that:

$$\phi^\dagger = \bigotimes_{l=0}^{L} \bigotimes_{j=1}^{b_l} \phi_{(l,j)}^\dagger,$$

with $\phi_{(l,j)}^\dagger \in \mathbb{R}^b$ for any $l \in [|0, L|]$, $j \in [|1, b_l|]$. The operator $\bigotimes$ is the concatenation operator. Each vector $\phi_{(l,j)}^\dagger$ is a solution of the following optimization sub-problem:

$$\begin{aligned} &\max_{\phi_{(l,j)} \in \mathbb{R}^b} \quad \sum_{k=1}^{b} \log(\phi_{(l,j,k)}^2) \\ &\text{subject to:} \quad \sum_{k=1}^{b} a_{(l,k)}^2 {\phi_{(l,j,k)}}^2 = \sigma_{(l,j)}^2. \end{aligned}$$

Then, by writing the Karush–Kuhn–Tucker conditions of the above optimization problem we get the following expression for the solution:

$${\phi_{(l,j,k)}^\dagger}^2 = \frac{\sigma_{(l,j)}^2}{b\, a_{(l,k)}^2} \quad \forall\, k \in [|1, b|].$$

Thus, $\phi^\dagger$ verifies Equation (12).

We now need to show that $\phi^\dagger$ provides the same empirical risk than ϕ^*. For this purpose, we consider $l \in [|0, L-1|]$ and assume that the first and the second moments of the neuron activation in layer l are the same for ϕ^* and $\phi^\dagger$, we will then show that this property is true in layer $l+1$. Let's then assume that:

$$\sum_{i=1}^{n} \mathbb{E}_{q_{\phi^*}} \left[\psi_{(l,j)}(x_i) \right] = \sum_{i=1}^{n} \mathbb{E}_{q_{\phi^\dagger}} \left[\psi_{(l,j)}(x_i) \right] \quad \forall\, j \in [|1, b|] \tag{28}$$

$$\sum_{i=1}^{n} \mathbb{E}_{q_{\phi^*}} \left[\psi_{(l)}(x_i) \psi_{(l)}(x_i)^T \right] = \sum_{i=1}^{n} \mathbb{E}_{q_{\phi^\dagger}} \left[\psi_{(l)}(x_i) \psi_{(l)}(x_i)^T \right]. \tag{29}$$

Let's define $U_i = (U_{i1}, ..., U_{ib})$ with $U_{ij} = \psi_{(l)}(x_i)^T w_{(l,j)}$ $\forall i \in [|1, n|],\ \forall j \in [|1, b|]$. Considering Equation (28), for any $j \in [|1, b|]$, we have:

$$\sum_{i=1}^{n} \mathbb{E}_{q_{\phi^\dagger}} \left[U_{ij} \right] = \sum_{i=1}^{n} \mathbb{E}_{q_{\phi^\dagger}} \left[\psi_{(l)}(x_i) \right]^T \overline{w}_{(l,j)} = \sum_{i=1}^{n} \mathbb{E}_{q_{\phi^*}} \left[\psi_{(l)}(x_i) \right]^T \overline{w}_{(l,j)} = \sum_{i=1}^{n} \mathbb{E}_{q_{\phi^*}} \left[U_{ij} \right]. \quad (30)$$

Moreover, for any $k, j \in [|1, b|]$ such that $k \neq j$, we have:

$$\begin{aligned}
\sum_{i=1}^{n} \mathbb{E}_{q_{\phi^\dagger}} \left[U_i U_i^T \right]_{kj} &= \sum_{i=1}^{n} \mathbb{E}_{q_{\phi^\dagger}} \left[U_{ik} U_{ij} \right] \\
&= \sum_{i=1}^{n} \mathbb{E}_{q_{\phi^\dagger}} \left[\left(\psi_{(l)}(x_i)^T w_{(l,k)} \right) \left(\psi_{(l)}(x_i)^T w_{(l,j)} \right) \right] \\
&= \sum_{i=1}^{n} \sum_{u=1}^{b} \sum_{v=1}^{b} \mathbb{E}_{q_{\phi^\dagger}} \left[\psi_{(l,u)}(x_i) \psi_{(l,v)}(x_i) \right] \mathbb{E}_{q_{\phi^\dagger}} \left[w_{(l,k,u)} w_{(l,j,v)} \right] \\
&= \sum_{u=1}^{b} \sum_{v=1}^{b} \left(\sum_{i=1}^{n} \mathbb{E}_{q_{\phi^\dagger}} \left[\psi_{(l,u)}(x_i) \psi_{(l,v)}(x_i) \right] \right) \overline{w}_{(l,k,u)} \overline{w}_{(l,j,v)} \\
&= \sum_{i=1}^{n} \overline{w}_{(l,k)}^T \left(\sum_{i=1}^{n} \mathbb{E}_{q_{\phi^\dagger}} \left[\psi_{(l)}(x_i) \psi_{(l)}(x_i)^T \right] \right) \overline{w}_{(l,j)} \\
&= \sum_{i=1}^{n} \overline{w}_{(l,k)}^T \left(\sum_{i=1}^{n} \mathbb{E}_{q_{\phi^*}} \left[\psi_{(l)}(x_i) \psi_{(l)}(x_i)^T \right] \right) \overline{w}_{(l,j)} \quad \text{(considering Equation (29))} \\
&= \sum_{i=1}^{n} \mathbb{E}_{q_{\phi^*}} \left[U_i U_i^T \right]_{kj}.
\end{aligned} \quad (31)$$

Then, for any $j \in [|1, b|]$, we have:

$$\begin{aligned}
\sum_{i=1}^{n} \mathbb{E}_{q_{\phi^\dagger}} \left[U_i U_i^T \right]_{jj} &= \sum_{i=1}^{n} \mathbb{E}_{q_{\phi^\dagger}} \left[\left(\psi_{(l)}(x_i)^T w_{(l,j)} \right)^2 \right] \\
&= \sum_{i=1}^{n} \left(\mathbb{V}_{q_{\phi^\dagger}} \left[\psi_{(l)}(x_i)^T (w_{(l,j)} - \overline{w}_{(l,j)}) \right] + \mathbb{E}_{q_{\phi^\dagger}} \left[\left(\psi_{(l)}(x_i)^T \overline{w}_{(l,j)} \right)^2 \right] \right) \\
&= \sum_{i=1}^{n} \left(\sum_{k=1}^{b} \mathbb{E}_{q_{\phi^\dagger}} [\psi_{(l,k)}(x_i)^2] {\phi^\dagger_{(l,j,k)}}^2 + \overline{w}_{(l,j)}^T \mathbb{E}_{q_{\phi^\dagger}} \left[\psi_{(l)}(x_i) \psi_{(l)}(x_i)^T \right] \overline{w}_{(l,j)} \right) \\
&= \sum_{i=1}^{n} \left(\sum_{k=1}^{b} \mathbb{E}_{q_{\phi^*}} [\psi_{(l,k)}(x_i)^2] {\phi^\dagger_{(l,j,k)}}^2 + \overline{w}_{(l,j)}^T \mathbb{E}_{q_{\phi^*}} \left[\psi_{(l)}(x_i) \psi_{(l)}(x_i)^T \right] \overline{w}_{(l,j)} \right).
\end{aligned}$$

Where the last equality is deducted from Equation (29). Moreover, the first term can be developed as follows:

$$\begin{aligned}
\sum_{i=1}^{n}\sum_{k=1}^{b}\mathbb{E}_{q_{\phi^*}}[\psi_{(l,k)}(x_i)^2]{\phi^\dagger_{(l,j,k)}}^2 &= \sum_{k=1}^{b} n\, a_{(l,k)}^2 {\phi^\dagger_{(l,j,k)}}^2 \\
&= \sum_{k=1}^{b} n\, a_{(l,k)}^2 \frac{\sigma_{(l,j)}^2}{b\, a_{(l,k)}^2} \quad \text{by definition of } \phi^\dagger \\
&= n\, \sigma_{(l,j)}^2 \\
&= \sum_{i=1}^{n} \mathbb{V}_{q_{\phi^*}}\left[\psi_{(l)}(x_i)^T\left(w_{(l,j)} - \overline{w}_{(l,j)}\right)\right].
\end{aligned}$$

We then deduce that:

$$\sum_{i=1}^{n}\mathbb{E}_{q_{\phi^\dagger}}\left[U_i U_i^T\right]_{jj} = \sum_{i=1}^{n}\mathbb{E}_{q_{\phi^*}}\left[U_i U_i^T\right]_{jj}. \tag{32}$$

Equations (31) and (32) implies that $\sum_{i=1}^{n}\mathbb{E}_{q_{\phi^\dagger}}\left[U_i U_i^T\right] = \sum_{i=1}^{n}\mathbb{E}_{q_{\phi^*}}\left[U_i U_i^T\right]$. Considering this last equality, Equation (30) and Assumption (5), we then conclude that:

$$\sum_{i=1}^{n}\mathbb{E}_{q_{\phi^\dagger}}\left[\zeta\left(U_i\right)\right] = \sum_{i=1}^{n}\mathbb{E}_{q_{\phi^*}}\left[\zeta\left(U_i\right)\right] \tag{33}$$

$$\sum_{i=1}^{n}\mathbb{E}_{q_{\phi^\dagger}}\left[\zeta\left(U_i\right)\zeta\left(U_i\right)^T\right] = \sum_{i=1}^{n}\mathbb{E}_{q_{\phi^*}}\left[\zeta\left(U_i\right)\zeta\left(U_i\right)^T\right]. \tag{34}$$

Where,

$$\zeta\left(U_i\right) = \left(\zeta\left(\psi_{(l)}(x_i)w_{(l,1)}\right), ..., \zeta\left(\psi_{(l)}^T(x_i)w_{(l,p)}\right)\right) = \psi_{(l+1)}(x_i).$$

Then Equations (33) and (34) are equivalent to the moments' equality in Equations (28) and (29) applied to layer $l+1$. As these equations are true for $l=0$, then, by recurrence, we have Equations (28) and (29) for $l = L+1$, then:

$$\sum_{i=1}^{n}\mathbb{E}_{q_{\phi^\dagger}}\left[h(x_i)\right] = \sum_{i=1}^{n}\mathbb{E}_{q_{\phi^*}}\left[h(x_i)\right] \quad \text{and} \quad \sum_{i=1}^{n}\mathbb{E}_{q_{\phi^\dagger}}\left[h(x_i)^2\right] = \sum_{i=1}^{n}\mathbb{E}_{q_{\phi^*}}\left[h(x_i)^2\right].$$

Moreover, by developing the empirical risk, we have:

$$\mathcal{L}_{\mathcal{S}}(w) = \sum_{i=1}^{n}\left(h(x_i) - y_i\right)^2 = \sum_{i=1}^{n}\left(h(x_i)^2 - 2h(x_i)y_i + y_i^2\right).$$

From which we deduce that:

$$\mathbb{E}_{q_{\phi^\dagger}}\left[\mathcal{L}_{\mathcal{S}}(w)\right] = \mathbb{E}_{q_{\phi^*}}\left[\mathcal{L}_{\mathcal{S}}(w)\right].$$

Then, considering Equation (27) and the uniqueness of the solution of Problem (24), we conclude that $\phi^\dagger = \phi^*$.

■

Appendix B. Hyperparameters Impact Analysis

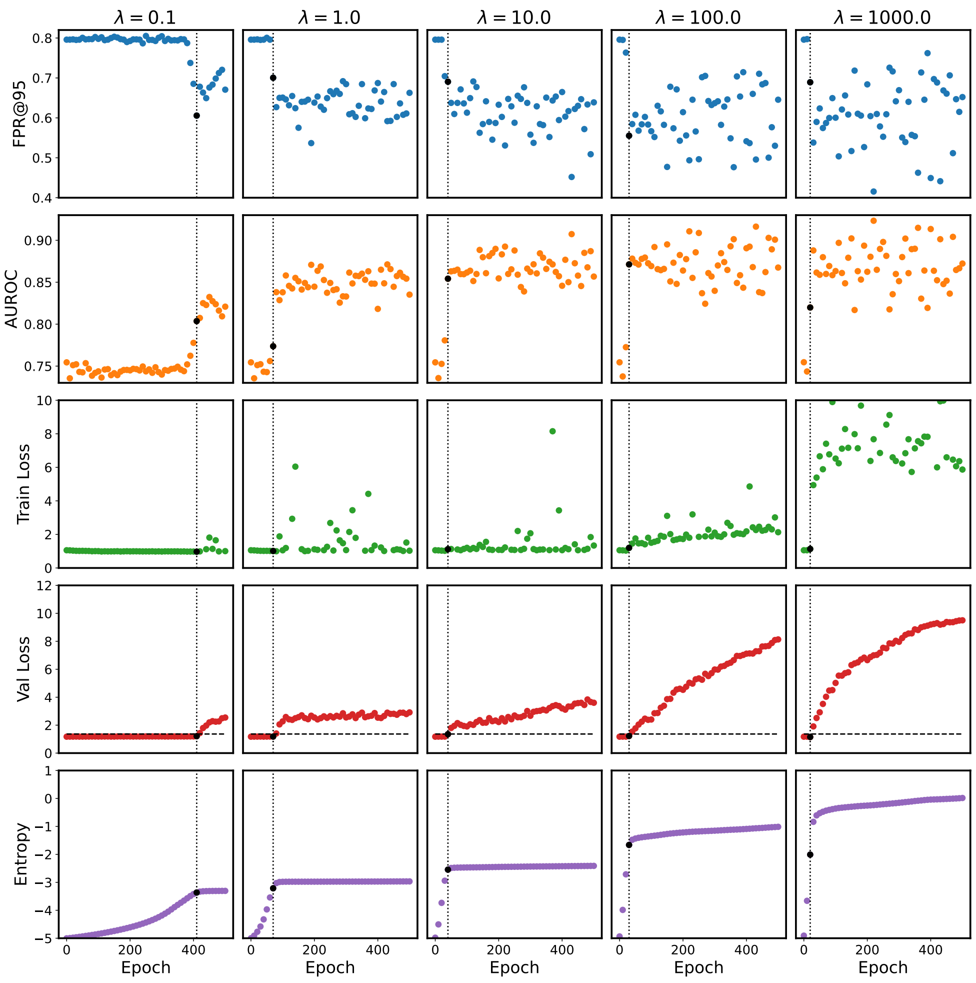

Figure 9: Hyperparameter analysis of MaxWEntSVD for the Weather-Shift experiment. Evolution of the five metrics: FPR@95, AUROC, training loss, validation loss, and weight entropy across epochs for different values of λ (note that a scaling factor of $1/d$ is further applied to λ). The horizontal dashed lines in the validation loss plots represent the threshold τ and the dotted vertical lines indicate the stopping epoch (after which the validation loss exceeds τ). We observe that higher λ values lead to better FPR and AUROC, along with higher entropy. At a certain epoch, entropy increases rapidly, coinciding with improved OOD detection performance but also an increase in validation loss. For high λ values and late epochs, the variance in OOD detection metrics between epochs becomes large. The stopping criterion ensures that training stops when AUROC is high but with reduced variance. For $\lambda = 1000$, the training loss is large and fluctuating, with high variance in OOD detection metrics, suggesting that the training loss stability should be taken into account when selecting the λ value.

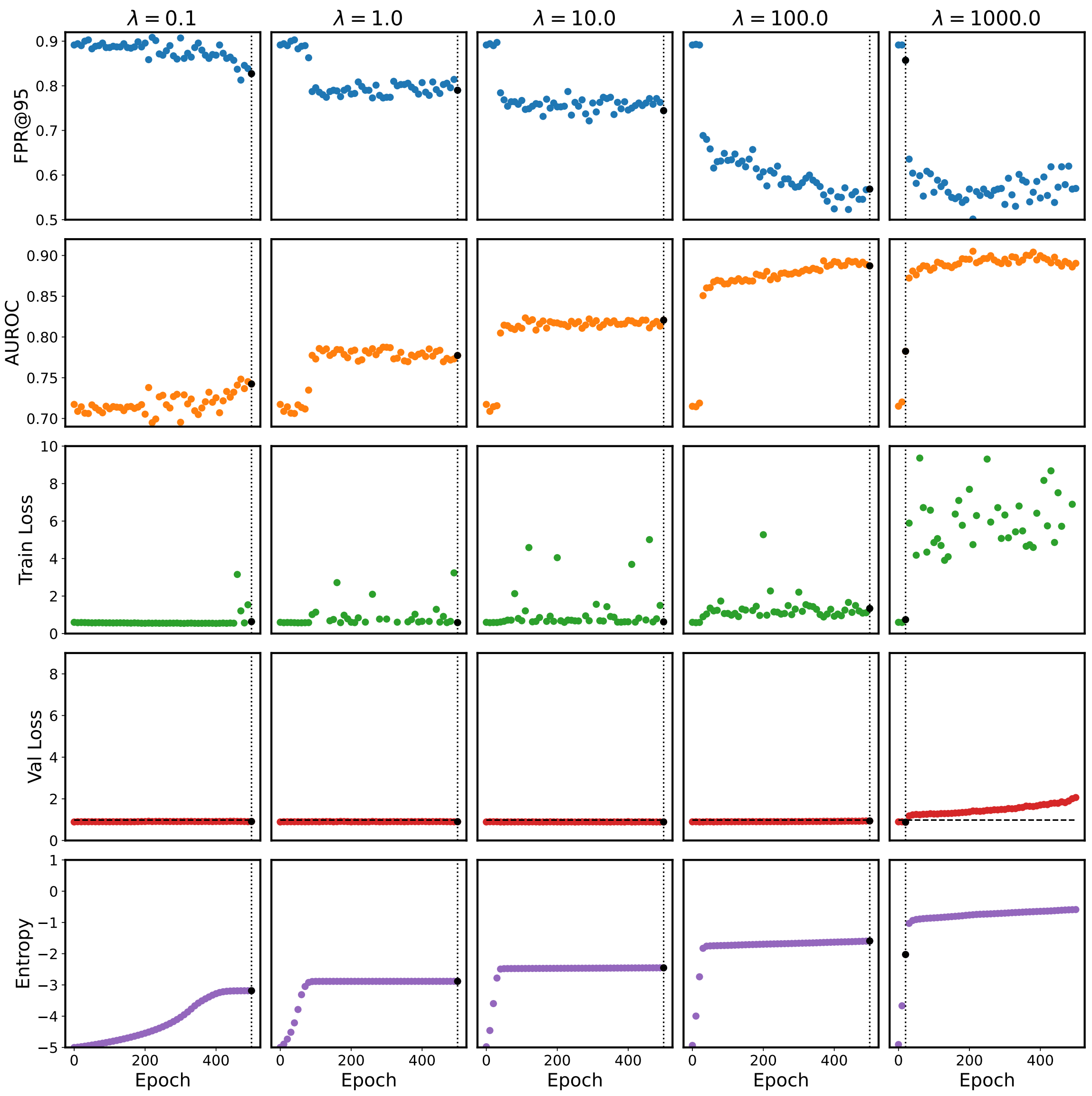

Figure 10: Hyperparameter analysis of MaxWEntSVD for the BigBus-Shift experiment. Evolution of the five metrics: FPR@95, AUROC, training loss, validation loss, and entropy across epochs for different values of λ (note that a scaling factor of $1/d$ is further applied to λ). The horizontal dashed lines in the validation loss plots represent the threshold τ and the dotted vertical lines indicate the stopping epoch (after which the validation loss exceeds τ). We observe that higher λ values lead to better FPR and AUROC, along with higher entropy. At a certain epoch, entropy increases rapidly, coinciding with improved OOD detection performance. The increase in validation loss is only observed for $\lambda = 1000$. In this setting, the OOD detection performance remains stable for late epochs although the training loss is unstable.

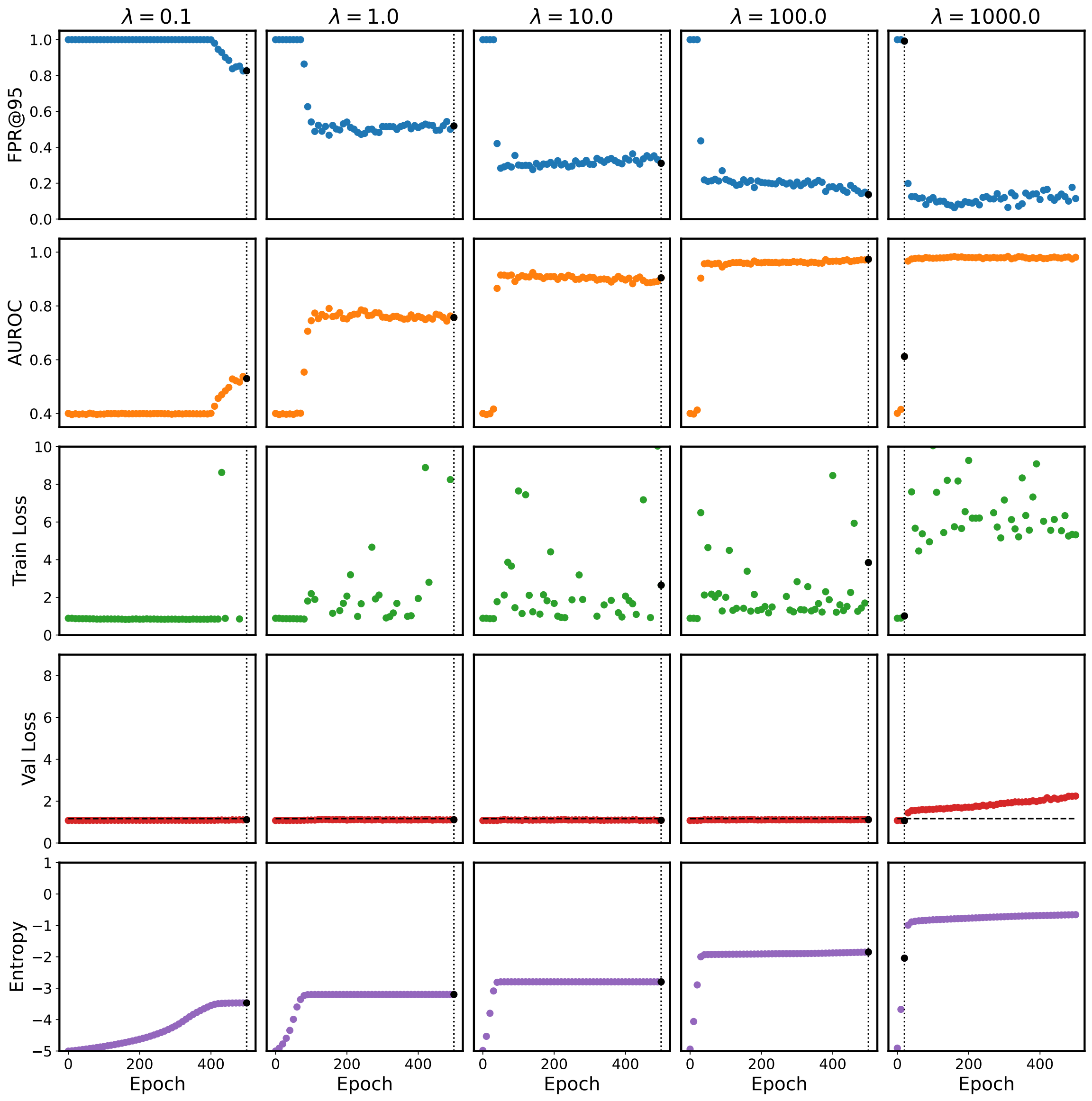

Figure 11: Hyperparameter analysis of MaxWEntSVD for the Cameras-Shift experiment. Evolution of the five metrics: FPR@95, AUROC, training loss, validation loss, and entropy across epochs for different values of λ (note that a scaling factor of $1/d$ is further applied to λ). The horizontal dashed lines in the validation loss plots represent the threshold τ and the dotted vertical lines indicate the stopping epoch (after which the validation loss exceeds τ). We observe that higher λ values lead to better FPR and AUROC, along with higher entropy. At a certain epoch, entropy increases rapidly, coinciding with improved OOD detection performance. The increase in validation loss is only observed for $\lambda = 1000$. In this setting, the OOD detection performance remains stable for late epochs although the training loss is unstable.

The analysis of the hyperparameter impact across the three experiments Weather, BigBus, and Camera Shift (Figures 9, 10, 11) demonstrates that larger values of λ generally result in improved OOD detection performances. In the Weather Shift experiment, however, a significant variance in OOD detection metrics is observed for high λ values during later epochs. Furthermore, for $\lambda = 1000$, the training loss is highly unstable across all three experiments, indicating that while larger λ values tend to improve performance, excessively large values can lead to instability during training. Additionally, it should be noted that, in the Weather Shift experiment, the stopping criterion effectively selects an epoch with lower variance in OOD metrics and a reasonable validation loss.

The detailed metrics obtained at the stopping epoch are reported for all λ values in Table 7. The results reveal that weight entropy is closely aligned with OOD performance: higher entropy corresponds to better AUROC and lower FPR. Although $\lambda = 1000$ yields the highest entropy after 500 epochs, the stopping criterion stops the training at an epoch where the entropy is lower than that for $\lambda = 100$. This observation suggests that hyperparameter selection should be guided by both entropy and validation loss. Specifically, users should select a λ value that produces a model with the highest entropy, while ensuring the validation loss remains below the threshold τ. Importantly, it should be highlighted that the lowest validation loss does not correspond to the best OOD detection performance.

In summary, while OOD metrics tend to improve with more epochs, the variance between epochs also increases in some cases. OOD performance and entropy generally increase with higher λ values, but when λ is too large, training becomes unstable and validation loss quickly exceeds the threshold. Therefore, the recommended approach is to use the stopping criterion to maintain a reasonable validation loss and select λ based on the resulting entropy. A well-performing model is characterized by high entropy and reasonable validation loss. Both metrics can be measured without using OOD data, which enables a practical approach to select the hyperparameter λ.

Exp	BigBus				Cameras				Weather			
λ	AUC	FPR95	Ent.	Val	AUC	FPR95	Ent.	Val	AUC	FPR95	Ent.	Val
0.1	0.74	0.83	-3.19	0.91	0.53	0.83	-3.47	1.11	0.8	0.61	-3.36	1.21
1.0	0.78	0.79	-2.88	0.9	0.76	0.52	-3.2	1.11	0.77	0.7	-3.21	1.18
10.0	0.82	0.74	-2.45	0.89	0.9	0.31	-2.8	1.09	0.85	0.69	-2.55	1.35
100.0	**0.89**	**0.57**	**-1.59**	0.94	**0.97**	**0.14**	**-1.85**	1.12	**0.87**	**0.56**	**-1.66**	1.22
1000.0	0.78	0.86	-2.03	**0.88**	0.61	0.99	-2.04	**1.07**	0.82	0.69	-2.01	**1.15**

Table 7: Metrics for different values of λ obtained at the stopping epoch. The table presents the AUC, FPR95, weight entropy (Ent.), and validation NLL (Val) for the three datasets BigBus, Cameras, and Weather. Lower FPR95 values and higher AUC scores indicate better OOD detection performance, while lower validation NLL account for better ID performance. The entropy measures the diversity of the weight distribution. We observe that the λ providing the highest weight entropy at the stopping epoch achieves the best AUC and FPR. In contrast, the λ corresponding to the lowest validation loss does not yield the best overall performance.

Appendix C. Achieving MaxWEnt's Behavior in Bayesian Neural Networks

In this section, we conduct an ablation study to identify the key components that enable a Bayesian Neural Network (BNN) with a Gaussian prior to exhibit behaviors similar to those of MaxWEnt and MaxWEnt-SVD. We identified three critical factors: frozen mean, large prior variance, and SVD parameterization. Experiments were performed on the synthetic classification dataset and the eight UCI regression datasets introduced in Section 7.5.

In this study, we consider a non-MC-Dropout BNN trained with stochastic variational inference (Hoffman et al., 2013) using the reparameterization trick (Kingma and Welling, 2014). We use the KL-weighted ELBO optimization involving a λ parameter to weight the KL term as follows:

$$\max_{\theta \in \mathbb{R}^D} \mathbb{E}_{q_\theta} \left[\sum_{(x,y) \in \mathcal{S}} \log(p(y|h_w(x)) \right] - \lambda D_{\text{KL}} \left(q_\theta(w), p(w) \right).$$

This formulation is commonly adopted in practice for the variational Bayes approach to Bayesian neural networks (Wenzel et al., 2020a). The use of a trade-off parameter enables the direct comparison with the MaxWEnt objective. In the following, we adopt the same trade-off factor as for MaxWEnt, such that $\lambda = 10\frac{n}{d}$. We consider a Gaussian isotropic prior $p(w)$ of variance σ^2 and a Gaussian posterior $q_\theta(w) \sim \mathcal{N}(\mu, \Sigma)$, with $\theta = (\mu, \Sigma)$ the posterior parameters.

The following settings are examined:

- **SVD vs. No SVD**: In both settings, the posterior variance Σ is parameterized by the vector $\phi \in \mathbb{R}^d$, such that $\Sigma = \text{diag}(\phi^2)$ (No SVD) or $\Sigma = V\text{diag}(\phi^2)V^T$ (SVD), using the matrix V defined in Section 3.3.2.

- **Frozen vs. Unfrozen Mean**: For the frozen mean case, the posterior mean μ is trained along with Σ; the prior is centered on 0 such that $p(w) \sim \mathcal{N}(0, \sigma^2 \text{Id}_d)$, which corresponds to the usual setting for BNNs. For the unfrozen mean case, the posterior mean is equal to the weights of a pretrained neural network, such that $\mu = \overline{w}$ is fixed during training, as implemented in MaxWEnt. Accordingly, the prior is set to $\mathcal{N}(\overline{w}, \sigma^2 \text{Id}_d)$.

- **Large vs. Small Prior Variance $\boldsymbol{\sigma}^2$**: We have highlighted in Section 5.2 that the MaxWEnt optimization is related to the BNN training with Gaussian prior of large variance. To showcase the impact of the prior variance we consider both setting $\sigma^2 \ll 1$ $(\sigma^2 = 0.1)$ and $\sigma^2 \gg 1$ $(\sigma^2 = 10^{10})$.

It should be noted that the SVD parameterization requires a frozen posterior mean. Hence, the implementation choices above results in six different setup combinations. For all experiments, all networks are trained during 500 epochs and implement the stopping criterion presented in Section 7.5.4, providing a consistent basis for comparison.

C.1 Synthetic Classification

We consider the synthetic classification dataset described in Section 7.1. The results for the six setting combinations are reported in Figure 8. The left and right columns respectively present the results obtained with low and large variance prior. We observe that for all settings enlarging the prior variance increases the contrast between in-distribution and out-of-distribution uncertainty.

		Low prior variance	**Large prior variance**
No SVD	**Unfrozen Mean**	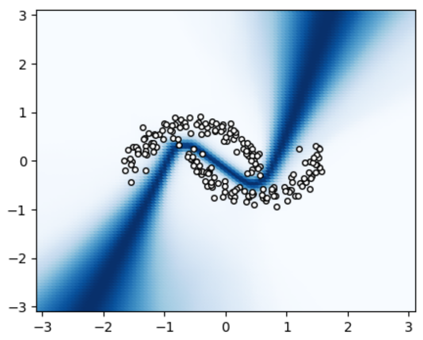	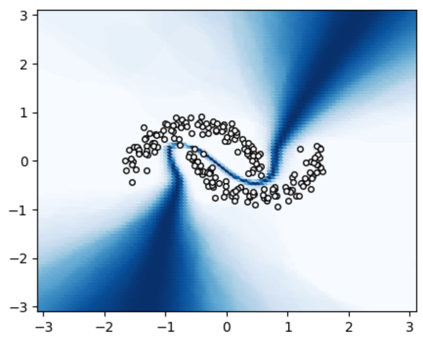
	Frozen Mean	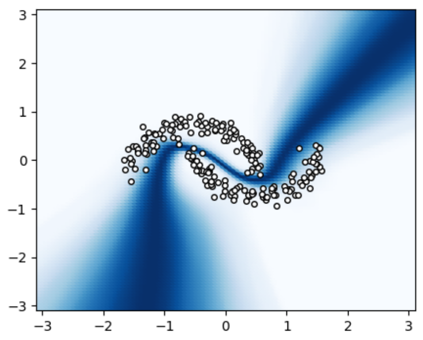	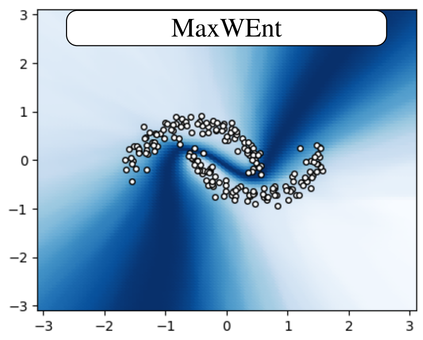
SVD	**Frozen Mean**	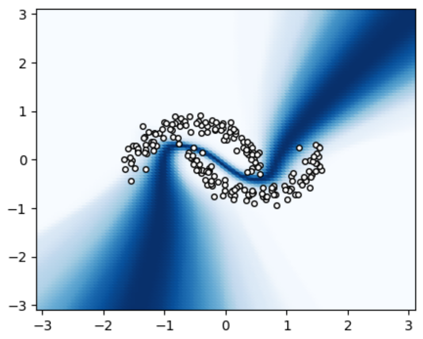	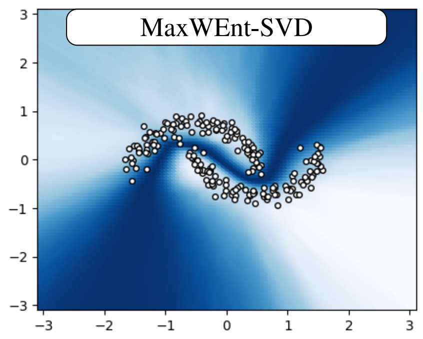

Table 8: Comparison of BNN settings on the synthetic classification dataset. White points represent training data, and shades of blue indicate uncertainty.

Additionally, the results highlight that the two settings "frozen mean" and SVD-parameterization, used for the MaxWEnt and MaxWEnt-SVD approaches, improve the epistemic uncertainty quantification.

C.2 UCI datasets

Table 9 presents the OOD detection performance for different BNN settings on the 8 UCI datasets. We report our observations as follows:

		No SVD				SVD	
		Unfrozen mean		Frozen mean		Frozen mean	
		$\sigma^2 \ll 1$	$\sigma^2 \gg 1$	$\sigma^2 \ll 1$	$\sigma^2 \gg 1$	$\sigma^2 \ll 1$	$\sigma^2 \gg 1$
AUC	extrapol	0.659	0.692	0.761	0.775	0.795	**0.843**
	interpol	0.450	0.556	0.524	0.559	0.656	**0.783**
FPR	extrapol	0.698	0.639	0.594	0.576	0.503	**0.407**
	interpol	0.950	0.897	0.895	0.852	0.765	**0.535**
Val	extrapol	-0.318	-0.100	-0.638	-0.623	**-0.649**	-0.62
	interpol	-0.169	0.633	-0.359	-0.342	**-0.409**	-0.371

Table 9: Comparison of the BNN settings for the UCI experiments. The table presents the average OOD detection metrics (AUC, FPR) and Validation NLL (Val) across the 8 UCI datasets for interpolation (interpol) and extrapolation (extrapol) settings. Higher AUC and lower FPR are better. Columns compare BNN settings with and without SVD parameterization and "frozen mean", under small ($\sigma^2 \ll 1$) and large ($\sigma^2 \gg 1$) prior variances.

- **Effectiveness of large variance prior.** For frozen and unfrozen mean, SVD and No SVD settings, the use of a large variance prior instead of a low variance significantly improves the OOD detection performances (e.g., for the interpolation experiments with the SVD parameterization the FPR drops from 0.765 to 0.535).
- **Impact of frozen mean.** Freezing the mean improves the OOD detection performances compared to the unfrozen mean setting. For instance, with large prior variance in the extrapolation experiments, the FPR decreases from 0.639 to 0.576 when using a frozen mean. A similar effect is observed in the synthetic experiment, where the uncertainty between the two classes is lower for the unfrozen mean setting. A possible explanation to this phenomenon is that using a frozen mean shifts the training focus to the scale parameters, which are directly related to weight entropy, hence promoting an increase in entropy.
- **Impact of SVD parameterization.** Incorporating the SVD parameterization to the BNN significantly increase the OOD detection performances, even with low prior variance. Further improvements are obtained when enlarging the prior variance.
- **The validation NLL is smaller when using the low variance prior.** The use of a large prior consistently degrades the validation NLL. For example, in the Unfrozen mean case, NLL increases from -0.169 to 0.633 in the interpolation setting. This observation highlights that validation NLL is not a suitable metric for promoting weight entropy and improving OOD performances. Interestingly, the best validation NLL is obtained with the SVD parameterization and low prior variance, suggesting that traditional BNNs could benefit from SVD parameterization to improve in-distribution performance.

In conclusion, enlarging the prior variance, and then the weight entropy, effectively improves OOD detection performances in all settings. While the SVD parameterization with small prior variance already improves OOD detection performance, increasing the variance further yields a significant improvement, especially in the challenging interpolation setting.

References

Moloud Abdar, Farhad Pourpanah, Sadiq Hussain, Dana Rezazadegan, Li Liu, Mohammad Ghavamzadeh, Paul Fieguth, Xiaochun Cao, Abbas Khosravi, U Rajendra Acharya, et al. A review of uncertainty quantification in deep learning: Techniques, applications and challenges. *Information Fusion*, 76:243–297, 2021.

Alexander Amini, Wilko Schwarting, Ava Soleimany, and Daniela Rus. Deep evidential regression. *Advances in Neural Information Processing Systems*, 33:14927–14937, 2020.

Anastasios Nikolas Angelopoulos, Stephen Bates, Michael Jordan, and Jitendra Malik. Uncertainty sets for image classifiers using conformal prediction. In *International Conference on Learning Representations*, 2020.

Martin Arjovsky, Soumith Chintala, and Léon Bottou. Wasserstein generative adversarial networks. In Doina Precup and Yee Whye Teh, editors, *Proceedings of the 34th International Conference on Machine Learning*, volume 70 of *Proceedings of Machine Learning Research*, pages 214–223, International Convention Centre, Sydney, Australia, 06–11 Aug 2017. PMLR. URL `http://proceedings.mlr.press/v70/arjovsky17a.html`.

Arsenii Ashukha, Alexander Lyzhov, Dmitry Molchanov, and Dmitry Vetrov. Pitfalls of in-domain uncertainty estimation and ensembling in deep learning. In *International Conference on Learning Representations*, 2019.

Andrei Atanov, Arsenii Ashukha, Kirill Struminsky, Dmitriy Vetrov, and Max Welling. The deep weight prior. In *International Conference on Learning Representations*, 2018.

Abhijit Bendale and Terrance E Boult. Towards open set deep networks. In *Proceedings of the IEEE conference on computer vision and pattern recognition*, pages 1563–1572, 2016.

Adam Berger, Stephen A Della Pietra, and Vincent J Della Pietra. A maximum entropy approach to natural language processing. *Computational linguistics*, 22(1):39–71, 1996.

Charles Blundell, Julien Cornebise, Koray Kavukcuoglu, and Daan Wierstra. Weight uncertainty in neural network. In *International conference on machine learning*, pages 1613–1622. PMLR, 2015.

Shahin Boluki, Randy Ardywibowo, Siamak Zamani Dadaneh, Mingyuan Zhou, and Xiaoning Qian. Learnable bernoulli dropout for bayesian deep learning. In *International Conference on Artificial Intelligence and Statistics*, pages 3905–3916. PMLR, 2020.

S Boyd, L Vandenberghe, and L Faybusovich. Convex optimization. *IEEE Transactions on Automatic Control*, 51(11):1859–1859, 2006.

Senqi Cao and Zhongfei Zhang. Deep hybrid models for out-of-distribution detection. In *Proceedings of the IEEE/CVF Conference on Computer Vision and Pattern Recognition*, pages 4733–4743, 2022.

Guangyao Chen, Peixi Peng, Xiangqian Wang, and Yonghong Tian. Adversarial reciprocal points learning for open set recognition. *IEEE Transactions on Pattern Analysis and Machine Intelligence*, 44(11):8065–8081, 2021.

Francesco D'Angelo and Vincent Fortuin. Repulsive deep ensembles are bayesian. *Advances in Neural Information Processing Systems*, 34, 2021.

Antoine de Mathelin, François Deheeger, Mathilde Mougeot, and Nicolas Vayatis. Discrepancy-based active learning for domain adaptation. In *International Conference on Learning Representations*, 2022.

Antoine de Mathelin, Francois Deheeger, Mathilde Mougeot, and Nicolas Vayatis. Deep anti-regularized ensembles provide reliable out-of-distribution uncertainty quantification. *arXiv preprint arXiv:2304.04042*, 2023.

Jia Deng, Wei Dong, Richard Socher, Li-Jia Li, Kai Li, and Li Fei-Fei. Imagenet: A large-scale hierarchical image database. In *2009 IEEE conference on computer vision and pattern recognition*, pages 248–255. Ieee, 2009.

Li Deng. The mnist database of handwritten digit images for machine learning research [best of the web]. *IEEE signal processing magazine*, 29(6):141–142, 2012.

Terrance DeVries and Graham W Taylor. Learning confidence for out-of-distribution detection in neural networks. *arXiv preprint arXiv:1802.04865*, 2018.

Xuefeng Du, Zhaoning Wang, Mu Cai, and Yixuan Li. Vos: Learning what you don't know by virtual outlier synthesis. In *International Conference on Learning Representations*, 2022.

John Duchi. Derivations for linear algebra and optimization. *Berkeley, California*, 3(1):2325–5870, 2007.

Andrew YK Foong, Yingzhen Li, José Miguel Hernández-Lobato, and Richard E Turner. 'in-between'uncertainty in bayesian neural networks. *arXiv preprint arXiv:1906.11537*, 2019.

Vincent Fortuin. Priors in bayesian deep learning: A review. *International Statistical Review*, 90 (3):563–591, 2022.

Vincent Fortuin, Adrià Garriga-Alonso, Sebastian W Ober, Florian Wenzel, Gunnar Ratsch, Richard E Turner, Mark van der Wilk, and Laurence Aitchison. Bayesian neural network priors revisited. In *International Conference on Learning Representations*, 2021.

Yarin Gal and Zoubin Ghahramani. Dropout as a bayesian approximation: Representing model uncertainty in deep learning. In *international conference on machine learning*, pages 1050–1059. PMLR, 2016.

Yarin Gal, Jiri Hron, and Alex Kendall. Concrete dropout. *Advances in neural information processing systems*, 30, 2017.

Andrew Gelman. Prior choice recommendations, 2020. URL `https://github.com/standev/stan/wiki/Prior-Choice-Recommendations`.

Soumya Ghosh, Jiayu Yao, and Finale Doshi-Velez. Model selection in bayesian neural networks via horseshoe priors. *J. Mach. Learn. Res.*, 20(182):1–46, 2019.

Xavier Glorot and Yoshua Bengio. Understanding the difficulty of training deep feedforward neural networks. In *In Proceedings of the International Conference on Artificial Intelligence and Statistics (AISTATS'10). Society for Artificial Intelligence and Statistics*, 2010.

James-A Goulet, Luong Ha Nguyen, and Saeid Amiri. Tractable approximate gaussian inference for bayesian neural networks. *The Journal of Machine Learning Research*, 22(1):11374–11396, 2021.

Alex Graves. Practical variational inference for neural networks. *Advances in neural information processing systems*, 24, 2011.

Chuan Guo, Geoff Pleiss, Yu Sun, and Kilian Q Weinberger. On calibration of modern neural networks. In *International conference on machine learning*, pages 1321–1330. PMLR, 2017a.

Chuan Guo, Geoff Pleiss, Yu Sun, and Kilian Q Weinberger. On calibration of modern neural networks. In *International conference on machine learning*, pages 1321–1330. PMLR, 2017b.

Kaiming He, Xiangyu Zhang, Shaoqing Ren, and Jian Sun. Deep residual learning for image recognition. In *Proceedings of the IEEE conference on computer vision and pattern recognition*, pages 770–778, 2016.

Dan Hendrycks and Kevin Gimpel. A baseline for detecting misclassified and out-of-distribution examples in neural networks. In *International Conference on Learning Representations*, 2017.

Dan Hendrycks, Steven Basart, Mantas Mazeika, Andy Zou, Joseph Kwon, Mohammadreza Mostajabi, Jacob Steinhardt, and Dawn Song. Scaling out-of-distribution detection for real-world settings. In *International Conference on Machine Learning*, pages 8759–8773. PMLR, 2022a.

Dan Hendrycks, Andy Zou, Mantas Mazeika, Leonard Tang, Bo Li, Dawn Song, and Jacob Steinhardt. Pixmix: Dreamlike pictures comprehensively improve safety measures. In *Proceedings of the IEEE/CVF Conference on Computer Vision and Pattern Recognition*, pages 16783–16792, 2022b.

Christian Henning, Francesco D'Angelo, and Benjamin F Grewe. Are bayesian neural networks intrinsically good at out-of-distribution detection? *arXiv preprint arXiv:2107.12248*, 2021.

Matthew D Hoffman, David M Blei, Chong Wang, and John Paisley. Stochastic variational inference. *Journal of Machine Learning Research*, 2013.

Yen-Chang Hsu, Yilin Shen, Hongxia Jin, and Zsolt Kira. Generalized odin: Detecting out-of-distribution image without learning from out-of-distribution data. In *Proceedings of the IEEE/CVF Conference on Computer Vision and Pattern Recognition*, pages 10951–10960, 2020.

Rui Huang and Yixuan Li. Mos: Towards scaling out-of-distribution detection for large semantic space. In *Proceedings of the IEEE/CVF Conference on Computer Vision and Pattern Recognition*, pages 8710–8719, 2021.

Rui Huang, Andrew Geng, and Yixuan Li. On the importance of gradients for detecting distributional shifts in the wild. *Advances in Neural Information Processing Systems*, 34:677–689, 2021a.

Ziyi Huang, Henry Lam, and Haofeng Zhang. Quantifying epistemic uncertainty in deep learning. *arXiv preprint arXiv:2110.12122*, 2021b.

Eyke Hüllermeier and Willem Waegeman. Aleatoric and epistemic uncertainty in machine learning: An introduction to concepts and methods. *Machine Learning*, 110:457–506, 2021.

Pavel Izmailov, Wesley J Maddox, Polina Kirichenko, Timur Garipov, Dmitry Vetrov, and Andrew Gordon Wilson. Subspace inference for bayesian deep learning. In *Uncertainty in Artificial Intelligence*, pages 1169–1179. PMLR, 2020.

Siddhartha Jain, Ge Liu, Jonas Mueller, and David Gifford. Maximizing overall diversity for improved uncertainty estimates in deep ensembles. In *Proceedings of the AAAI Conference on Artificial Intelligence*, volume 34, pages 4264–4271, 2020.

Edwin T Jaynes. Information theory and statistical mechanics. *Physical review*, 106(4):620, 1957.

Edwin T Jaynes. Prior probabilities. *IEEE Transactions on systems science and cybernetics*, 4(3): 227–241, 1968.

Laurent Valentin Jospin, Hamid Laga, Farid Boussaid, Wray Buntine, and Mohammed Bennamoun. Hands-on bayesian neural networks—a tutorial for deep learning users. *IEEE Computational Intelligence Magazine*, 17(2):29–48, 2022.

Alex Kendall and Yarin Gal. What uncertainties do we need in bayesian deep learning for computer vision? *Advances in neural information processing systems*, 30, 2017.

Diederik P. Kingma and Jimmy Ba. Adam: A method for stochastic optimization. In Yoshua Bengio and Yann LeCun, editors, *3rd International Conference on Learning Representations, ICLR 2015, San Diego, CA, USA, May 7-9, 2015, Conference Track Proceedings*, 2015.

Diederik P. Kingma and Max Welling. Auto-encoding variational bayes. In Yoshua Bengio and Yann LeCun, editors, *2nd International Conference on Learning Representations, ICLR 2014, Banff, AB, Canada, April 14-16, 2014, Conference Track Proceedings*, 2014.

Shu Kong and Deva Ramanan. Opengan: Open-set recognition via open data generation. In *Proceedings of the IEEE/CVF International Conference on Computer Vision*, pages 813–822, 2021.

Agustinus Kristiadi, Matthias Hein, and Philipp Hennig. Being bayesian, even just a bit, fixes overconfidence in relu networks. In *International conference on machine learning*, pages 5436–5446. PMLR, 2020.

Agustinus Kristiadi, Matthias Hein, and Philipp Hennig. Being a bit frequentist improves bayesian neural networks. In *International Conference on Artificial Intelligence and Statistics*, pages 529–545. PMLR, 2022.

Alex Krizhevsky, Geoffrey Hinton, et al. Learning multiple layers of features from tiny images. 2009.

Anders Krogh and John Hertz. A simple weight decay can improve generalization. *Advances in neural information processing systems*, 4, 1991.

Volodymyr Kuleshov, Nathan Fenner, and Stefano Ermon. Accurate uncertainties for deep learning using calibrated regression. In *International conference on machine learning*, pages 2796–2804. PMLR, 2018.

Balaji Lakshminarayanan, Alexander Pritzel, and Charles Blundell. Simple and scalable predictive uncertainty estimation using deep ensembles. *Advances in neural information processing systems*, 30, 2017.

Kimin Lee, Kibok Lee, Honglak Lee, and Jinwoo Shin. A simple unified framework for detecting out-of-distribution samples and adversarial attacks. *Advances in neural information processing systems*, 31, 2018a.

Kimin Lee, Kibok Lee, Honglak Lee, and Jinwoo Shin. A simple unified framework for detecting out-of-distribution samples and adversarial attacks. *Advances in neural information processing systems*, 31, 2018b.

Jing Lei, Max G'Sell, Alessandro Rinaldo, Ryan J Tibshirani, and Larry Wasserman. Distribution-free predictive inference for regression. *Journal of the American Statistical Association*, 113 (523):1094–1111, 2018.

Dan Levi, Liran Gispan, Niv Giladi, and Ethan Fetaya. Evaluating and calibrating uncertainty prediction in regression tasks. *Sensors*, 22(15):5540, 2022.

Chun-Liang Li, Kihyuk Sohn, Jinsung Yoon, and Tomas Pfister. Cutpaste: Self-supervised learning for anomaly detection and localization. In *Proceedings of the IEEE/CVF Conference on Computer Vision and Pattern Recognition*, pages 9664–9674, 2021.

Shiyu Liang, Yixuan Li, and Rayadurgam Srikant. Enhancing the reliability of out-of-distribution image detection in neural networks. *arXiv preprint arXiv:1706.02690*, 2017.

Jeremiah Zhe Liu, Shreyas Padhy, Jie Ren, Zi Lin, Yeming Wen, Ghassen Jerfel, Zack Nado, Jasper Snoek, Dustin Tran, and Balaji Lakshminarayanan. A simple approach to improve single-model deep uncertainty via distance-awareness. *arXiv preprint arXiv:2205.00403*, 2022.

Weitang Liu, Xiaoyun Wang, John Owens, and Yixuan Li. Energy-based out-of-distribution detection. *Advances in neural information processing systems*, 33:21464–21475, 2020.

Yehao Liu, Matteo Pagliardini, Tatjana Chavdarova, and Sebastian U Stich. The peril of popular deep learning uncertainty estimation methods. *arXiv preprint arXiv:2112.05000*, 2021.

Yong Liu and Xin Yao. Ensemble learning via negative correlation. *Neural networks*, 12(10): 1399–1404, 1999.

Christos Louizos and Max Welling. Structured and efficient variational deep learning with matrix gaussian posteriors. In *International conference on machine learning*, pages 1708–1716. PMLR, 2016.

Christos Louizos and Max Welling. Multiplicative normalizing flows for variational bayesian neural networks. In *International Conference on Machine Learning*, pages 2218–2227. PMLR, 2017.

Christos Louizos, Xiahan Shi, Klamer Schutte, and Max Welling. The functional neural process. *Advances in Neural Information Processing Systems*, 32, 2019.

David JC MacKay. A practical bayesian framework for backpropagation networks. *Neural computation*, 4(3):448–472, 1992.

David JC MacKay. *Information theory, inference and learning algorithms*. Cambridge university press, 2003.

David John Cameron Mackay. *Bayesian methods for adaptive models*. PhD thesis, California Institute of Technology, 1992.

Cédric Malherbe and Nicolas Vayatis. Global optimization of lipschitz functions. In *International Conference on Machine Learning*, pages 2314–2323. PMLR, 2017.

Hendrik Alexander Mehrtens, Camila González, and Anirban Mukhopadhyay. Improving robustness and calibration in ensembles with diversity regularization. *arXiv preprint arXiv:2201.10908*, 2022.

Tom M Mitchell. Version spaces: A candidate elimination approach to rule learning. In *Proceedings of the 5th international joint conference on Artificial intelligence-Volume 1*, pages 305–310, 1977.

Chandra Nair, Balaji Prabhakar, and Devavrat Shah. On entropy for mixtures of discrete and continuous variables. *arXiv preprint cs/0607075*, 2006.

Andre T Nguyen, Fred Lu, Gary Lopez Munoz, Edward Raff, Charles Nicholas, and James Holt. Out of distribution data detection using dropout bayesian neural networks. In *Proceedings of the AAAI Conference on Artificial Intelligence*, volume 36, pages 7877–7885, 2022.

David A Nix and Andreas S Weigend. Estimating the mean and variance of the target probability distribution. In *Proceedings of 1994 ieee international conference on neural networks (ICNN'94)*, volume 1, pages 55–60. IEEE, 1994.

Kazuki Osawa, Siddharth Swaroop, Mohammad Emtiyaz E Khan, Anirudh Jain, Runa Eschenhagen, Richard E Turner, and Rio Yokota. Practical deep learning with bayesian principles. *Advances in neural information processing systems*, 32, 2019.

Yaniv Ovadia, Emily Fertig, Jie Ren, Zachary Nado, David Sculley, Sebastian Nowozin, Joshua Dillon, Balaji Lakshminarayanan, and Jasper Snoek. Can you trust your model's uncertainty? evaluating predictive uncertainty under dataset shift. *Advances in neural information processing systems*, 32, 2019.

Matteo Pagliardini, Martin Jaggi, François Fleuret, and Sai Praneeth Karimireddy. Agree to disagree: Diversity through disagreement for better transferability. *arXiv preprint arXiv:2202.04414*, 2022.

Victor Y Pan and Zhao Q Chen. The complexity of the matrix eigenproblem. In *Proceedings of the thirty-first annual ACM symposium on Theory of computing*, pages 507–516, 1999.

Nick Pawlowski, Andrew Brock, Matthew CH Lee, Martin Rajchl, and Ben Glocker. Implicit weight uncertainty in neural networks. *arXiv preprint arXiv:1711.01297*, 2017.

Tim Pearce, Mohamed Zaki, Alexandra Brintrup, N Anastassacos, and A Neely. Uncertainty in neural networks: Bayesian ensembling. *stat*, 1050:12, 2018.

Alexandre Ramé and Matthieu Cord. Dice: Diversity in deep ensembles via conditional redundancy adversarial estimation. In *ICLR 2021-9th International Conference on Learning Representations*, 2021.

Carl Edward Rasmussen. Gaussian processes in machine learning. In *Summer school on machine learning*, pages 63–71. Springer, 2003.

Danilo Rezende and Shakir Mohamed. Variational inference with normalizing flows. In *International conference on machine learning*, pages 1530–1538. PMLR, 2015.

Danilo Jimenez Rezende, Shakir Mohamed, and Daan Wierstra. Stochastic backpropagation and approximate inference in deep generative models. In *International conference on machine learning*, pages 1278–1286. PMLR, 2014.

Hippolyt Ritter, Aleksandar Botev, and David Barber. A scalable laplace approximation for neural networks. In *6th International Conference on Learning Representations, ICLR 2018-Conference Track Proceedings*, volume 6. International Conference on Representation Learning, 2018.

Andrew Ross, Weiwei Pan, Leo Celi, and Finale Doshi-Velez. Ensembles of locally independent prediction models. In *Proceedings of the AAAI Conference on Artificial Intelligence*, volume 34, pages 5527–5536, 2020.

Tim GJ Rudner, Sanyam Kapoor, Shikai Qiu, and Andrew Gordon Wilson. Function-space regularization in neural networks: A probabilistic perspective. 2023.

Lukas Ruff, Robert Vandermeulen, Nico Goernitz, Lucas Deecke, Shoaib Ahmed Siddiqui, Alexander Binder, Emmanuel Müller, and Marius Kloft. Deep one-class classification. In *International conference on machine learning*, pages 4393–4402. PMLR, 2018.

Seonghan Ryu, Sangjun Koo, Hwanjo Yu, and Gary Geunbae Lee. Out-of-domain detection based on generative adversarial network. In *Proceedings of the 2018 Conference on Empirical Methods in Natural Language Processing*, pages 714–718, 2018.

Chandramouli Shama Sastry and Sageev Oore. Detecting out-of-distribution examples with gram matrices. In *International Conference on Machine Learning*, pages 8491–8501. PMLR, 2020.

Pierre Segonne, Yevgen Zainchkovskyy, and Søren Hauberg. Robust uncertainty estimates with out-of-distribution pseudo-inputs training. *arXiv preprint arXiv:2201.05890*, 2022.

Murat Sensoy, Lance Kaplan, and Melih Kandemir. Evidential deep learning to quantify classification uncertainty. *Advances in neural information processing systems*, 31, 2018.

Zheyan Shen, Jiashuo Liu, Yue He, Xingxuan Zhang, Renzhe Xu, Han Yu, and Peng Cui. Towards out-of-distribution generalization: A survey. *arXiv preprint arXiv:2108.13624*, 2021.

Changjian Shui, Azadeh Sadat Mozafari, Jonathan Marek, Ihsen Hedhli, and Christian Gagné. Diversity regularization in deep ensembles. *arXiv preprint arXiv:1802.07881*, 2018.

Samarth Sinha, Homanga Bharadhwaj, Anirudh Goyal, Hugo Larochelle, Animesh Garg, and Florian Shkurti. Dibs: Diversity inducing information bottleneck in model ensembles. In *Proceedings of the AAAI Conference on Artificial Intelligence*, volume 35, pages 9666–9674, 2021.

Timothy John Sullivan, Mike McKerns, Dominik Meyer, Florian Theil, Houman Owhadi, and Michael Ortiz. Optimal uncertainty quantification for legacy data observations of lipschitz functions. *ESAIM: Mathematical Modelling and Numerical Analysis*, 47(6):1657–1689, 2013.

Shengyang Sun, Changyou Chen, and Lawrence Carin. Learning structured weight uncertainty in bayesian neural networks. In *Artificial Intelligence and Statistics*, pages 1283–1292. PMLR, 2017.

Shengyang Sun, Guodong Zhang, Jiaxin Shi, and Roger Grosse. Functional variational bayesian neural networks. In *International Conference on Learning Representations*, 2018.

Yiyou Sun and Yixuan Li. Dice: Leveraging sparsification for out-of-distribution detection. In *Computer Vision–ECCV 2022: 17th European Conference, Tel Aviv, Israel, October 23–27, 2022, Proceedings, Part XXIV*, pages 691–708. Springer, 2022.

Yiyou Sun, Chuan Guo, and Yixuan Li. React: Out-of-distribution detection with rectified activations. *Advances in Neural Information Processing Systems*, 34:144–157, 2021.

Yiyou Sun, Yifei Ming, Xiaojin Zhu, and Yixuan Li. Out-of-distribution detection with deep nearest neighbors. In *International Conference on Machine Learning*, pages 20827–20840. PMLR, 2022.

Jihoon Tack, Sangwoo Mo, Jongheon Jeong, and Jinwoo Shin. Csi: Novelty detection via contrastive learning on distributionally shifted instances. *Advances in neural information processing systems*, 33:11839–11852, 2020.

Natasa Tagasovska and David Lopez-Paz. Single-model uncertainties for deep learning. *Advances in Neural Information Processing Systems*, 32, 2019.

Sunil Thulasidasan, Gopinath Chennupati, Jeff A Bilmes, Tanmoy Bhattacharya, and Sarah Michalak. On mixup training: Improved calibration and predictive uncertainty for deep neural networks. *Advances in Neural Information Processing Systems*, 32, 2019.

Alexandru Tifrea, Eric Petru Stavarache, and Fanny Yang. Semi-supervised novelty detection using ensembles with regularized disagreement. In *The 38th Conference on Uncertainty in Artificial Intelligence*, 2022.

Antonio Torralba, Rob Fergus, and William T Freeman. 80 million tiny images: A large data set for nonparametric object and scene recognition. *IEEE transactions on pattern analysis and machine intelligence*, 30(11):1958–1970, 2008.

Ba-Hien Tran, Simone Rossi, Dimitrios Milios, and Maurizio Filippone. All you need is a good functional prior for bayesian deep learning. *The Journal of Machine Learning Research*, 23(1): 3210–3265, 2022.

Joost Van Amersfoort, Lewis Smith, Yee Whye Teh, and Yarin Gal. Uncertainty estimation using a single deep deterministic neural network. In *International conference on machine learning*, pages 9690–9700. PMLR, 2020.

Vladimir Vovk, Alexander Gammerman, and Glenn Shafer. *Algorithmic learning in a random world*, volume 29. Springer, 2005.

Haoqi Wang, Zhizhong Li, Litong Feng, and Wayne Zhang. Vim: Out-of-distribution with virtual-logit matching. In *Proceedings of the IEEE/CVF Conference on Computer Vision and Pattern Recognition*, pages 4921–4930, 2022a.

Haotao Wang, Aston Zhang, Yi Zhu, Shuai Zheng, Mu Li, Alex J Smola, and Zhangyang Wang. Partial and asymmetric contrastive learning for out-of-distribution detection in long-tailed recognition. In *International Conference on Machine Learning*, pages 23446–23458. PMLR, 2022b.

Hongxin Wei, Renchunzi Xie, Hao Cheng, Lei Feng, Bo An, and Yixuan Li. Mitigating neural network overconfidence with logit normalization. In *International Conference on Machine Learning*, pages 23631–23644. PMLR, 2022.

Yeming Wen, Dustin Tran, and Jimmy Ba. Batchensemble: an alternative approach to efficient ensemble and lifelong learning. *arXiv preprint arXiv:2002.06715*, 2020.

Florian Wenzel, Kevin Roth, Bastiaan Veeling, Jakub Swiatkowski, Linh Tran, Stephan Mandt, Jasper Snoek, Tim Salimans, Rodolphe Jenatton, and Sebastian Nowozin. How good is the bayes posterior in deep neural networks really? In *International Conference on Machine Learning*, pages 10248–10259. PMLR, 2020a.

Florian Wenzel, Jasper Snoek, Dustin Tran, and Rodolphe Jenatton. Hyperparameter ensembles for robustness and uncertainty quantification. *Advances in Neural Information Processing Systems*, 33:6514–6527, 2020b.

Andrew Gordon Wilson. The case for bayesian deep learning. *arXiv preprint arXiv:2001.10995*, 2020.

Anqi Wu, Sebastian Nowozin, Edward Meeds, Richard E Turner, José Miguel Hernández-Lobato, and Alexander L Gaunt. Deterministic variational inference for robust bayesian neural networks. In *International Conference on Learning Representations*, 2018.

Jingkang Yang, Pengyun Wang, Dejian Zou, Zitang Zhou, Kunyuan Ding, Wenxuan Peng, Haoqi Wang, Guangyao Chen, Bo Li, Yiyou Sun, et al. Openood: Benchmarking generalized out-of-distribution detection. *arXiv preprint arXiv:2210.07242*, 2022.

Qing Yu and Kiyoharu Aizawa. Unsupervised out-of-distribution detection by maximum classifier discrepancy. In *Proceedings of the IEEE/CVF international conference on computer vision*, pages 9518–9526, 2019.

Sangdoo Yun, Dongyoon Han, Seong Joon Oh, Sanghyuk Chun, Junsuk Choe, and Youngjoon Yoo. Cutmix: Regularization strategy to train strong classifiers with localizable features. In *Proceedings of the IEEE/CVF international conference on computer vision*, pages 6023–6032, 2019.

Sheheryar Zaidi, Arber Zela, Thomas Elsken, Chris C Holmes, Frank Hutter, and Yee Teh. Neural ensemble search for uncertainty estimation and dataset shift. *Advances in Neural Information Processing Systems*, 34:7898–7911, 2021.

Vitjan Zavrtanik, Matej Kristan, and Danijel Skočaj. Draem-a discriminatively trained reconstruction embedding for surface anomaly detection. In *Proceedings of the IEEE/CVF International Conference on Computer Vision*, pages 8330–8339, 2021.

Guodong Zhang, Shengyang Sun, David Duvenaud, and Roger Grosse. Noisy natural gradient as variational inference. In *International conference on machine learning*, pages 5852–5861. PMLR, 2018.

Shanghang Zhang, Guanhang Wu, Joao P Costeira, and Jose MF Moura. Understanding traffic density from large-scale web camera data. In *Proceedings of the IEEE Conference on Computer Vision and Pattern Recognition*, pages 5898–5907, 2017.

Shaofeng Zhang, Meng Liu, and Junchi Yan. The diversified ensemble neural network. *Advances in Neural Information Processing Systems*, 33:16001–16011, 2020.

Yibo Zhou. Rethinking reconstruction autoencoder-based out-of-distribution detection. In *Proceedings of the IEEE/CVF Conference on Computer Vision and Pattern Recognition*, pages 7379–7387, 2022.